BiFeO3-BaTiO3: A new generation of lead-free electroceramics

WANG, Dawei <http://orcid.org/0000-0001-6957-2494>, WANG, Ge, MURAKAMI, Shunsuke, FAN, Zhongming, FETEIRA, Antonio <http://orcid.org/0000-0001-8151-7009>, ZHOU, Di, SUN, Shikuan, ZHAO, Quanliang and REANEY, Ian M.

Published version

WANG, Dawei, WANG, Ge, MURAKAMI, Shunsuke, FAN, Zhongming, FETEIRA, Antonio, ZHOU, Di, SUN, Shikuan, ZHAO, Quanliang and REANEY, Ian M. (2018). BiFeO3-BaTiO3: A new generation of lead-free electroceramics. Journal of advanced dielectrics, p. 1830004.

Copyright and re-use policy

Review

JOURNAL OF ADVANCED DIELECTRICS
Vol. 8, No. 6 (2018) 1830004 (35 pages)

DOI: 10.1142/S2010135X18300049

World Scientific
www.worldscientific.com

$BiFeO_3$-$BaTiO_3$: A new generation of lead-free electroceramics

Dawei Wang*,‖,††, Ge Wang*,††, Shunsuke Murakami*,††, Zhongming Fan†, Antonio Feteira‡, Di Zhou§, Shikuan Sun*, Quanliang Zhao¶ and Ian M. Reaney*,**

*Department of Materials Science and Engineering
University of Sheffield, Sheffield S1 3JD, UK

†Department of Materials Science and Engineering
Iowa State University, Ames, Iowa 50011, USA

‡Christian Doppler Laboratory for Advanced Ferroic Oxides
Sheffield Hallam University, Sheffield S1 1WB, UK

§Electronic Materials Research Laboratory
Key Laboratory of the Ministry of Education
& International Center for Dielectric Research
Xi'an Jiaotong University, Xi'an 710049, Shaanxi, P. R. China

¶School of Mechanical and Materials Engineering
North China University of Technology
Beijing 100144, P. R. China

‖dawei.wang@sheffield.ac.uk

**i.m.reaney@sheffield.ac.uk

Received 17 September 2018; Revised 19 September 2018; Accepted 15 October 2018; Published 17 December 2018

Lead-based electroceramics such as Pb(Zr.Ti)O_3 (PZT) and its derivatives have excellent piezoelectric, pyroelectric and energy storage properties and can be used in a wide range of applications. Potential lead-free replacements for PZT such as potassium sodium niobate (KNN) and sodium bismuth titanate (NBT) have a much more limited range of useful properties and have been optimized primarily for piezoelectric applications. Here, we review the initial results on a new generation of lead-free electroceramics based on $BiFeO_3$-$BaTiO_3$ (BF-BT) highlighting the essential crystal chemistry that permits a wide range of functional properties. We demonstrate that with the appropriate dopants and heat treatment, BF-BT can be used to fabricate commercially viable ceramics for applications, ranging from sensors, multilayer actuators, capacitors and high-density energy storage devices. We also assess the potential of BF-BT-based ceramics for electrocaloric and pyroelectric applications.

Keywords: $BiFeO_3$-$BaTiO_3$; lead-free; piezoelectrics; energy storage; dielectrics; capacitors.

1. Introduction

Electroceramics is a class of materials used for their unique electrical, optical and magnetic properties in communications, energy conversion and storage, electronics and automation.[1] Electroceramics have subclasses which include dielectrics, piezoelectrics, pyroelectrics, ferroelectrics, ion conductors, and magnetic ceramics.[1] Currently, the market for electroceramics is dominated by $BaTiO_3$ (BT) and Pb(Zr,Ti)O_3 (PZT). $BaTiO_3$ is utilized in dielectric applications in multilayer ceramic capacitors (MLCCs), produced in trillions of parts per year, whereas PZT is the basis for pyro-, piezo- and ferroelectric application as well as novel energy storage technology at the antiferroelectric/ferroelectric (AFE/FE) phase boundary within the PZT phase diagram.

2. Piezoelectricity and Lead Zirconate Titanate

Piezoelectricity was first discovered in quartz by Pierre and Jacques Curie in 1880[2] who determined that mechanical stress generated electric charge on the surface of quartz, now referred to as the direct piezoelectric effect. The inverse piezoelectric effect was mathematically deduced from fundamental thermodynamic principles by Gabriel Lippmann in 1881 and experimentally confirmed by the Curie brothers.[3] Over the next few decades, 20 natural crystals were found to show piezoelectricity and their properties were rigorously defined using tensor analysis. The first application using piezoelectric material was conducted by Paul Lengvin in 1917 during World War I when quartz was used in ultrasonic submarine detectors, called sonar. During World War II, $BaTiO_3$ was simultaneously discovered in USA, Russia, and

‖,**Corresponding authors.
††Author Contributions: D. Wang, G. Wang and S. Murakami contributed equally to this work and should be considered as co-first authors.

Japan. Since $BaTiO_3$ has much higher dielectric and piezoelectric properties than natural materials, the development of piezoelectric materials was accelerated, leading to the discovery of PZT after World War II.[4–7] PZT has a morphotropic phase boundary (MPB), separating rhombohedral (R) and tetragonal (T) phase, and hence shows high piezoelectric properties with high Curie temperature (T_C, Fig. 1). Since this compositionally driven phase transition is nearly independent of temperature, PZT has been widely applied to many applications. T and R phases have six spontaneous polarization directions along $\langle 001 \rangle$ and eight along $\langle 111 \rangle$, respectively. Therefore, at the MPB, there exist many possible polarization directions and hence high piezoelectric properties are generated. In addition, Noheda *et al.*[8,9] reported a monoclinic (M) phase between the T and R phase in PZT in 1999. The M phase has 24 possible polarization directions which enhance the electromechanical properties. The properties of commercial PZTs are controlled by dopants which are broadly categorized as soft PZT (donor doped) and hard PZT (acceptor doped).[10–14] These features have made PZTs the most widely used piezoelectrics to date.

3. Lead-Free Piezoelectrics

Following increased environmental awareness during the latter part of the 20th century, lead has become subject to increasing legal restraints that prohibit its usage, alongside mercury, cadmium and hexavalent chromium, in electronic devices. The Restriction of Hazardous Substances Directive (RoHS) was adopted in 2003 by the European Union[15] and has effectively driven the development of lead-free substitutes. However, to date there is no lead-free piezoelectric able to replace fully PZT. Rather, there are a number of candidates such as $(K,Na)NbO_3$ (KNN), $Bi_{1/2}Na_{1/2}TiO_3$ (BNT), and $(Ba,Ca)(Zr,Ti)O_3$ (BCZT) each of which has strengths and weaknesses. Extensive research on KNN based materials was triggered by Saito *et al.* in 2004[16] when textured $(K_{0.44}N_{a0.52}Li_{0.04})(Nb_{0.86}Ta_{0.10}Sb_{0.04})O_3$ achieved high piezoelectric coefficient (d_{33}) = 416 pC/N, an electro-strain (S_{max}) ~ 0.15% at 2 kV/mm (inverse piezoelectric coefficient d^*_{33} = 750 pm/V) and a $T_C = 253°C$, as shown in Fig. 2. d_{33} is comparable to that of PZT but the orthorhombic (O) to T phase transition temperature close to room temperature (RT) results in a decrease in piezoactivity with increase in temperature.[17–19] Recently, KNN-based ceramics have been reported with high $d_{33} = 300 \sim 570$ pC/N and R-T phase coexistence at room temperature but whose properties deteriorate with increasing temperature, unlike PZT.[20–31] Giant strain in BNT has been reported by Zhang *et al.*[32] with the ternary system of $(0.94\text{-}x)Bi_{0.5}Na_{0.5}TiO_3$-$0.06BaTiO_3$-$xK_{0.5}Na_{0.5}NbO_3$ (BNT-BT-xKNN) exhibiting a S_{max} of 0.45% at 8 kV/mm (d^*_{33} = 562 pm/V), as shown in Fig. 3. Since then, many researchers have studied NBT-based materials,[33–41] and recently Liu *et al.*[41] reported polycrystalline $[Bi_{1/2}(Na_{0.8}K_{0.2})_{1/2}](Ti_{0.985}Ta_{0.015})O_3$ ceramics with a S_{max} of 0.62% under a moderate bipolar field of 5 kV/mm (d^*_{33} = 1240 pm/V). However, BNT-based materials undergo depolarization (T_d) at ~ 100°C and are thus difficult to utilize for high temperature applications.[33–41] Liu and Ren[42] reported $0.50Ba(Zr_{0.2}Ti_{0.8})O_3$-$0.50(Ba_{0.7}Ca_{0.3})TiO_3$ (BZT-50BCT) with a high d_{33} of 620 pC/N and a S_{max} of 0.057% at 0.5 kV/mm (d^*_{33} = 1140 pm/V), Fig. 4, purportedly due to an MPB but more accurately described as a tri-critical point (TCP) consisting of T, R, and cubic (C) phases which gives a low energy barrier for polarization rotation and lattice distortion.[42–47] BCZT cannot be used at high temperature due to the low T_C(< 100°C) but compositions do not contain volatile and endangered raw materials and hence they are considered environmentally friendly, sustainable and easy to process.

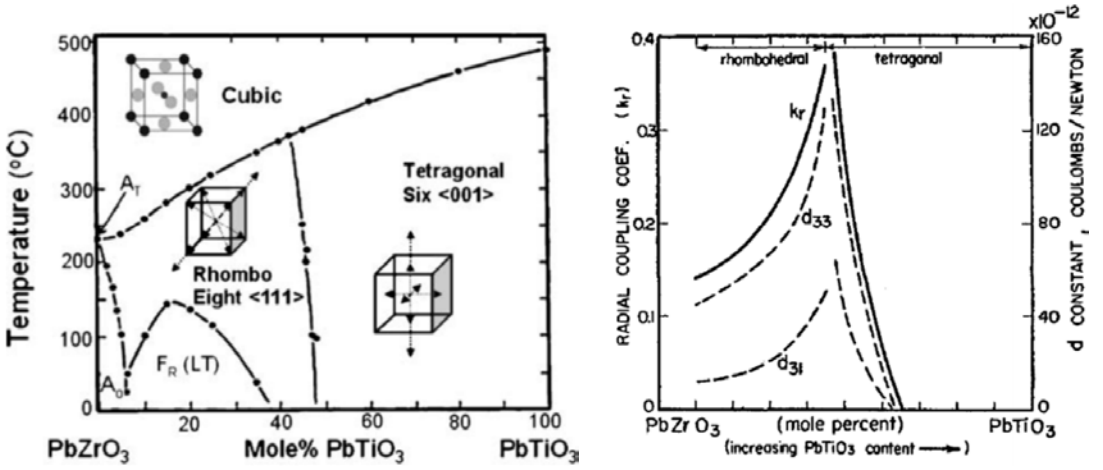

(a) (b)

Fig. 1. (a) Phase diagram[5] and (b) electromechanical properties[6] of $Pb(Zr,Ti)O_3$ (PZT).

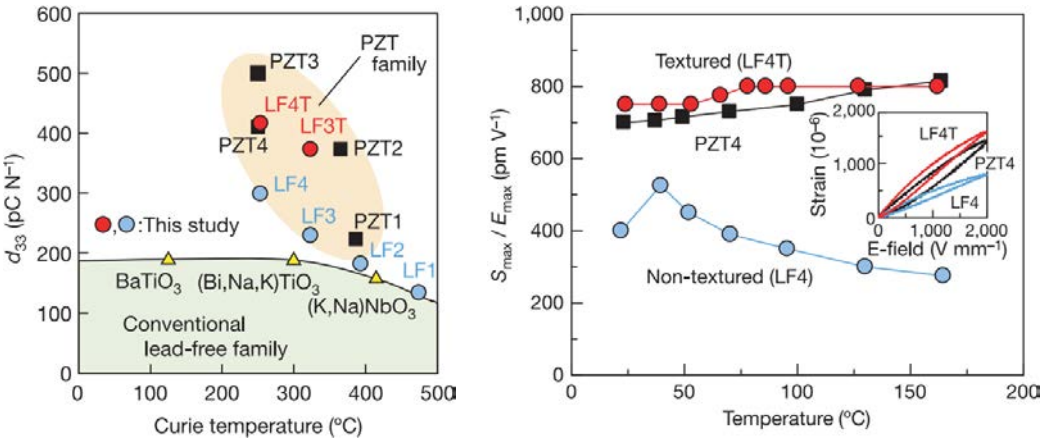

(a) (b)

Fig. 2. (a) Comparison of d_{33} at 25°C among developed $(K_{0.44}N_{a0.52}Li_{0.04})(Nb_{0.86}Ta_{0.10}Sb_{0.04})O_3$ (LF) ceramics, and conventional PZT and lead free ceramics as a function of T_C. (b) Temperature dependences of d_{33}^* for the textured (LF4T), nontextured (LF4) and PZT4 ceramics. Inset, electric-field-induced strain curve for LF4T, LF4 and PZT4 ceramics at 25°C.[16]

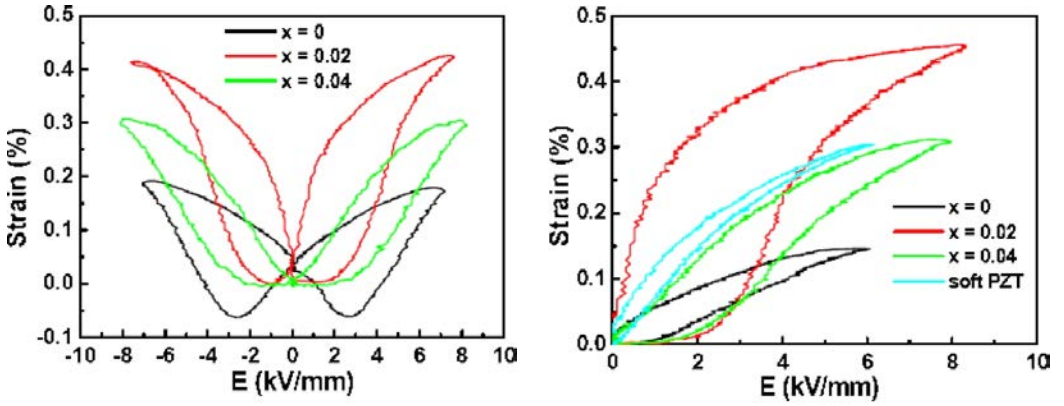

(a) (b)

Fig. 3. Field-induced strain in $(0.94\text{-}x)Bi_{0.5}Na_{0.5}TiO_3\text{-}0.06BaTiO_3\text{-}xK_{0.5}Na_{0.5}NbO_3$ (BNT-BT-KNN) ceramics. (a) Bipolar strain curves of BNT-BT-xKNN with $x = 0$, 0.02, and 0.04. (b) Unipolar strain curves of BNT-BT-KNN with $x = 0$, 0.02, and 0.04 in comparison to that of commercial soft PZT.[32]

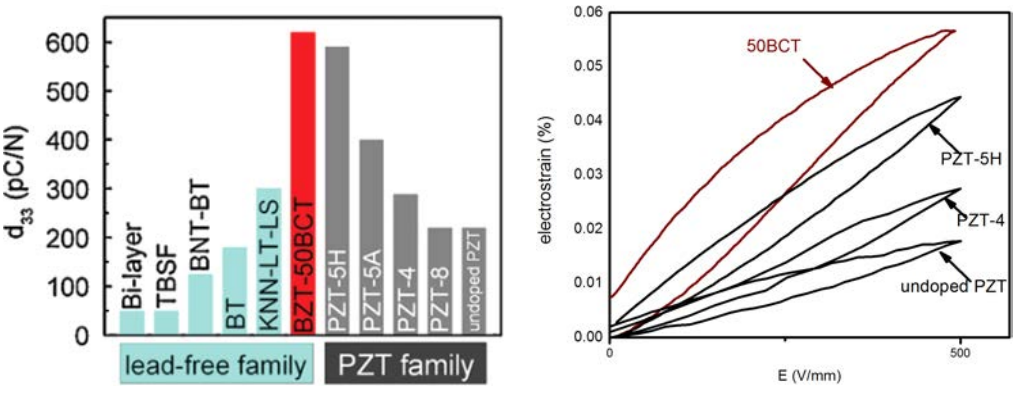

(a) (b)

Fig. 4. (a) Comparison of d_{33} among $0.50Ba(Zr_{0.2}Ti_{0.8})O_3\text{-}0.50(Ba_{0.7}Ca_{0.3})TiO_3$ (BZT-50BCT) and other lead-free piezoelectrics and PZT family. (b) Electric-field-induced strain of BZT-50BCT in comparison with several typical PZT ceramics.[42]

4. The $BiFeO_3$-$BaTiO_3$ System

The ceramics discussed in Sec. 3 show great promise for the development of lead-free piezoelectrics, but PZT also exhibits several further useful physical properties and can be used in different applications. Ideally, therefore an alternative lead-free system is required which can be used not only as a piezoelectric but also in other applications, potentially simplifying industrial production of lead-free electroceramics. $BiFeO_3$-$BaTiO_3$ (BF-BT) ceramics have recently emerged as a contender to replace PZT. $BaTiO_3$ and $BiFeO_3$ have T and R structures, respectively, at RT with the latter having a particularly high T_C (825°C).[48–50] As early as 1964, Venevtsev *et al.*[51] claimed that BF-BT formed a continuous solid solution at RT with three crystal structures: R (100-67% BF), C (67-7.5% BF) and T (7.5-0% BF), which was later confirmed by Kumar *et al.*[52] In 2009, Leontsevw and Eitel[53] gave a revised phase diagram for BF-BT system, Fig. 5, based on temperature dependence of dielectric constant (ε_r) and differential scanning calorimetry (DSC) measurements. They reported a broad, temperature-independent MPB (0.25-0.4BT) between R and C phases, with enhanced piezoelectricity. Subsequently, Lee *et al.*[54] reported a PZT-like R-T MPB in quenched BF-BT based ceramics, with high $d_{33} = 402$ pC/N and $T_C = 454$°C, as shown in Fig. 6.

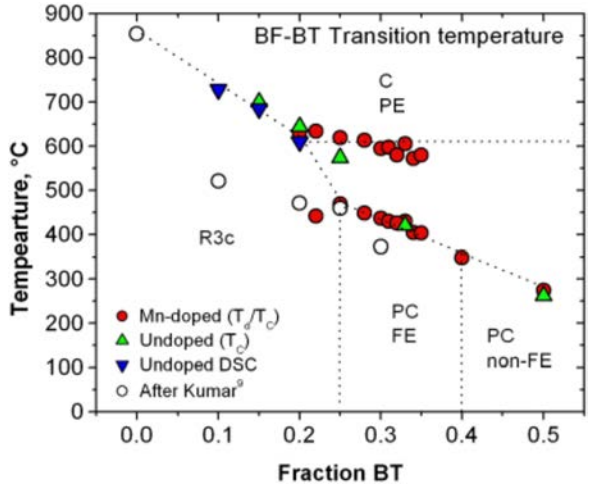

Fig. 5. Phase diagram of $BiFeO_3$-$BaTiO_3$ (BF-BT) solid solution.[53]

There is clear similarity between PZT and BF-BT solid solutions with a general trend from R to T as BT and PT concentration increase, respectively. However, in BF-BT, both the A- and B-sites are occupied by more than one ionic species as opposed to just the B-site in PZT. This rather obvious statement accounts for the differences in the compositional phase transformations between PZT and BF-BT. In PZT, Ti and Zr compete to influence the displacement of the contiguous Pb-site with its highly polarizable lone pair of electrons. In contrast in BF-BT, Ba acts as a large blocking ion for displacements of the Bi lone pair species. On the B-site, Fe compete with Ti displacements. The presence of competition for uniform displacements on each site results in a greater driving force for the formation of short-range ordered pseudosymmetric structures, as observed by Leontsevw and Eitel[53] and subsequent researchers. There is therefore, a greater tendency in the system for the formation of broad relaxor-like dielectric behavior than within PZT. Although this may not be ideal to obtain large d_{33}, it does not preclude a high strain electrostrictive response (large d^*_{33}) and is ideal for high energy density storage, electrocaloric and possibly pyroelectric applications.

The many recent publications over the last decade, as shown in Fig. 7, indicate that the BF-BT system is one of most promising candidates for lead-free ceramics. In this

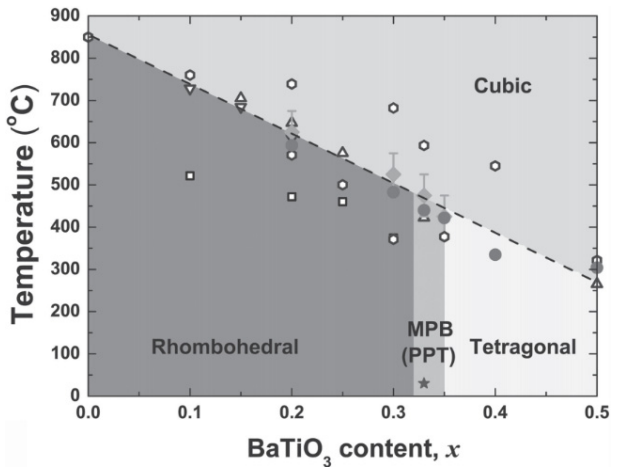

(a)

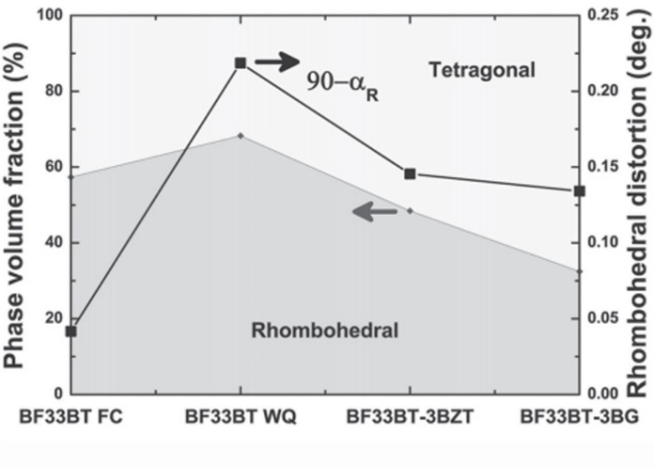

(b)

Fig. 6. (a) Suggested phase diagram of $BiFeO_3$-$BaTiO_3$ (BF-BT) system; (b) rhombohedral distortions (90°-α_R) and phase volume fractions of furnace-cooled $0.67BiFeO_3$-$0.33BaTiO_3$ (BF33BT), water-quenched BF33BT, 3%$Bi(Zn_{1/2}Ti_{1/2})O_3$ (BZT) doped BF33BT (BF33BT-3BZT) and 3%$BiGaO_3$ (BG) doped BF33BT (BF33BT-3BG) ceramics.[54]

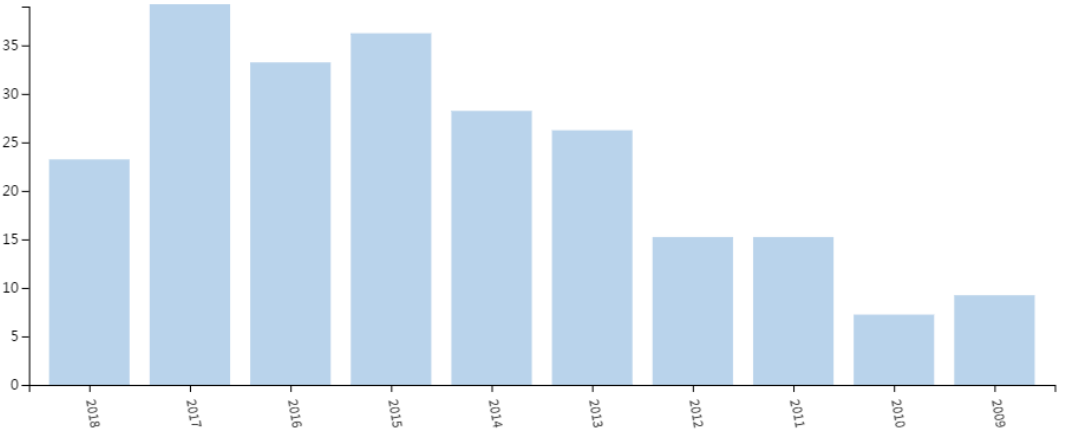

Fig. 7. The number of publications on BF-BT lead-free ceramics from 2000 to 2018. (Collected from ISI Web of Science using the keywords of BF-BT and $BiFeO_3$-$BaTiO_3$).

paper, we will review the current development of BF-BT lead-free ceramics, focusing on the crystal/domain structure, compositional inhomogeneity, piezoelectricity and energy storage properties. We demonstrate that with the appropriate dopants and heat treatment, BF-BT can be used to fabricate commercially viable ceramics for applications ranging from sensors, multilayer actuators, high temperature capacitors and high-density energy storage capacitors with potential for, but as yet unexplored, electrocaloric and pyroelectric applications.

5. $BiFeO_3$-$BaTiO_3$ Based Ceramics

5.1. *Crystal/domain structure and compositional inhomogeneity*

5.1.1. *Crystal structure*

Furnace cooled BF-BT solid solutions are widely considered to have an *R*-*C* phase boundary (albeit broad) at which the electromechanical properties are optimized.[51–54] Gotardo *et al.*[55] are one of the few authors who disagree with this perception and have ascribed xBF-(1-x)BT ($0.3 \leq x \leq 0.9$) ceramics to a combination of *R*3*c* and *Cm* phases, as shown in Fig. 8. Moreover, Lee *et al.*[54] reported an MPB in quenched Ga-doped BF-BT between *R*3*c* and *P*4*mm* (Fig. 6), with $d_{33} = 402$ pC/N. Despite these observations, the general consensus is that doping BF-BT pushes the system towards relaxor behavior accompanied by promotion of a core-shell microstructure,[56] particularly if samples are furnace cooled.

Even though the low signal d_{33} reported by Lee *et al.*[54] has not to date been repeated, many authors have observed large S_{max} and (high signal) d^*_{33} in quenched compositions with $BiMeO_3$ dopants, such as $Bi(Zn_{2/3}Nb_{1/3})O_3$ (BZN), $Bi(Mg_{2/3}Nb_{1/3})O_3$ (BMN) and $BiScO_3$ (BSc).[56–58] Only Murakami *et al.*,[56,57] deliberately eradicated quenching using BMN and BSc as dopants to give high $S_{max}(> 0.4\%)$ in furnace cooled ceramics in which *R* and *C* phases (*C* dominant) coexisted. These authors argued that avoiding quenching was advantageous for industrial manufacturing. Overall, these reports point to the potential of the BF-BT ceramics as high strain actuators but demonstrate that the structure and thus properties are sensitive to dopant concentration, type and heat treatment.

5.1.2. *Domain structure*

Ferroelectric domain structure and its evolution as a function of composition, temperature and electric field are critical to

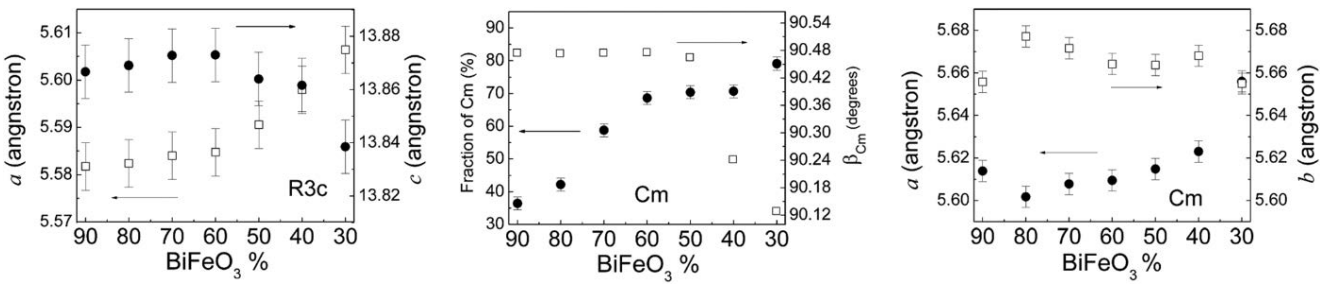

(a) (b) (c)

Fig. 8. (a) Lattice parameters for *R*3*c* unit cell, (b) fraction of the *Cm* phase and the monoclinic (*M*) phase angle β, (c) lattice parameters for *Cm* unit cell.[55]

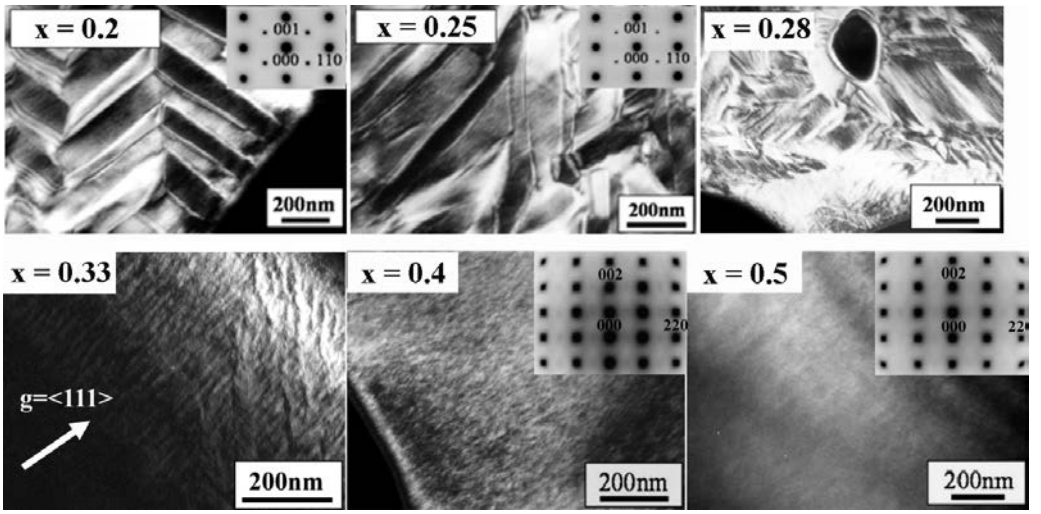

Fig. 9. Domain evolution and diffraction patterns of $(1-x)$BF-xBT.[59,60]

understanding the performance of any given ferroelectric solid solution. Mori *et al.*[59,60] examined the domain structure evolution of BF-BT across the *R* to *C* transformation and found that the lamellar domain morphology changed from well-defined herringbone type in 0.8BF-0.2BT to a more complex configuration in 0.72BF-0.28BT, to tweed-like small domains in 0.67BF-0.33BT, and then to a nano-domain structure for 0.4 and 0.5 BT, as shown in Fig. 9. Even though d_{33} is a maximum at the *R* to *C* phase boundary, the highest S_{max} and d^*_{33} appear in compositions with a dominant nano-domain structure. Wang and Murakami *et al.*[56,61] have elucidated such correlations through systematic TEM observations in Nd- and BMN-doped BF-BT compositions (Figs. 10 and 11) but further work is required to understand the field induced transition behavior in these complex systems. Kim *et al.*[62] compared the domain structure between furnace-cooled and air-quenched 0.75BF-0.25BT and showed that the air-quenched sample contained more regular domain structure than furnace cooled, as shown in Fig. 12. This data is consistent with a larger piezoelectric response and implies that in quenched samples composition/microstructure/defect structure may be very different from furnace cooled. Most authors note that quenching tends to suppress the core-shell structure, hinting at complex changes to phase equilibria as a function of temperature.

5.1.3. *Compositional inhomogeneity*

Compositional inhomogeneity is often observed in doped BF-BT ceramics as evidenced by a core-shell microstructure composed of dark and light contrast relating to Ba/Ti-rich and Bi/Fe-rich regions in backscattered electron images (BSE, Figs. 13(a)–13(c)) as confirmed by elemental mapping (Figs. 13(d)–13(k)), transmission electron microscopy (TEM), temperature dependence of ε_r and impedance spectroscopy.[56–58,63–67] Wang *et al.*[58] recently examined the core-shell microstructure of BZN-doped BF-BT by TEM and found that the Bi/Fe-rich core regions had $\{1/21/21/2\}$ superstructure reflections consistent with an *R*3*c* phase while Ba/Ti-rich shell regions were composed of a relaxor-like, nano-domain structured *C* phase, commensurate with a diffuse frequency-dependent Curie maximum, Fig. 14. Murakami *et al.*[56,57] observed compositional inhomogeneity in $Bi(Me)O_3$-doped BF-BT (Me=Y, Ga, Al, $Sc_{1/2}Y_{1/2}$, $Mg_{2/3}Nb_{1/3}$, Sc, $Zn_{2/3}Nb_{1/3}$, $Zn_{1/2}Ti_{1/2}$) and proved that

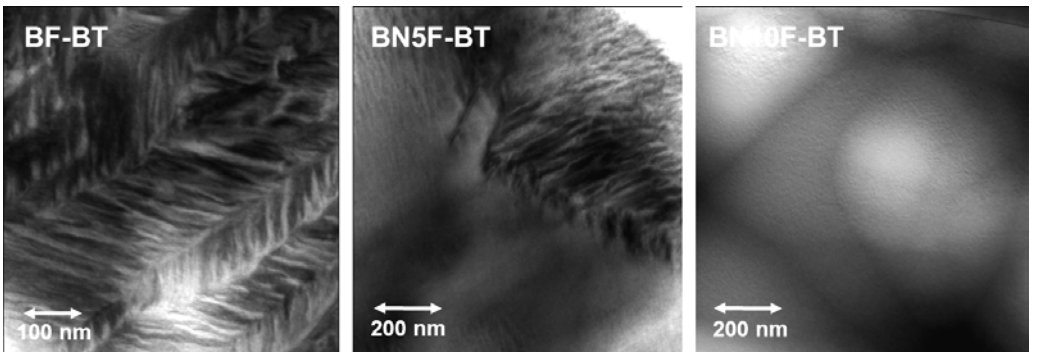

Fig. 10. TEM images of the domain structure in 0.7BF-0.3BT, 5%Nd-doped 0.7BF-0.3BT and 10%Nd-doped 0.7BF-0.3BT.[61]

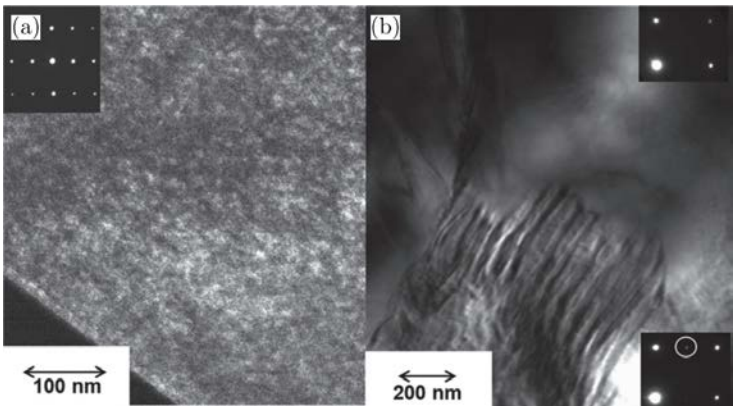

Fig. 11. TEM images and diffraction patterns in $Bi(Mg_{2/3}Nb_{1/3})O_3$ (BMN) doped BF-BT (a) 0.63BF-0.32BT-0.05BMN and (b) 0.7BF-0.25BT-0.05BMN.[56]

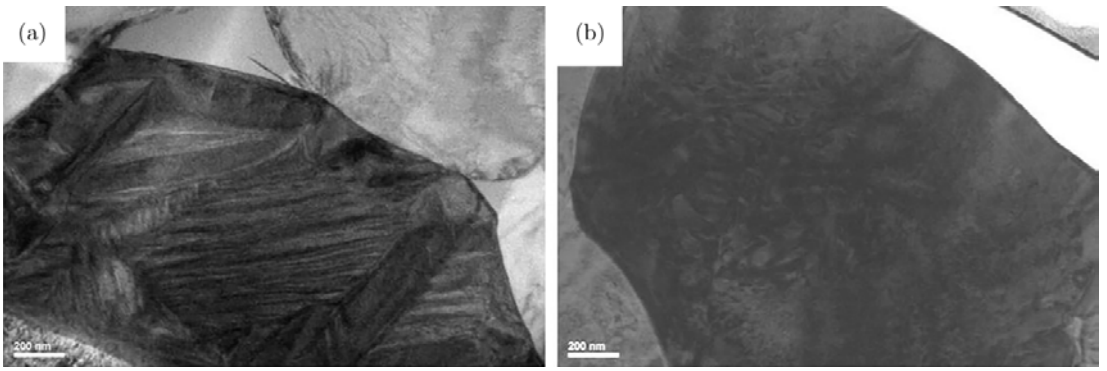

Fig. 12. Bright field TEM images for 800°C quenched (a) and (b) furnace cooled 0.75BF-0.25BT samples.[62]

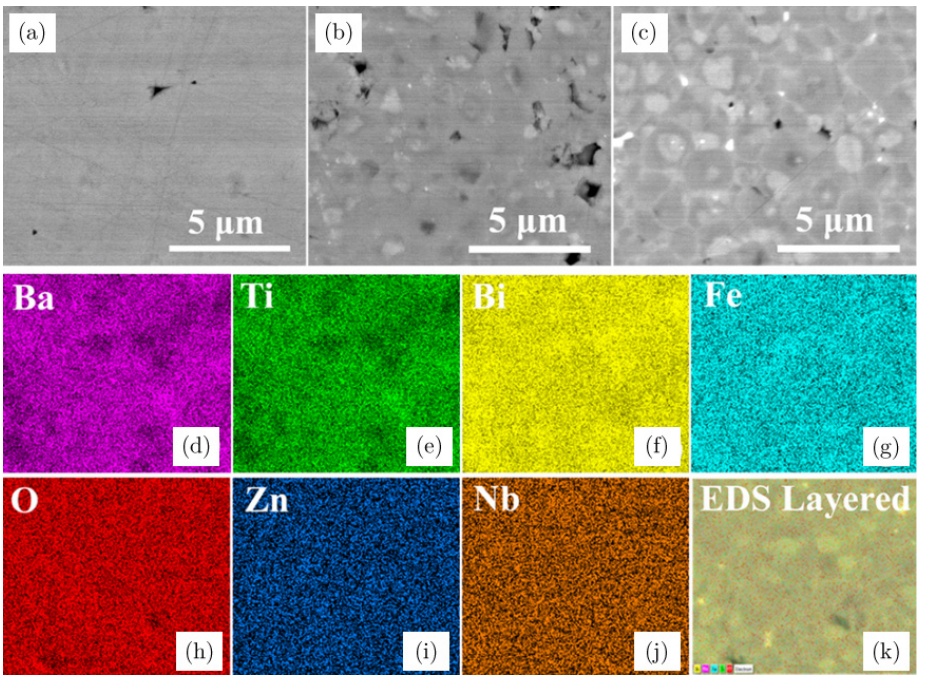

Fig. 13. Backscattered electron (BSE) images of polished surfaces for $Bi(Zn_{2/3}Nb_{1/3})O_3$ (BZN) doped BF-BT: (a) BF-BT, (b) BF-BT-0.02BZN, and (c) BF-BT-0.05BZN. EDS elemental mapping results of polished BF-BT-0.05BZN samples: (d) Ba, (e) Ti, (f) Bi, (g) Fe, (h) O, (i) Zn, (j) Nb, and (k) elemental layered image.[58]

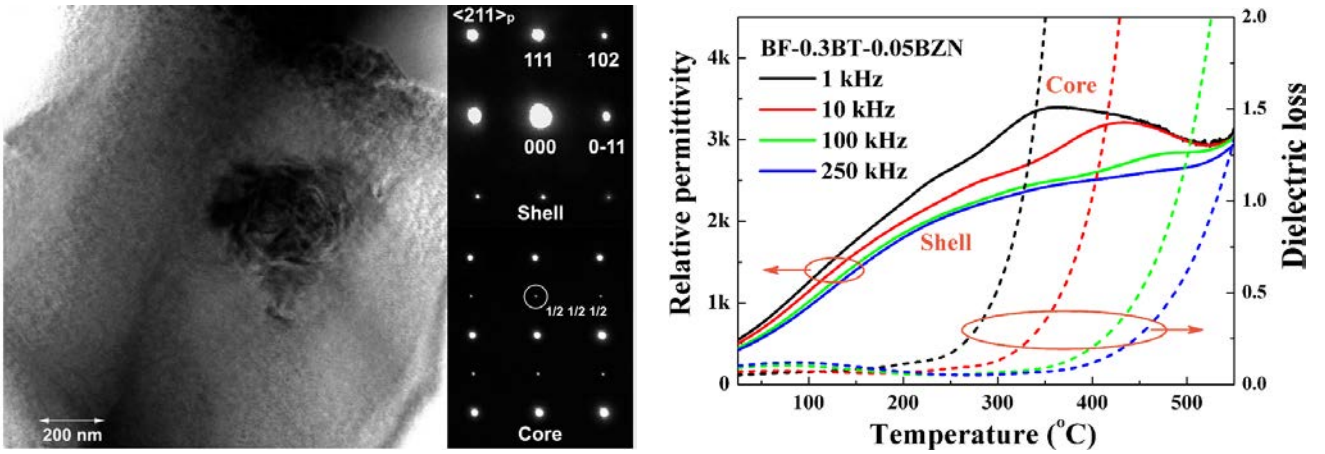

Fig. 14. (a) Bright field TEM image of a grain in $0.05Bi(Zn_{2/3}Nb_{1/3})O_3$ (BZN) doped BF-BT (BF-BT-0.05BZN), illustrating a Bi/Fe rich core and Ba/Ti rich shell; ⟨211⟩ zone axis diffraction patterns reveal the absence of $1/2\{ooo\}$ superstructure reflections in the shell (up) compared with core regions (down). (b) The $BiFeO_3$ and $BaTiO_3$ core-shell regions are tentatively ascribed to the high and low temperature dielectric anomalies.[58]

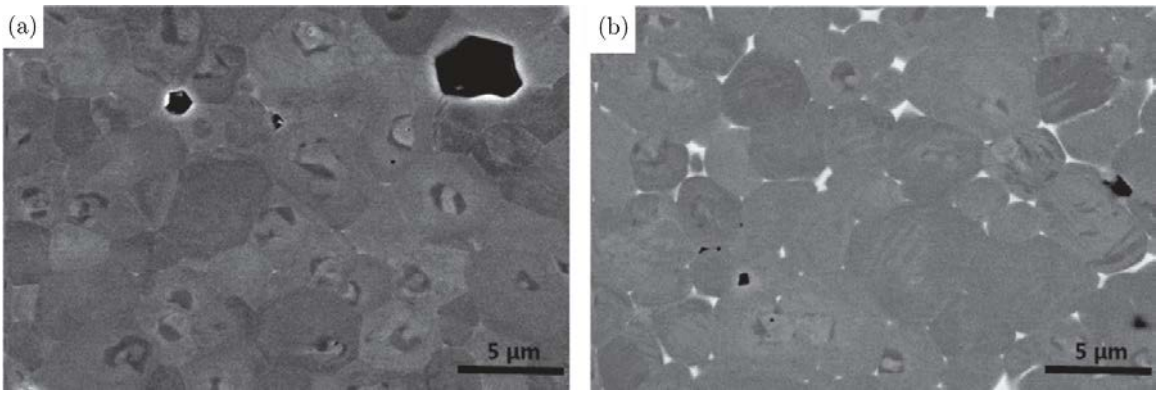

Fig. 15. BSE images of polished surface of (a) furnace cooled and (b) quenched $0.05Bi(Mg_{2/3}Nb_{1/3})O_3$ (BMN) doped BF-BT (0.75BF-0.25BT-0.05BMN) ceramics.[56]

quenching could effectively reduce inhomogeneity and increase polarization and strain, as shown in Figs. 15 and 16. They concluded that the major influence was the onset of immiscibility on cooling from the sintering temperature, driven by the electronegativity difference of the dopant species. Effectively, the more covalent the dopants are, the greater the tendency for immiscibility. Calisir *et al.*[64] studied La-doped BF-BT and they found that isovalent doping promoted solubility and led to a relatively homogeneous microstructure, while donor doping reduced solubility and caused chemical heterogeneity.

6. Piezoelectric Properties

6.1. *Dopant and piezoelectric properties*

One of the biggest concerns with $BiFeO_3$ containing systems is the high leakage current arising from either the loss of Bi or from the formation of Fe^{2+} as opposed to Fe^{3+} during sintering.[68–70] In each case, oxygen vacancies (V_O) are generated. To resolve these issues in BF-BT, excess Bi_2O_3 is added to compensate for volatilisation[71–73] and/or dopants[74–90] are used to accommodate changes in local defect chemistry associated with the multiple valence state of Fe. Dopants in the field of piezoelectric materials are classified into three groups: donor (higher valence), acceptor (lower valence) and self-compensated (average valence number remains the same). Donor dopants, such as Nb, Mn, are often reported to effectively increase the resistivity of BF-BT (Fig. 17).[74–79] And rare earth ions are reported to substitute on the A site of $BiFeO_3$ and improve d_{33} but there are conflicting reports as to whether they improve the resistivity/d_{33} of BF-BT ceramics.[80–83] However, a brief review of the literature suggests that the most successful dopants are stoichiometric or self-compensated (e.g., Cr, Co, Al, Ga, $Mg_{1/2}Ti_{1/2}$, $Zn_{1/2}Ti_{1/2}$ and $Ni_{1/2}Ti_{1/2}$).[84–90] Zhou *et al.*[84] reported that Al^{3+} promoted

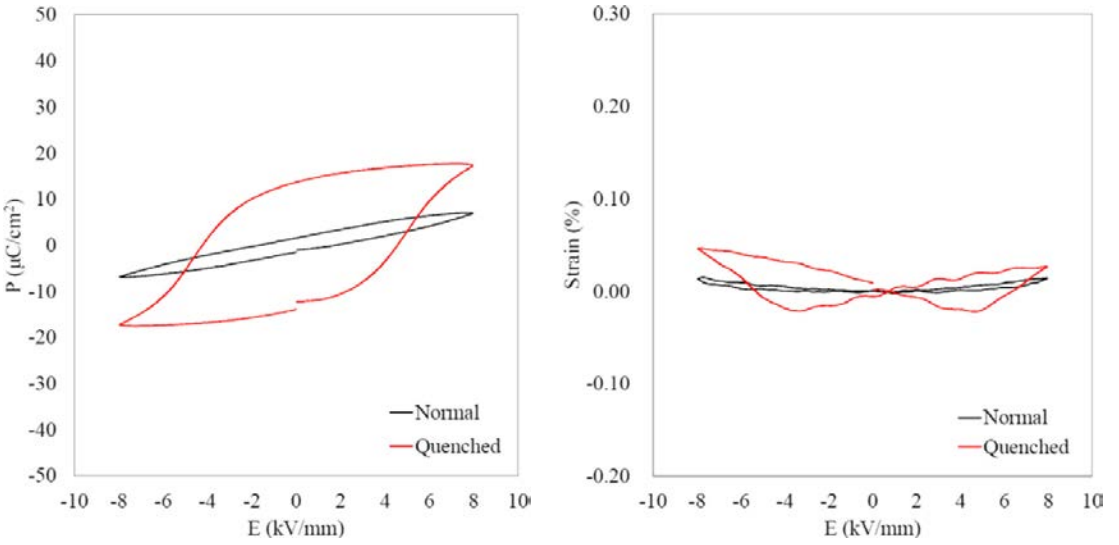

(a) (b)

Fig. 16. (a) *P-E* hysteresis loops and (b) bipolar *S-E* curves for furnace cooled and quenched 0.05Bi($Mg_{2/3}Nb_{1/3}$)O_3 (BMN) doped BF-BT (0.75BF-0.25BT-0.05BMN) ceramics.[56]

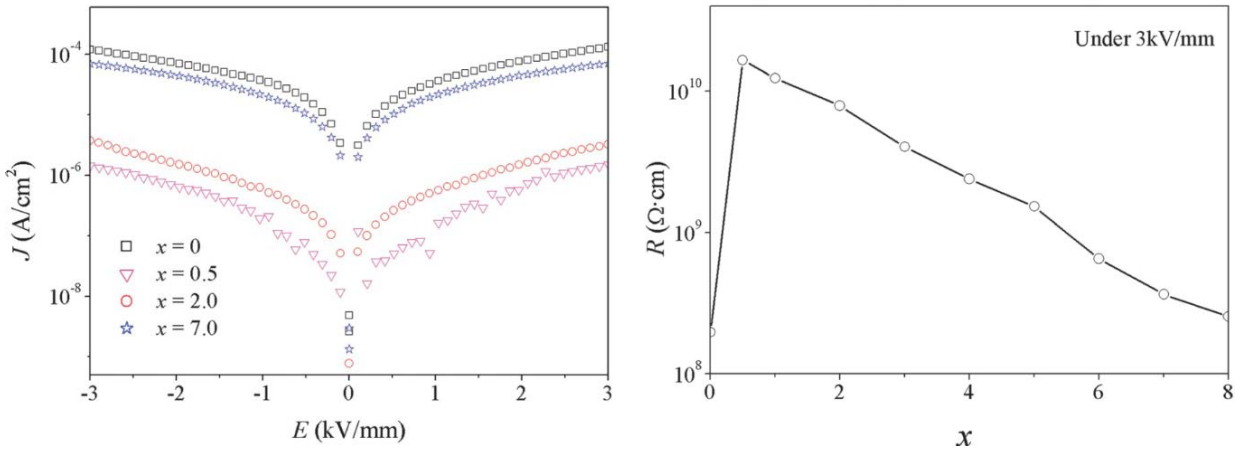

(a) (b)

Fig. 17. (a) Leakage current density J of $0.725BiFe_{0.96}Sc_{0.04}O_3$-$0.275BaTiO_3$ + x mol% MnO_2 (BFS-BT-xMn) ceramics at RT as a function of the electric field; (b) resistivity R of BFS-BT-xMn ceramics as a function of x under 3 kV/mm.[74]

the coexistence of R and O phases in $0.725BiFe_{1-x}Al_xO_3$-$0.275BaTiO_3$ + 1 mol% MnO_2 ceramics (BFAx-BT, Table 1) and improved d_{33} from 126 pC/N ($x = 0$) to 138 pC/N ($x = 0.01$). Zhou *et al.*[86] in a further study suggested that for $0.71BiFe_{1-x}(Ni_{1/2}Ti_{1/2})_xO_3$-$0.29BaTiO_3$ + 0.6 wt% MnO_2 ceramics (BFNTx-BT), $x = 0.03$ had the highest d_{33} = 156 pC/N and subsequently reported that $0.71BiFe_{1-x}Co_xO_3$-$0.29BaTiO_3$ + 0.6 wt% MnO_2 (BFCx-BT) with d_{33} = 167 pC/N[87] in which the grain size was largest, as shown in Fig. 18. Luo *et al.*[88] reported the piezoelectric properties for both A and B site doped BF-BT, (0.75-x)$BiFeO_3$-$0.25BaTiO_3$-xLa($Co_{0.5}Mn_{0.5}$)O_3 + 1 mol% MnO_2 ceramics (BF-BT-xLCM) in which they described a phase boundary consisting of R and O phases ($0.01 \le x \le 0.03$) with $d_{33} \sim$ 108 pC/N ($x = 0.02$), as shown in Fig. 19. As evidenced in the brief literature presented above, doped BF-BT ceramics exhibit coexistence of crystal structures (usually R and C), which are reputed to give rise to a large piezoelectric response but there are only Murakami *et al.*[57] have proposed crystallochemical trends to optimize dopants based on tolerance factor and electronegativity difference.

Quenching has been frequently used to improve the ferroelectric/piezoelectric properties of BF-BT based compositions, purportedly due to a reduction in the concentration of defects.[54,56,62,91–99] Lee *et al.*[54] reported a *R-T* MPB in quenched pure BF-BT and Ga/Bi($Zn_{0.5}Ti_{0.5}$)O_3 (BZT) doped

Table 1. Lattice parameters (a, b, c and V) and fitting parameters (R_{wp} and S) of the $0.725BiFe_{1-x}Al_xO_3$-$0.275BaTiO_3 + 1$ mol% MnO_2 ceramics (BFAx-BT) sintered at 970°C for 2 h.[84]

	Lattice parameters					R-factors (%)	
x	a (Å)	b (Å)	c (Å)	V (Å^3)	Weight (%)	R_{wp}	S
0	5.6456(6)	5.6456(6)	13.8615(4)	382.2023		8.11	1.73
0.01	5.6352(2)^R	5.6352(2)^R	13.8959(6)^R	382.157^R	80.68	8.17	1.81
	3.9869(5)^O	5.6570(1)^O	5.6404(7)^O	127.2169^O	19.31		
0.02	5.6368(2)^R	5.6368(2)^R	13.8726(8)^R	381.7328^R	75.63	7.6	1.43
	3.9949(5)^O	5.6395(8)^O	5.6568(2)^O	127.4476^O	24.36		
0.03	5.6338(6)^R	5.6338(6)^R	13.8844(9)^R	381.6566^R	45.35	9.1	1.58
	3.9791(8)^O	5.6465(8)^O	5.6594(8)^O	127.1619^O	54.64		
0.04	3.9919(5)	5.6475(3)	5.6440(6)	127.2437		8.2	1.74
0.05	3.9934(5)	5.6435(5)	5.6421(2)	127.1583		8.12	1.74
0.06	3.9954(5)	5.6465(3)	5.6350(4)	127.1292		8.8	1.74
0.07	3.9985(3)	5.6340(6)	5.6447(6)	127.1652		9.6	1.54
0.08	3.9980(4)	5.6393(5)	5.6407(9)	127.1794		9.2	1.61

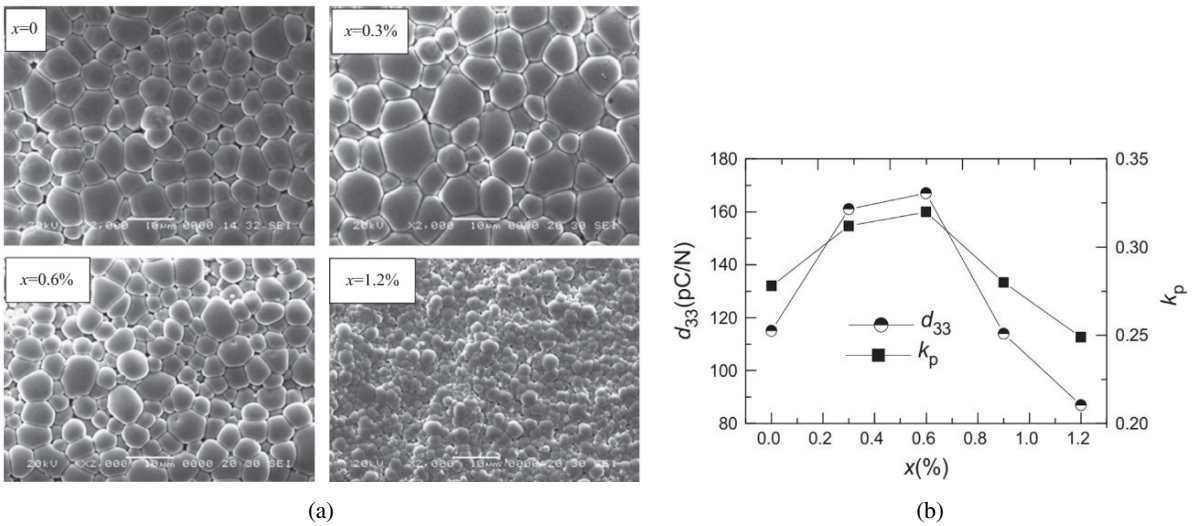

(a) (b)

Fig. 18. (a) SEM images and (b) d_{33} and planar electromechanical coupling factor k_p of $0.71BiFe_{1-x}Co_xO_3$-$0.29BaTiO_3 + 0.6$ wt% MnO_2 (BFCx-BT) ceramics.[87]

BF-BT with the highest d_{33} values (240–402 pC/N) (Fig. 20) to date. So far these results have not been reproduced by other researchers and typically much smaller values of d_{33} are reported, e.g., 160–200 pC/N by Zheng *et al.*,[91–97] Fig. 21. Kim *et al.*[62] found the cooling rate during quenching had a significant effect on phase transitions and ferroelectric/piezoelectric properties for BF-BT, as shown in Fig. 22. Wada *et al.*[98,99] studied the effect of annealing and quenching on the crystal structure and properties for BF-BT and they ascribed the enhancement of ferroelectric/piezoelectric properties to the domain wall de-pinning and the relaxation of lattice strain induced in the samples after heat treatment (Fig. 23). Quenched samples are thus reported to have useful values of d_{33} coupled with a high T_C. Although it is feasible that sensors could be fabricated from quenched compositions, it is highly unlikely that high strain monolithic actuators or bimorphs can be fabricated in this manner. Moreover, the formation of reliable multilayer actuators (MLAs) is difficult to rationalize given the differential thermal expansion between the electrode and ceramic layers.

6.2. *Compositions with high effective d^*_{33}*

In addition to d_{33}, large electric-field induced stain (S) and d^*_{33} and low strain hysteresis (SH) are important for actuator applications. Typical, field-induced bipolar and unipolar strain (S-E) curves of ferroelectrics are given in Fig. 24. Electric-field-induced positive strain (S_{pos}), negative strain (S_{neg}) and peak to peak strain ($S_{p\text{-}p}$) are obtained from the butterfly-shaped bipolar S-E loops (Fig. 24(a)). Generally,

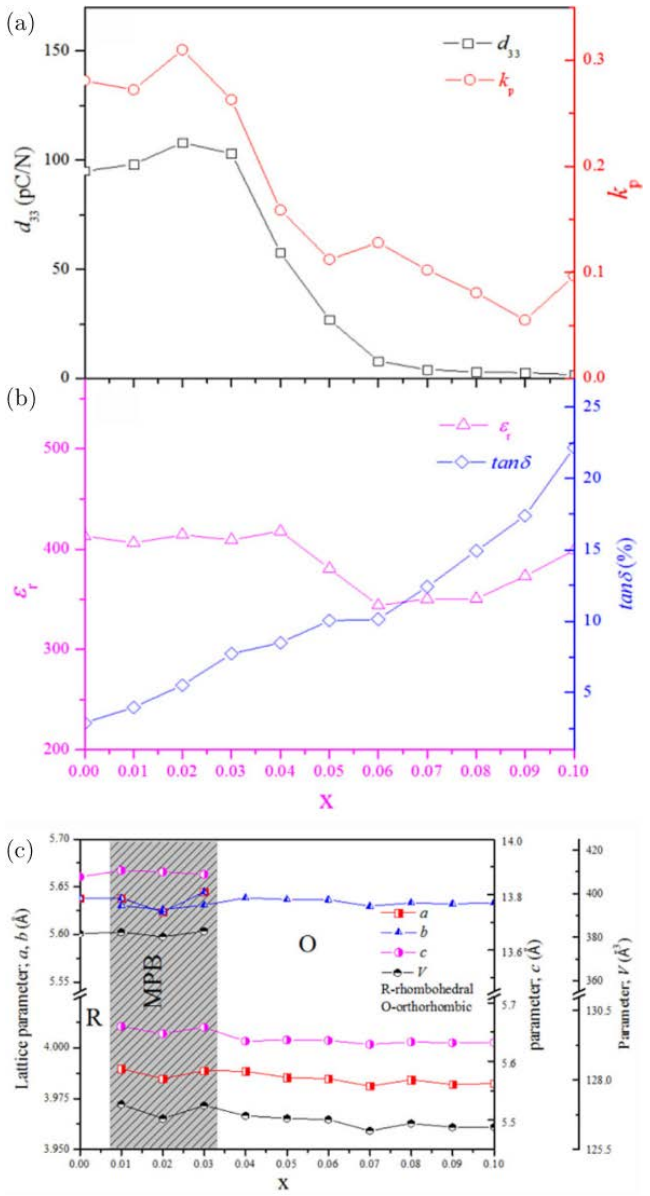

Fig. 19. Variations of (a) d_{33} and k_p, (b) ε_r and $\tan\delta$; (c) Lattice parameters a, b, c, and V of (0.75-x)$BiFeO_3$-0.25$BaTiO_3$-xLa$(Co_{0.5}Mn_{0.5})O_3$ + 1 mol% MnO_2 (BF-BT-xLCM) ceramics as a function of x.[88]

d^*_{33} and SH are calculated by

$$d^*_{33} = S_{\max}/E_{\max}, \quad (1)$$

$$\mathrm{SH} = H_{E\max/2}/S_{\max}, \quad (2)$$

where $S_{\max}$, $E_{\max}$ and $H_{E\max/2}$ is the average electric-field-induced maximum strain obtained from the unipolar S-E loops, the maximum electric field and the width of the loop at half the applied field, respectively, as shown in Fig. 24(b).

Undoped BF-BT at the R to C phase boundary have a value of d^*_{33} below 100 pm/V, mainly due to their high conductivity.[53] Leontsevw *et al.*[53] found Mn improved the DC resistivity by $1 \sim 5$ orders of magnitude and increased

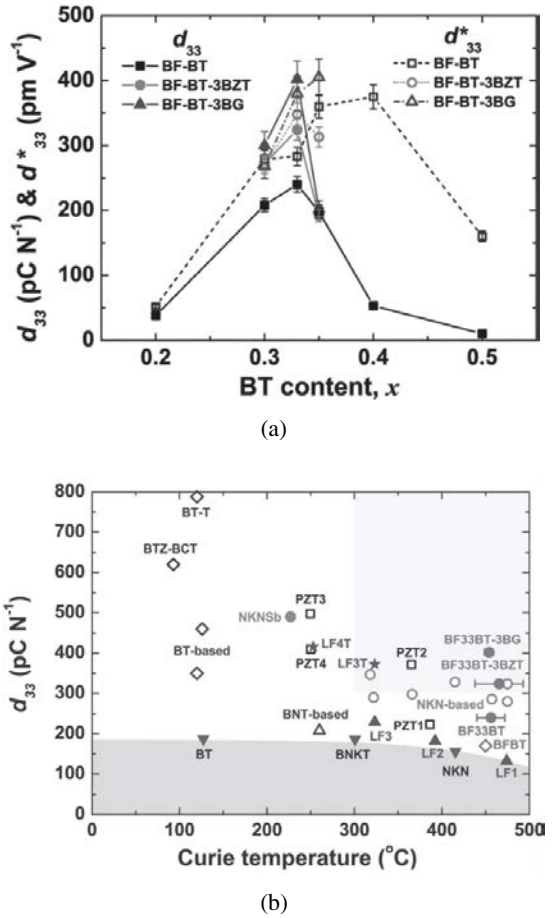

Fig. 20. (a) d_{33} (filled symbols) and d^*_{33} (empty symbols) values of the BF-BT, BF-BT-3BZT, and BF-BT-3BG ceramics as functions of BT content. (b) Comparison of d_{33} among other lead-free piezoelectrics and PZT family.[54]

d^*_{33} up to 331 pm/V with $S_{\max} = 0.166\%$ (Table 2). Wang *et al.*[58,61,83] doped Nd and BZN into BF-BT and obtained $S_{\text{pos}} \sim 0.463\%$ and $d^*_{33} \sim 424$ pm/V with SH of 37% for 0.5%BZN doped BF-BT (Fig. 25). The origin of the large strain was ascribed to a field-induced transition from short- to long-range dipolar order at the crossover from normal to a relaxor ferroelectric behavior. High $S_{\max}$ of 0.4% with large $d^*_{33} \sim 544$ pm/V was achieved in BMN doped BF-BT by Murakami *et al.*,[56] as shown in Fig. 26, who also suggested that $S_{\max}$ and d^*_{33} was optimized at the point of crossover from relaxor to ferroelectric which facilitates a macroscopic field induced transition to a ferroelectric state. The same authors fabricated a prototype MLA based on the composition 0.63BF-0.32BT-0.05BMN,[56] which gave a displacement of $\sim 1.5\,\mu$m at 7 kV/mm, as shown in Fig. 27. Importantly, the high strains reported by Murakami *et al.*[56–58] were achieved in ceramics and MLAs that were furnace cooled and hence might be considered more promising for commercial applications.

In contrast to Murakami *et al.* quenched BF-BT and Ga/BZT doped BF-BT were reported with high values of

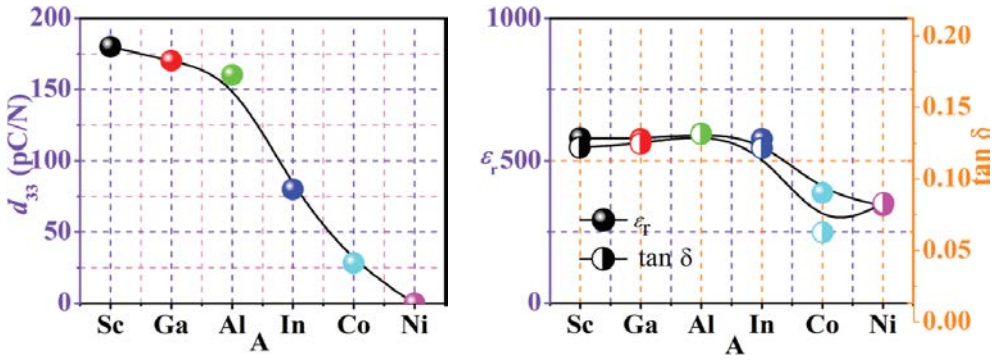

(a) (b)

Fig. 21. (a) d_{33}, (b) ε_r and $\tan\delta$; of $0.70Bi_{1.05}Fe_{0.97}A_{0.03}O_3$-$0.30BaTiO_3$ (BFA-BT, A: Sc, Ga, Al, In, Ni, Co) ceramics with different elements, A.[91]

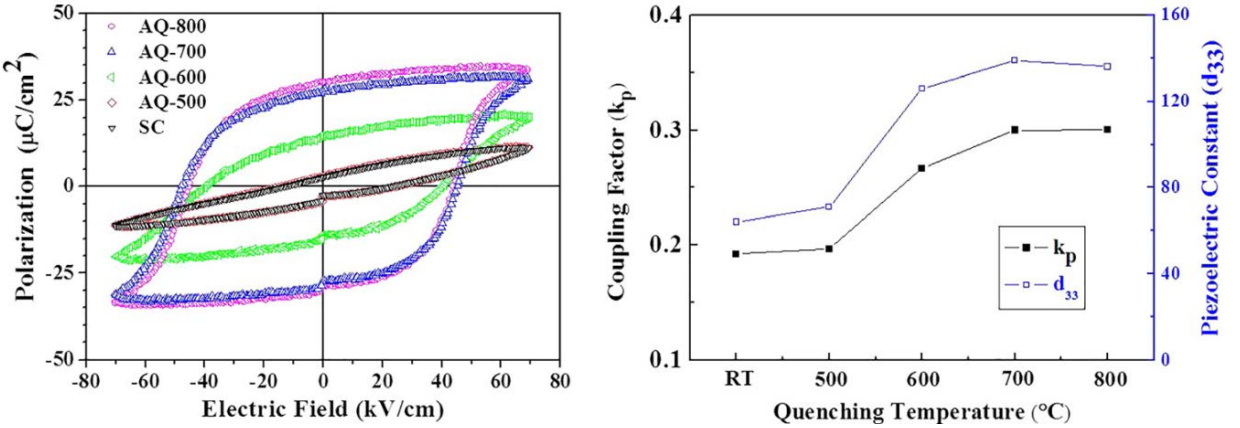

(a) (b)

Fig. 22. (a) *P-E* hysteresis loops and (b) d_{33} and k_p of the slowly cooled sample (SC) and air-quenched $0.75BiFeO_3$-$0.25BaTiO_3$ samples from 800, 700, 600, and 500°C (AQ-800, AQ-700, AQ-600, and AQ-500).[62]

$d^*_{33} = 375 \sim 410$ pm/V with S_{max} of $0.15 \sim 0.225\%$ by Lee *et al.* (Fig. 20),[54] but these authors attributed the large electromechanical response to coexisting *R* and *T* phases at MPB. Ryu *et al.*[96,97] prepared BZT and LN doped BF-BT by quenching process and high d^*_{33} of 600 pm/V was obtained at 30 kV/cm with SH of 38% (Fig. 28). These authors believed the high strain mainly came from the enhancement of domain wall density and mobility under the applied electric field. However, Wada *et al.*[100,101] investigated the effect of electric field on the phase structure and piezoelectric response for both pure BF-BT and $Bi(Mg_{1/2}Ti_{1/2})O_3$ (BMT) doped BF-BT by *in-situ* synchrotron radiation X-ray diffraction (SR-XRD). No peak splitting was observed in the diffraction peaks (Fig. 29) and they concluded that there was no electric-field-induced phase transition either in BF-BT nor BMT doped BF-BT ceramics.

Table 3 summaries results of BF-BT ceramics with the composition, the dopant, the sintering method, the piezoelectric properties and the T_C/the maximum dielectric permittivity (T_m) optimized. Optimized compositions fluctuate from 0.67BF-0.33BT to 0.75BF-0.25BT and d_{33} varies from 100 to 200 pC/N. The highest d_{33} reported to date is 402 pC/N for quenched 3 mol% Ga-doped 0.67BF-0.33BT but in this context appears anomalously high. d^*_{33} values are in the range of $128 \sim 600$ pm/V and consistently higher than d_{33}. d^*_{33} appears reproducible in so much as large value of strain can be routinely achieved, albeit at high fields (> 5 kV/cm). Given the complexity of the phase assemblage, microstructure and structure in the BF-BT system, a generalized overview of the crystal chemistry is difficult. However, the low d_{33} versus high d^*_{33} suggests that electrostriction dominates over piezoelectric behavior. The low d_{33} and absence of a *T* phase of similar free energy to *R* (*C* coexists with R phases according to most authors) also points to nonclassic MPB behavior. A more rational explanation of the dominant electrostrictive behavior is the growth of a long-range ferroelectric phase from relaxor-like nano-domains. The absence of *T* phase in the vicinity of optimized composition, suggests

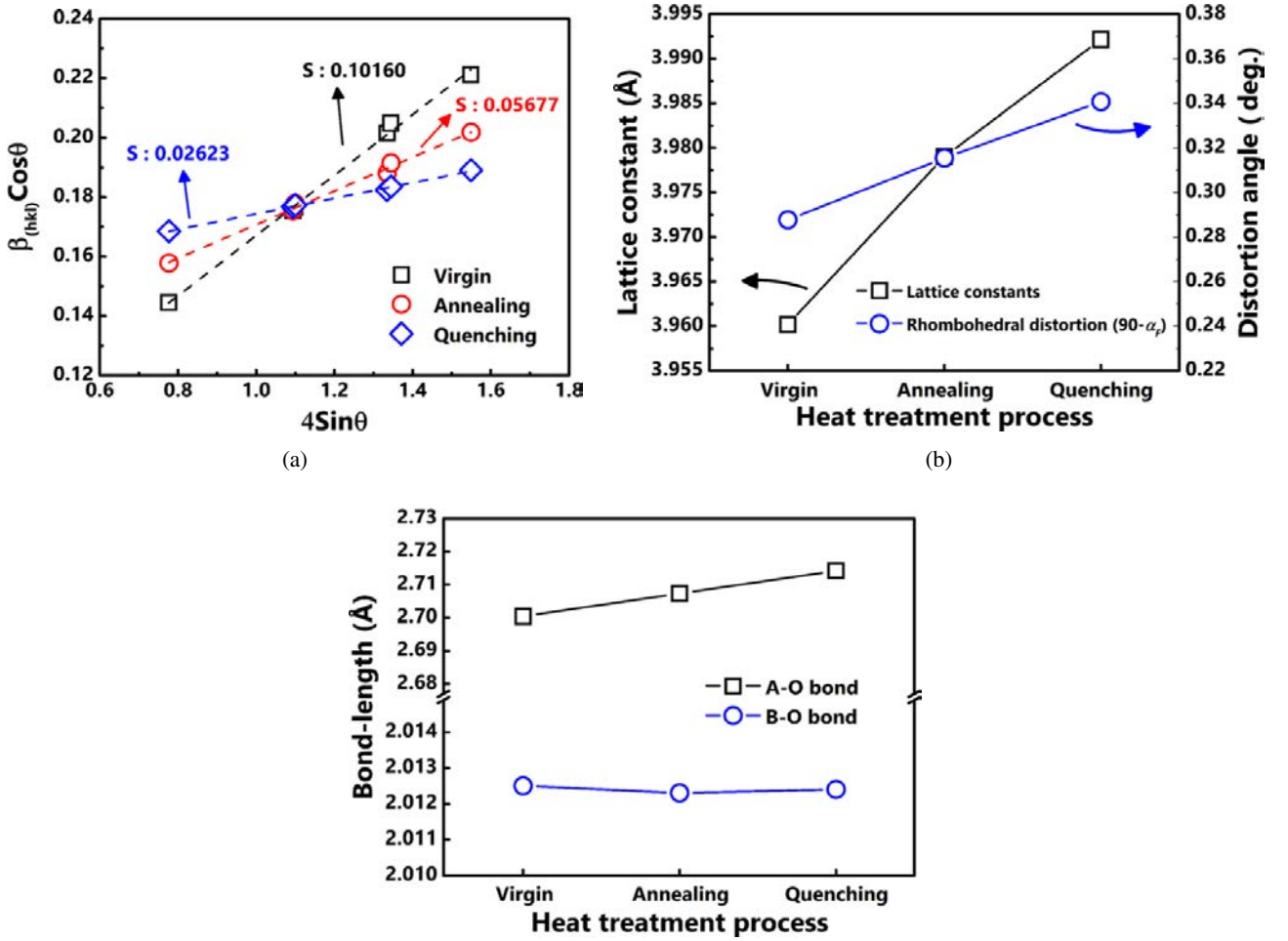

Fig. 23. Structural properties of BF-0.2BT$_V$, BF-0.2BT$_A$, and BF-0.2BT$_Q$. (a) Williamson Hall analysis; (b) Lattice constants and rhombohedral distortion (90-a_F); (c) A-O and B-O bond-length.[99]

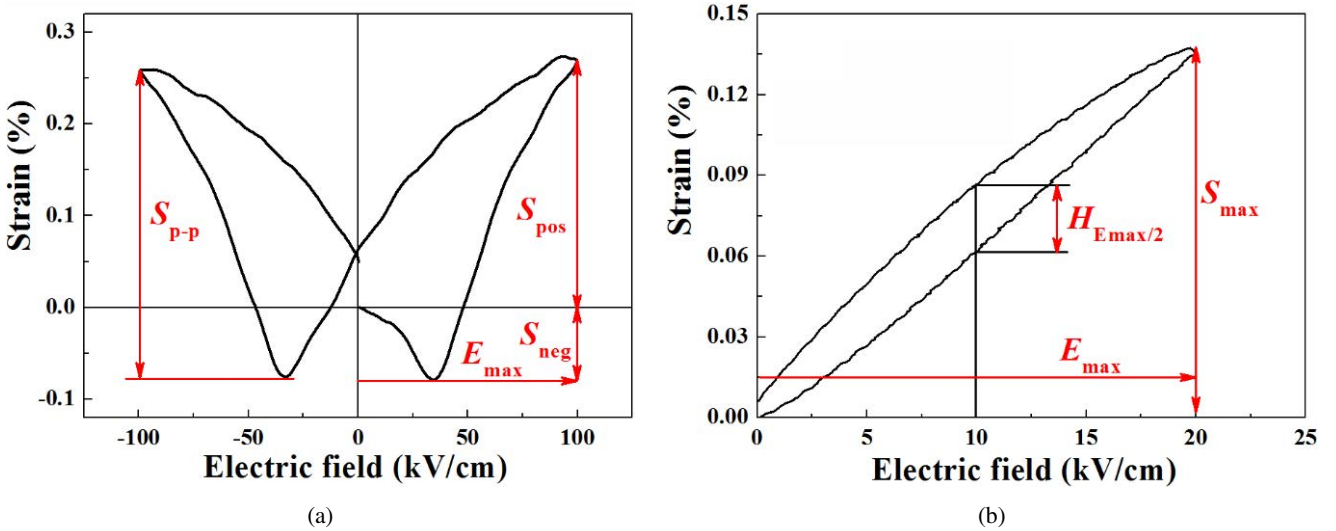

Fig. 24. The schematic figure of the field-induced (a) bipolar and (b) unipolar *S-E* curves of ferroelectrics.

Table 2. RT dielectric constant and loss values (measured at 1 kHz), Curie temperature (T_C) and depolarization temperatures (T_d), piezoelectric coefficient (d_{33}) and inverse piezoelectric coefficient (d^*_{33}), remnant polarization (P_r), and coercive field (E_C) for undoped and Mn-doped BF-xBT and other lead-free piezoelectric materials.[53]

Material	Dielectric constant	Loss	$T_C(R_d)$, °C	d_{33}, pC/N low (high) field	P_r, μC/cm^2	E_c, kV/cm	References
BF-xBT, Mn-doped							
$x = 0.15$	198	0.012	685				
$x = 0.25$	557	0.046	619 (469)	116 (142)	22.9	39.3	
$x = 0.31$	704	0.067	598 (430)	82 (331)	18.8	22.9	
$x = 0.33$	750	0.068	605 (430)	70 (327)	15.2	20.7	
$x = 0.35$	778	0.077	580 (403)	43 (306)	13.2	17.5	
BF-xBT, undoped							
$x = 0.15$	242	0.022	700				
$x = 0.25$	605	0.068	574	47 (128)			
$x = 0.33$	795	0.098	605 (420)	33 (151)			
$BaTiO_3$	1700	0.01	115	190			19
$BiFeO_3$ thin films	180	0.1	810	70			1 and 20
KNN	290	0.04	420 (195)	80			21
NBT-KBT–BT	730	0.02	290 (162)	173			22
PZT 5A	1700	0.002	365	400 (630)			23

Note: KNN $(K_{0.5}Na_{0.5})NbO_3$: NBT, $(Na_{0.5}Bi_{0.5})TiO_3$: KBT, $(K_{0.5}Bi_{0.5})TiO_3$; BT, $BaTiO_3$.

that the ferroelectric phase is most likely *R* and thus peak splitting is difficult to observe in *in-situ* studies.[100,101] This model however, requires further verification through *in-situ* studies that focus on determining the structure of the field induced state. Structural refinements however, are complicated by the core-shell microstructure often reported in undoped and doped compositions, and we recommend that future investigations are carried out on chemically homogeneous samples (by BSE images) such as those described by Murakami *et al.*[56,57]

A comparison of d_{33} versus T_C/T_m, d^*_{33} versus T_C/T_m and S_{max} versus d^*_{33} for lead-based and lead-free piezoelectric ceramics is plotted in Fig. 30.[10–138] Generally, the values of d_{33}/d^*_{33} decrease with the increase of T_C/T_m, but lead-based ceramics still exhibit larger d_{33}/d^*_{33} values compared to lead-free ceramics (Figs. 30(a) and 30(b)). In addition, some doped BF-BT ceramics exhibit high values of $S_{max} > 0.4\%$ amongst ferroelectric ceramics (Fig. 30(c)), with $d^*_{33} > 400$ pm/V and SH $< 40\%$.

7. Energy Storage Property

Dielectric capacitors are attractive for high-voltage pulse power application due to their high energy density and fast charge-discharge rate[139–142] with linear dielectrics (LD), antiferroelectrics (AFE) and relaxor-ferroelectrics (RFE) all considered excellent candidates. Energy density (W) for LD

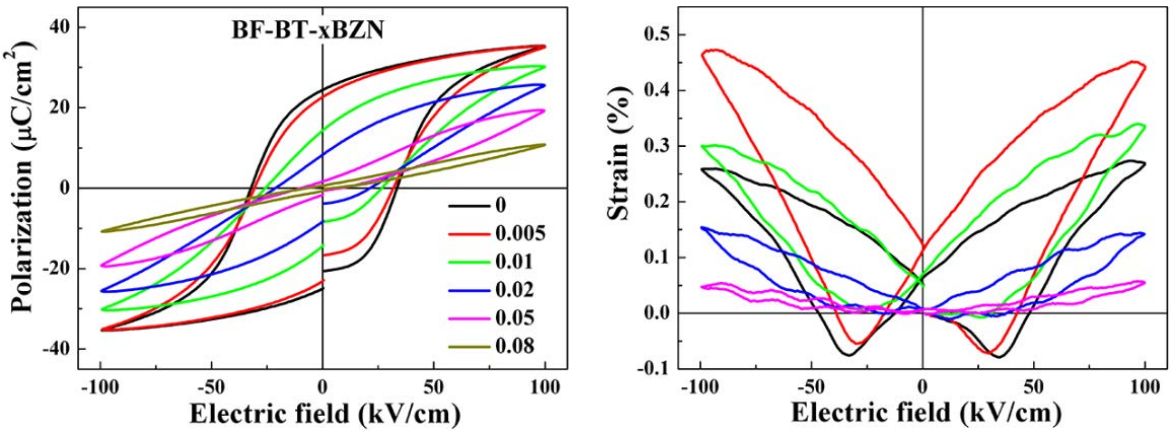

(a) (b)

Fig. 25. High electric field (a) bipolar *P-E*, (b) bipolar *S-E* and (c) unipolar *S-E* loops of $Bi(Zn_{2/3}Nb_{1/3})O_3$ (BZN) doped BF-BT (BF-BT-xBZN) samples at 100 kV/cm. (d) P_r and E_C as a function of BZN concentration. (e) S_{pos} and S_{neg} as a function of BZN concentration. (f) d^*_{33} and SH as a function of BZN concentration. d_{33} as a function of BZN concentration is in the inset of (d).[58]

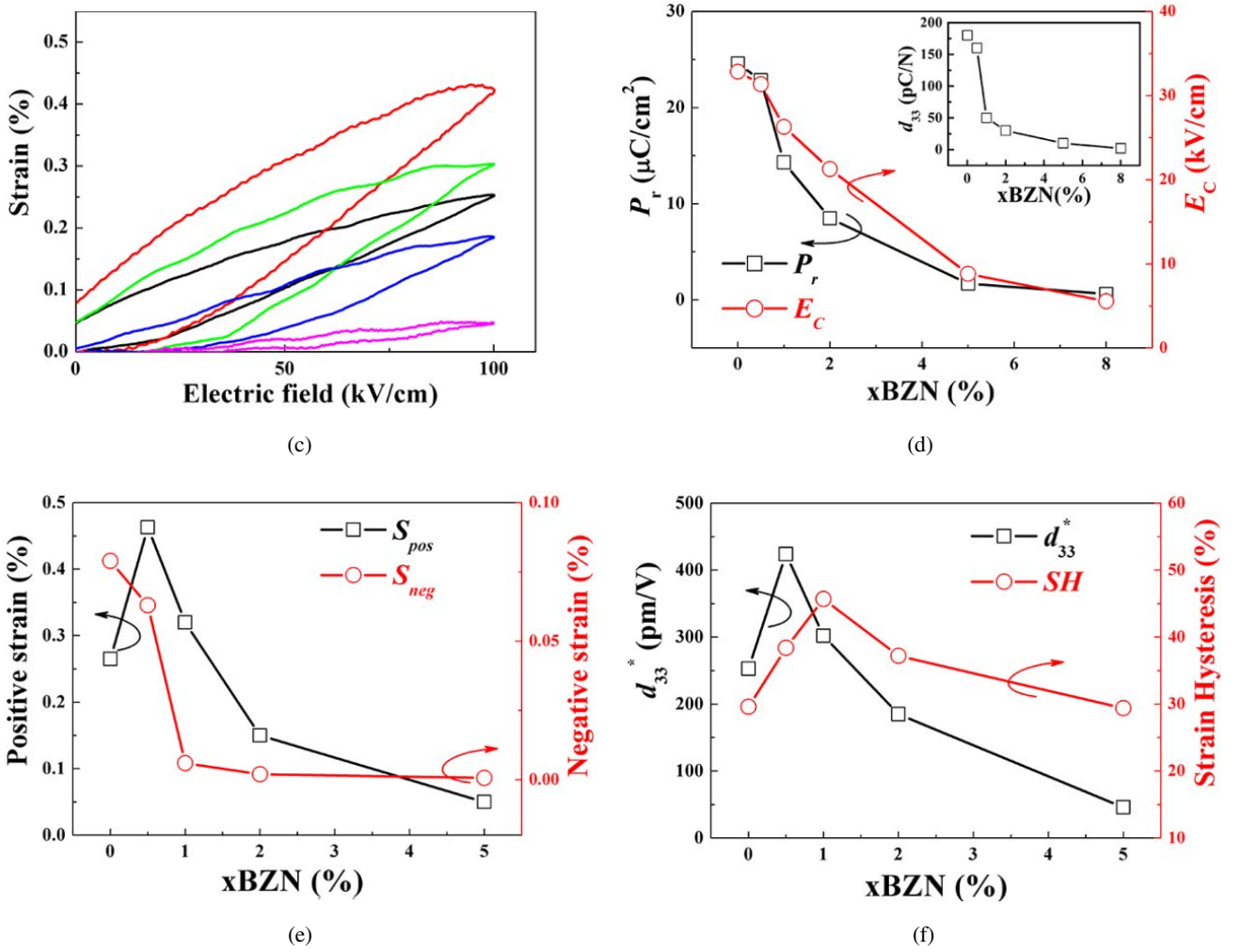

Fig. 25. (*Continued*)

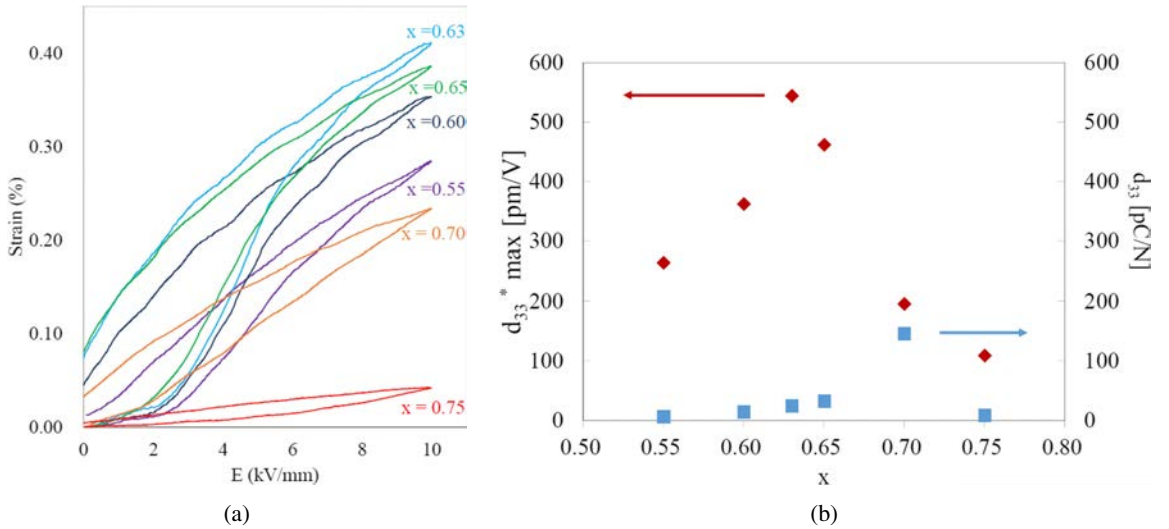

Fig. 26. (a) Unipolar *S-E* curves; (b) d_{33} and d_{33}^* of unpoled $Bi(Mg_{2/3}Nb_{1/3})O_3$ (BMN) doped BF-BT (BT-*x*BF-BMN, $x = 0.55$, 0.60, 0.63, 0.65, 0.70, and 0.75) ceramics.[56]

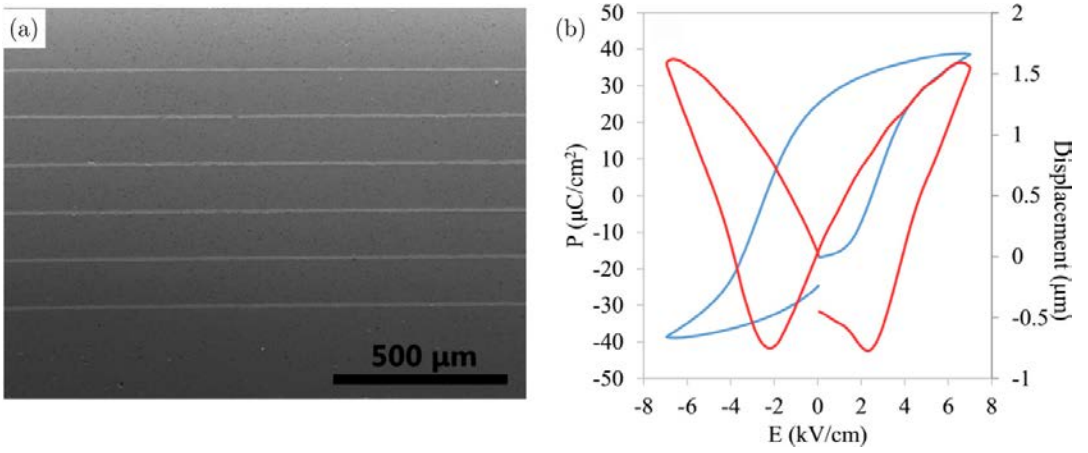

Fig. 27. (a) Cross-sectional SEM image of a $Bi(Mg_{2/3}Nb_{1/3})O_3$ (BMN) doped BF-BT (0.63BF-0.32BT-0.05BMN) multilayer actuator; (b) *P-E* loop and displacement-electric field (*D-E*) curve.[56]

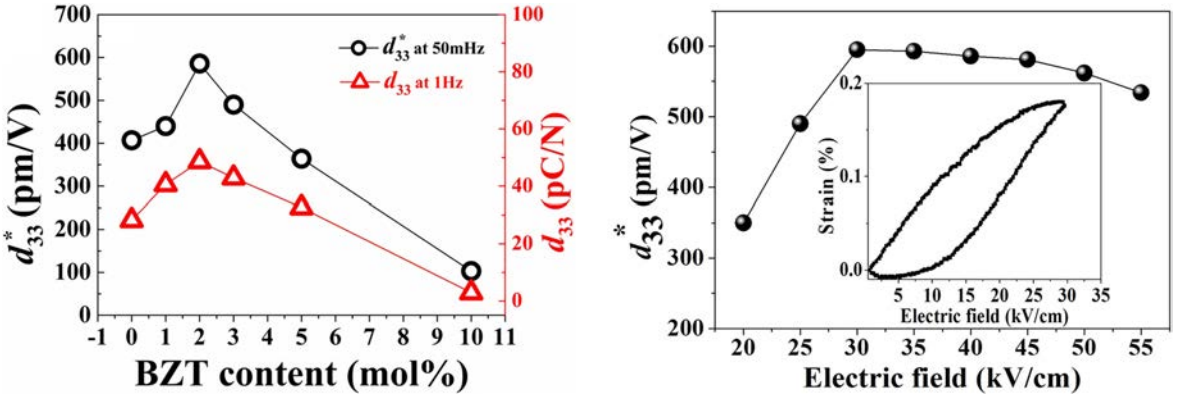

(a) (b)

Fig. 28. Piezoelectric response of $Bi(Zn_{1/2}Ti_{1/2})O_3$ (BZT)-modified BF-BT (BF-BT-*x*BZT) ceramics (a) d_{33} and d_{33}^* under 30 kV/cm; (b) d_{33}^* of BF-BT-0.02BZT ceramics as a function of different applied fields. Inset shows field-induced strain at 30 kV/cm.[96]

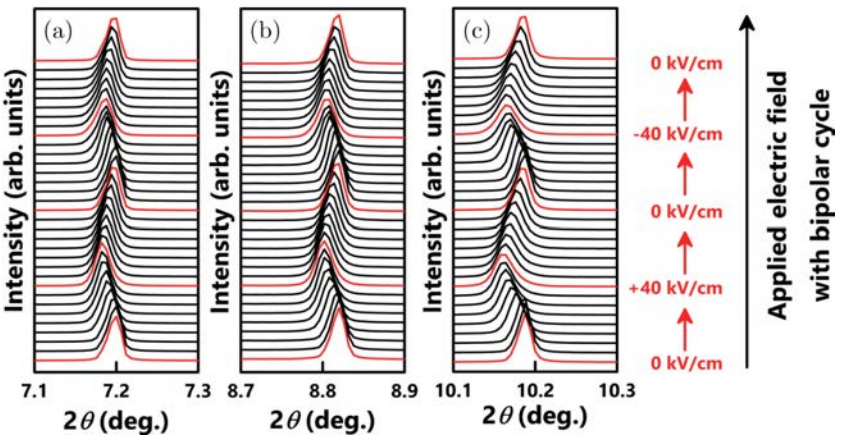

Fig. 29. The *in-situ* synchrotron radiation X-ray diffraction (SR-XRD) patterns of 0.67BF-0.33BT ceramics under the electric field with selected 2θ angles (a) from 7.1°–7.3° for (110), (b) from 8.7°–8.9° for (111), and (c) from 10.1°–10.3° for (200), respectively.[101]

is calculated using Eq. (3):

$$W = 1/2DE = 1/2\varepsilon_0\varepsilon_r E^2, \quad (3)$$

where D is the electrical displacement, E is the electric field, ε_0 and ε_r are the permittivity of free space and relative permittivity, respectively. Large values of W are obtained with both high ε_r and E for LD. For nonlinear dielectrics, the P-E loop is commonly used to calculate energy storage performance, as shown schematically in Fig. 31. The total energy density (W), recoverable energy density (W_{rec}) and energy conversion efficiency (η) are:

$$W = \int_0^{P_{max}} EdP, \quad (4)$$

$$W_{rec} = \int_{P_r}^{P_{max}} EdP, \quad (5)$$

$$\eta = W_{rec}/W \quad (6)$$

To obtain high W_{rec} and η, high P_{max}, low P_r and high breakdown strength (E_{BDS}) are essential. AFE and RFE are anticipated to display optimum W_{rec} and η since both exhibit high ΔP ($P_{max} - P_r$) and E_{BDS} values. Undoped BF-BT is a FE with high P_r and hysteresis but low ΔP and E_{BDS} and thus not suitable for energy storage. To decrease P_r/hysteresis and increase $\Delta P/E_{BDS}$, dopants may be substituted into the BF-BT solid solution in a deliberate attempt to force the phase transition from ferroelectric to relaxor.

7.1. *A or B site doping*

Slim P-E loops were observed by Calisir *et al.*[64] in $0.75BiFeO_3$-$0.25(Ba_{0.99}La_{0.01})TiO_3$ (BF-BLT) ceramics, exhibiting high $P_{max} \sim 0.15\,C/m^2$ and low $P_r \sim 0.04\,C/m^2$ with $W_{rec} \sim 0.61\,J/cm^3$ (Fig. 32). Double switching peaks were observed in J-E loop (Fig. 32(a)), indicating a reversible switching between an ergodic-relaxor (ER) and metastable

Table 3. Summary of the piezoelectric properties for BF-BT ceramics reported (BMN = $Bi(Mg_{2/3}Nb_{1/3})O_3$, LCM = $La(Co_{0.5}Mn_{0.5})O_3$, BZN = $Bi(Zn_{2/3}Nb_{1/3})O_3$, LN = $LiNbO_3$, BZT = $Bi(Zn_{1/2}Ti_{1/2})O_3$, BMT = $Bi(Mg_{1/2}Ti_{1/2})O_3$, BKT = $Bi_{0.5}K_{0.5}TiO_3$, BNT = $Bi_{0.5}Na_{0.5}TiO_3$).

Composition	Sintering method	d_{33} (pC/N)	d^*_{33} (pm/V)	S_{max} (%)	T_C/T_m (°C)	Ref.
0.75BF-0.25BT	Furnace cooled	47	128	0.064	574	53
0.67BF-0.33BT	Furnace cooled	33	151	0.0755	605	53
0.75BF-0.25BT + Mn	Furnace cooled	116	142	0.071	619	53
0.67BF-0.31BT + Mn	Furnace cooled	82	331	0.1655	598	53
0.67BF-0.33BT + Mn	Furnace cooled	70	327	0.1635	605	53
0.67BF-0.35BT + Mn	Furnace cooled	43	306	0.153	580	53
0.75BF-0.25BT + Mn	Furnace cooled	120	127	0.089	522	61
$0.75B_{0.975}Nd_{0.025}$F-0.25BT + Mn	Furnace cooled	140	144	0.101	490	61
$0.75B_{0.95}Nd_{0.05}$F-0.25BT + Mn	Furnace cooled	120	200	0.14	379	61
0.7BF-0.3BT + Mn	Furnace cooled	190	240	0.144	478	83
$0.7B_{0.98}Nd_{0.02}$F-0.3BT + Mn	Furnace cooled	50	333	0.2	390	83
$0.725BF_{0.96}Sc_{0.04}$-0.275BT + Mn	Furnace cooled	143	/	/	596	74
$0.71B_{0.98}La_{0.02}$F–0.29BT + Mn	Furnace cooled	168	/	/	400	80
0.7BF-0.25BT-0.05$BiScO_3$	Furnace cooled	145	465	0.233	400	57
$0.72BF_{0.99}Al_{0.01}$-0.28BT	Furnace cooled	151	/	/	450	84
0.73BF-0.25BT-0.02LCM + Mn	Furnace cooled	108	/	/	523	88
$0.71BF_{0.94}Co_{0.06}$-0.29BT + Mn	Furnace cooled	167	/	/	488	87
0.65BF-0.3BT-0.05BZT + Mn	Furnace cooled	139	/	/	523	89
0.695BF-0.3BT-0.005BZN + Mn	Furnace cooled	160	424	0.463	480	58
$0.71BF_{0.97}(Ni_{1/2}Ti_{1/2})_{0.03}$-0.29BT	Furnace cooled	156	/	/	431	86
0.725BF-0.25BT-0.025BKT + Mn	Furnace cooled	135	/	/	708/544	65
$B_{1.02}F_{0.96}Mg_{0.02}Ti_{0.02}$-0.3BT	Furnace cooled	198	/	/	497	73
0.7BF-0.25BT-0.05BMN	Furnace cooled	148	410	0.41	450	56
0.63BF-0.32BT-0.05BMN	Furnace cooled	20	544	0.272	380	56
0.715BF-0.275BT-0.01BNT + Mn	Furnace cooled	140	/	/	560	90
0.6BF-0.3BT-0.01BMT + Mn	Furnace cooled	94	189	0.0945	470	98
$0.7B_{1.05}$F-0.3BT	Quenched	180	/	/	506	71
$0.7B_{1.05}F_{0.97}Sc_{0.03}$-0.3BT	Quenched	180	/	/	500	91
0.7BF-0.3BT + 1 mol%Bi_2O_3	Quenched	200	333	0.1	500	92
0.7BF-0.3BT + 0.5 mol%CuO	Quenched	165	449	0.2694	503	94
0.71BF-0.29BT + 0.3 mol%MnO_2	Quenched	191	/	/	530	95
0.60BF-0.40BT-0.02BZT	Quenched	50	600	0.18	350	93
0.99(0.67BF-0.33BT)-0.01LN	Quenched	146	500	0.175	390	97
0.69B1.05F-0.28BT-0.03BZT	Quenched	195	200	0.13	505	96
0.67BF-0.33BT	Quenched	240	270	0.15	456	54
$0.64B_{1.05}$F-0.33T-0.03BZN	Quenched	324	345	0.19	466	54
$0.67B_{1.05}F_{0.97}Ga_{0.03}$-0.33T	Quenched	402	410	0.225	454	54

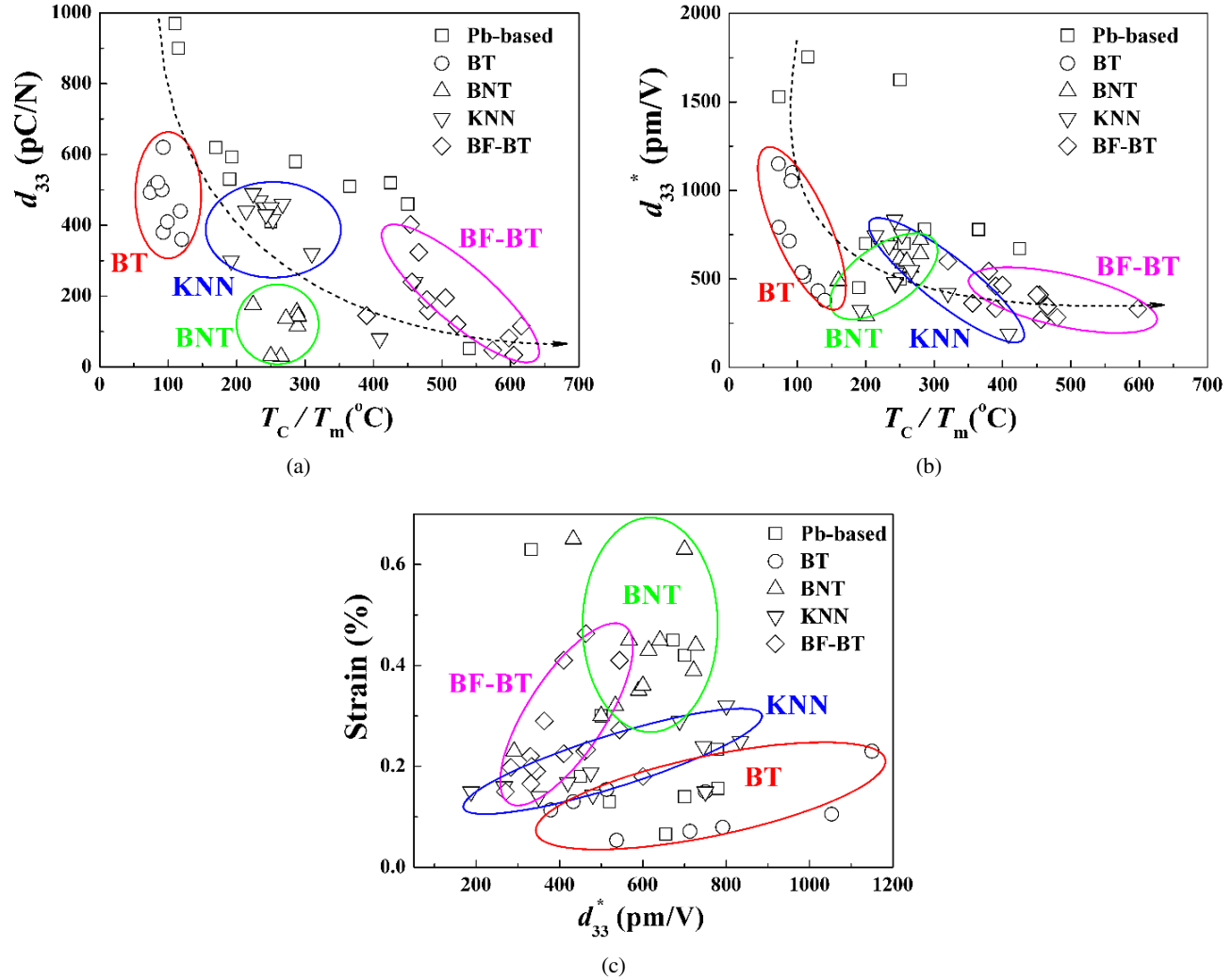

Fig. 30. A comparison of (a) d_{33} versus T_C/T_m, (b) d^*_{33} versus T_C/T_m and (c) S_{max} versus d^*_{33} for ceramics.[10–138]

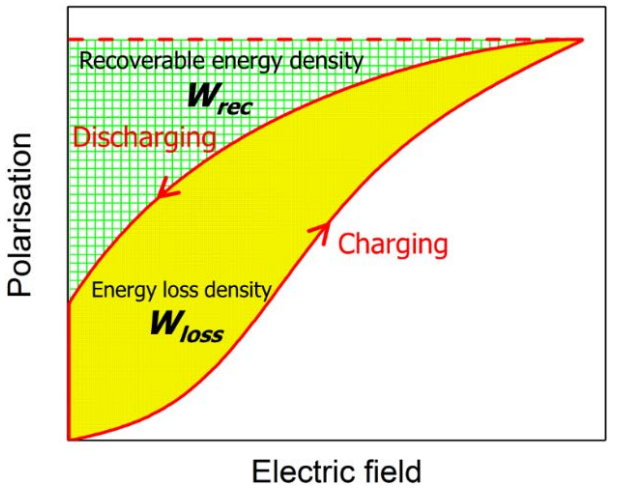

Fig. 31. Schematic diagram of the calculation of energy storage properties of nonlinear dielectrics.

FE states. Wang *et al.*[61] reported slim *P-E* loops, enhanced E_{BDS} and high ΔP in Nd doped BF-BT (Figs. 33 and 34), which they attributed to a phase transition to a RFE phase, enhanced density and reduced grain size, as shown in Fig. 35. High $W_{rec} \sim 1.82\,J\,cm^{-3}$ and $\eta \sim 87.8\%$ were obtained for 15% and 40% Nd-doped 0.7BF-0.3BT (BN15F-BT and BF40F-BT), respectively, Fig. 36. Multilayers (MLs) of BN15F-BT were fabricated with an exceptional high value of $W_{rec} \sim 6.74\,J\,cm^{-3}$ with $\eta \sim 77\%$ obtained under an electric field of 540 kV/cm, which exhibited good temperature stability $< 15\%$ up to 125°C, Fig. 37.[61] Beside lanthanide doping on the A site, Nb^{5+} on the B-site was substituted in 0.65BF-0.35BT which resulted in P_r to $\sim 5\,\mu C/cm^2$ but a less impressive $W_{rec} \sim 0.71\,J/cm^3$.[143]

7.2. *ABO_3 substitutions*

Other than utilizing direct A or B site doping, the formation of ternary solid solutions by the addition of a third ABO_3

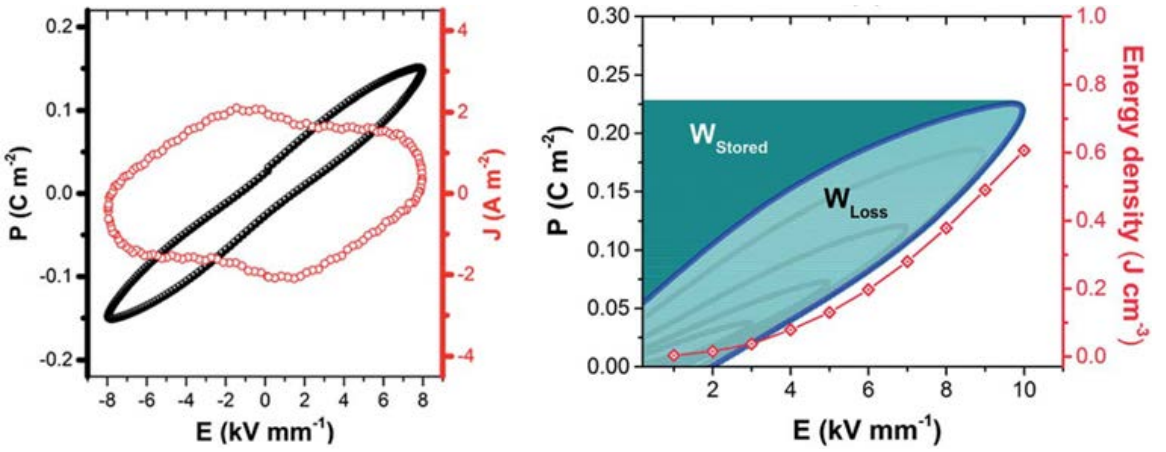

(a) (b)

Fig. 32. (a) *P-E* and *J-E* loops; (b) energy density properties for $0.75BiFeO_3$-$0.25(Ba_{0.99}La_{0.01})TiO_3$ (BF-BLT).[64]

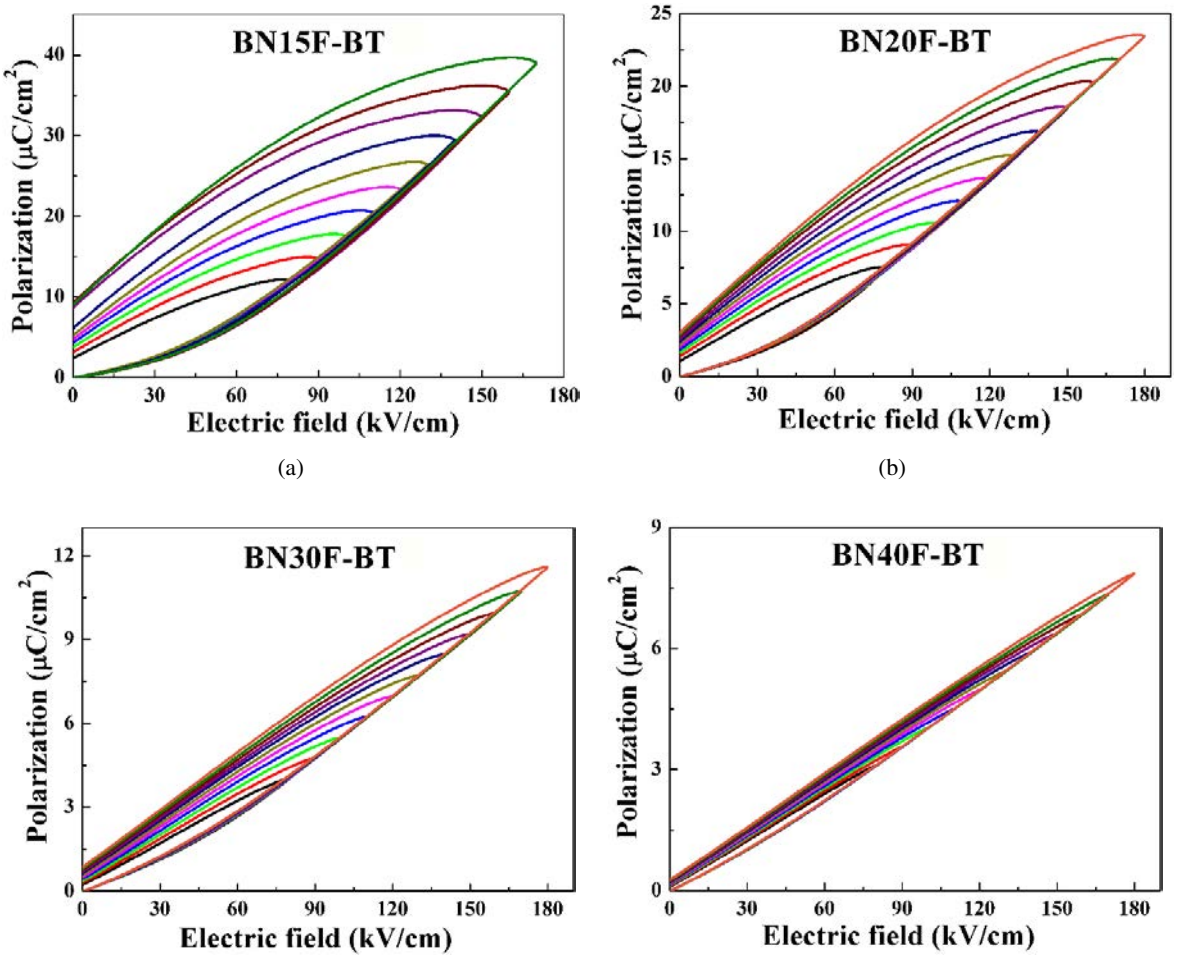

(a) (b)

(c) (d)

Fig. 33. Unipolar *P-E* loops under different electric fields for Nd doped 0.75BF-0.25BT (BN100*x*F-BT) (a) BN15F-BT, (b) BN20F-BT, (c) BN30F-BT and (d) BN40F-BT.[61]

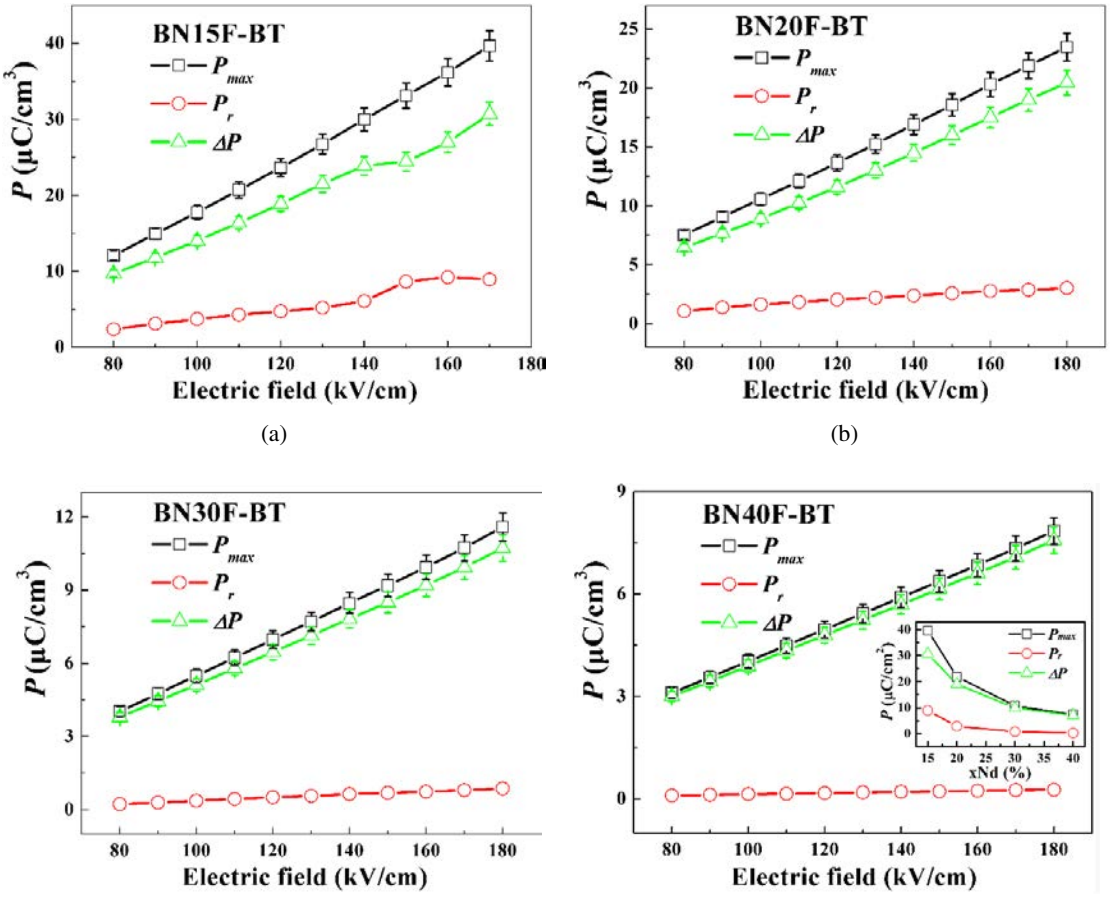

Fig. 34. P_{max}, P_r and ΔP as a function of electric field for Nd doped 0.75BF-0.25BT (BN100xF-BT) (a) BN15F-BT, (b) BN20F-BT, (c) BN30F-BT and (d) BN40F-BT; P_{max}, P_r and ΔP as a function of Nd concentration at 170 kv/cm are shown in the inset of (d).[61]

compound have been used to enhance energy storage properties. Zheng *et al.*[144] reported high $W_{rec} \sim 1.56\,J/cm^3$ with $\eta \sim 75\%$ under an electric field of 12.5 kV/mm in Ba$(Mg_{1/3}Nb_{2/3})O_3$ (BMN) doped BF-BT solid solution, as shown in Fig. 38, which had a good temperature stability from 25 to 190°C (Figs. 38(b) and 38(d)). They also found similar energy storage properties ($W_{rec} \sim 1.66\,J\,cm^{-3}$ with $\eta \sim 82\%$) in 0.61BF-0.33BT-0.06La$(Mg_{1/2}Ti_{1/2})O_3$ (BF-BT-0.06LMT), Fig. 39.[145] Liu *et al.* recently reported 0.06Sr$(Al_{0.5}Nb_{0.5})O_3$ (SAN)-0.6BF-0.34BT compositions with slim

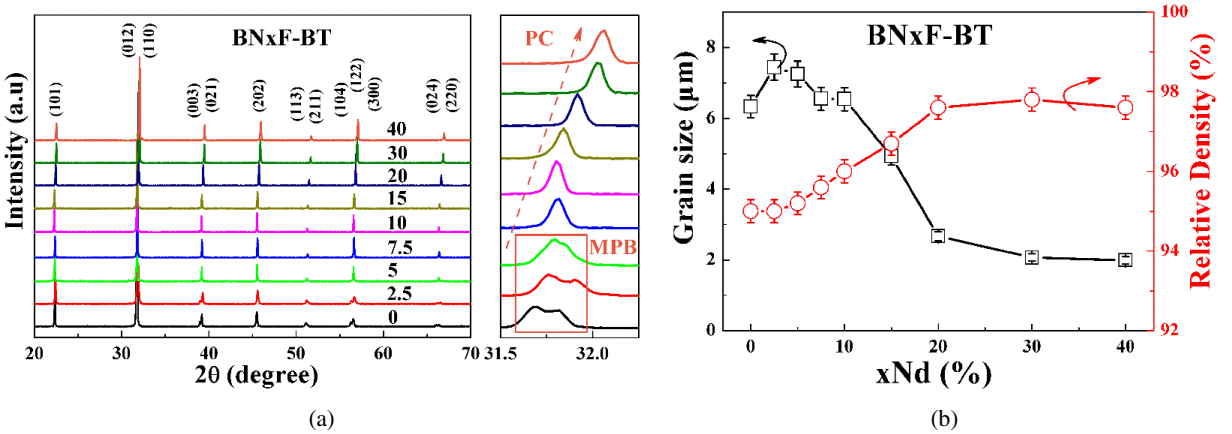

Fig. 35. (a) XRD patterns of Nd doped 0.75BF-0.25BT (BN100*x*F-BT); (b) average grain size and relative density of BN100*x*F-BT as a function of Nd concentration.[61]

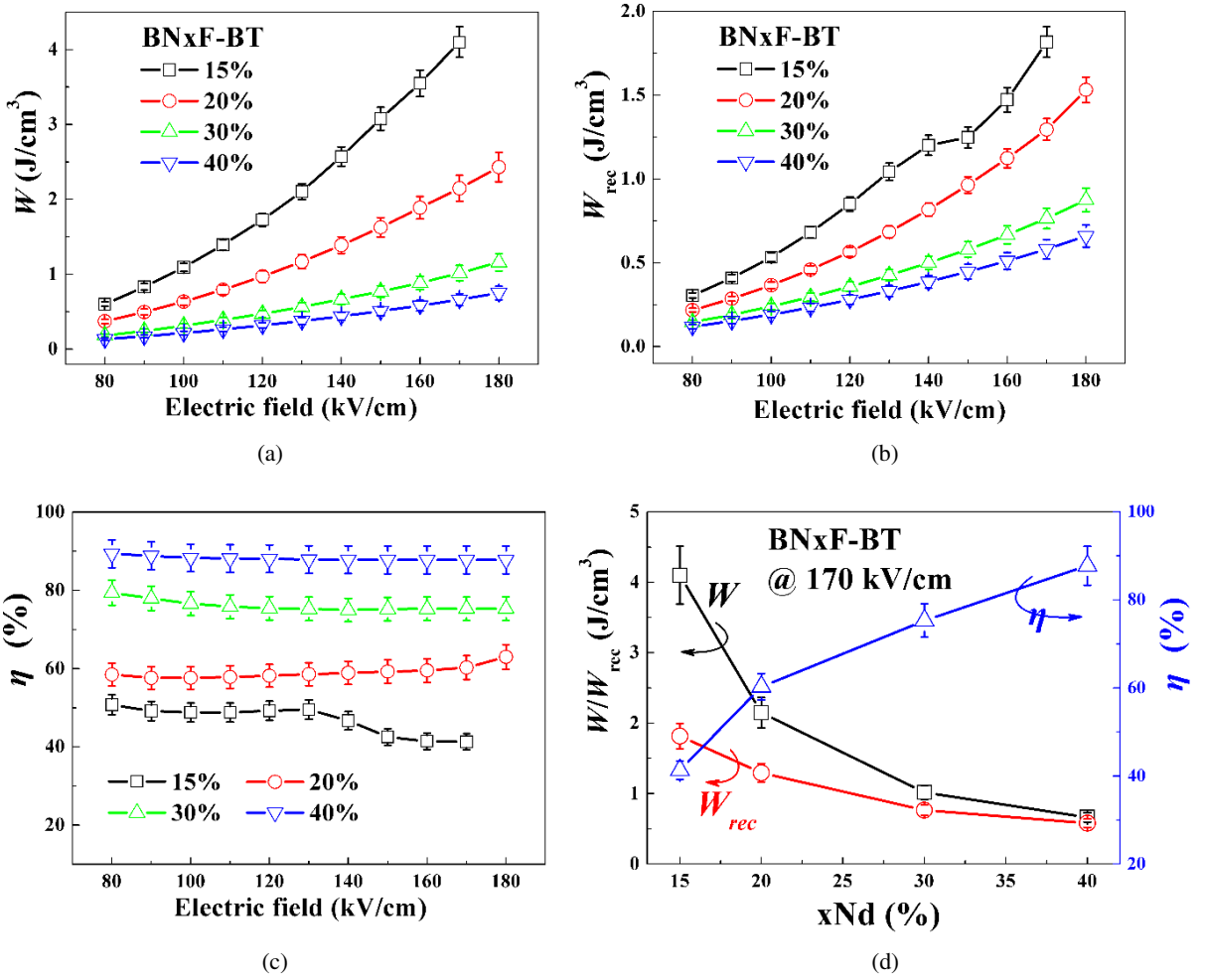

Fig. 36. (a) W, (b) W_{rec} and (c) η of Nd doped 0.75BF-0.25BT (BN100xF-BT): BN15F-BT, BN20F-BT, BN30F-BT and BN40F-BT as a function of electric field; (d) W, W_{rec} and η as a function of Nd concentration at 170 kV/cm.[61]

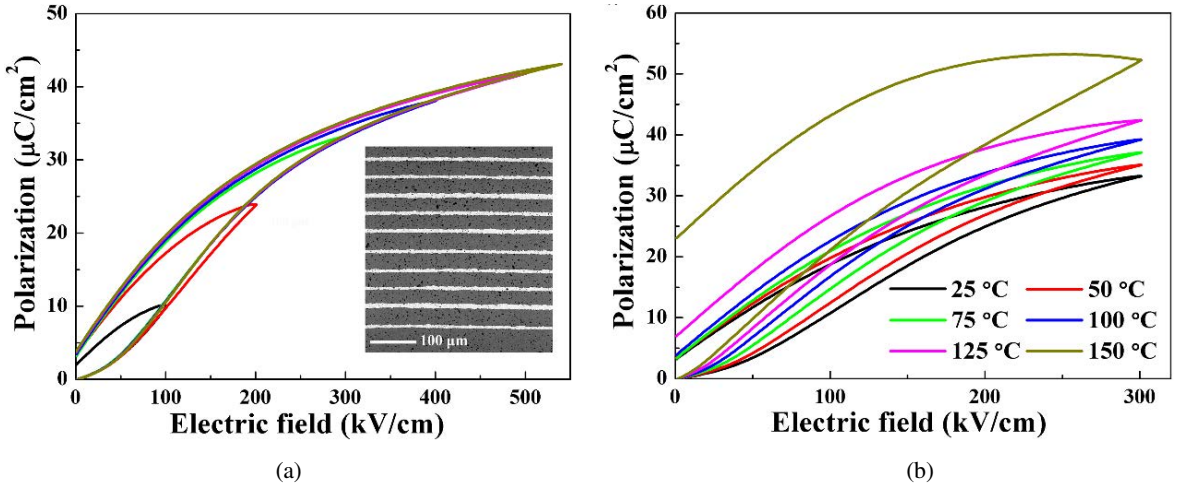

Fig. 37. (a) Unipolar P-E loops of BN15F-BT MLs under different electric fields at RT, (b) *in-situ* temperature dependence of unipolar P-E loops of MLs at an electric field of 300 kV/cm, (c) W, W_{rec} and η of MLs as a function of electric field at RT, and (d) W, W_{rec} and η of MLs as a function of temperature at 300 kV/cm; SEM image of MLs is in the inset of (a).[61]

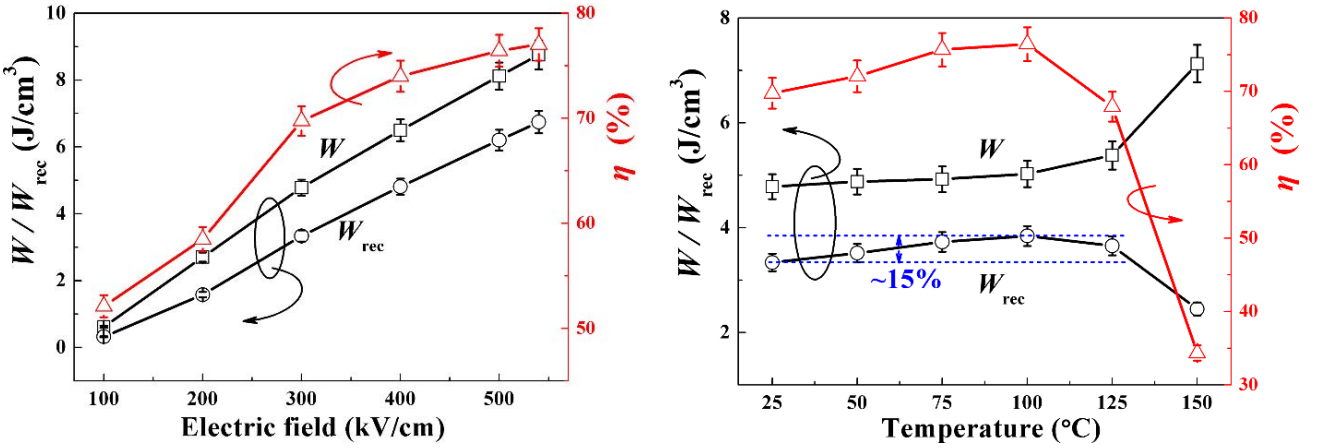

(c) (d)

Fig. 37. (*Continued*)

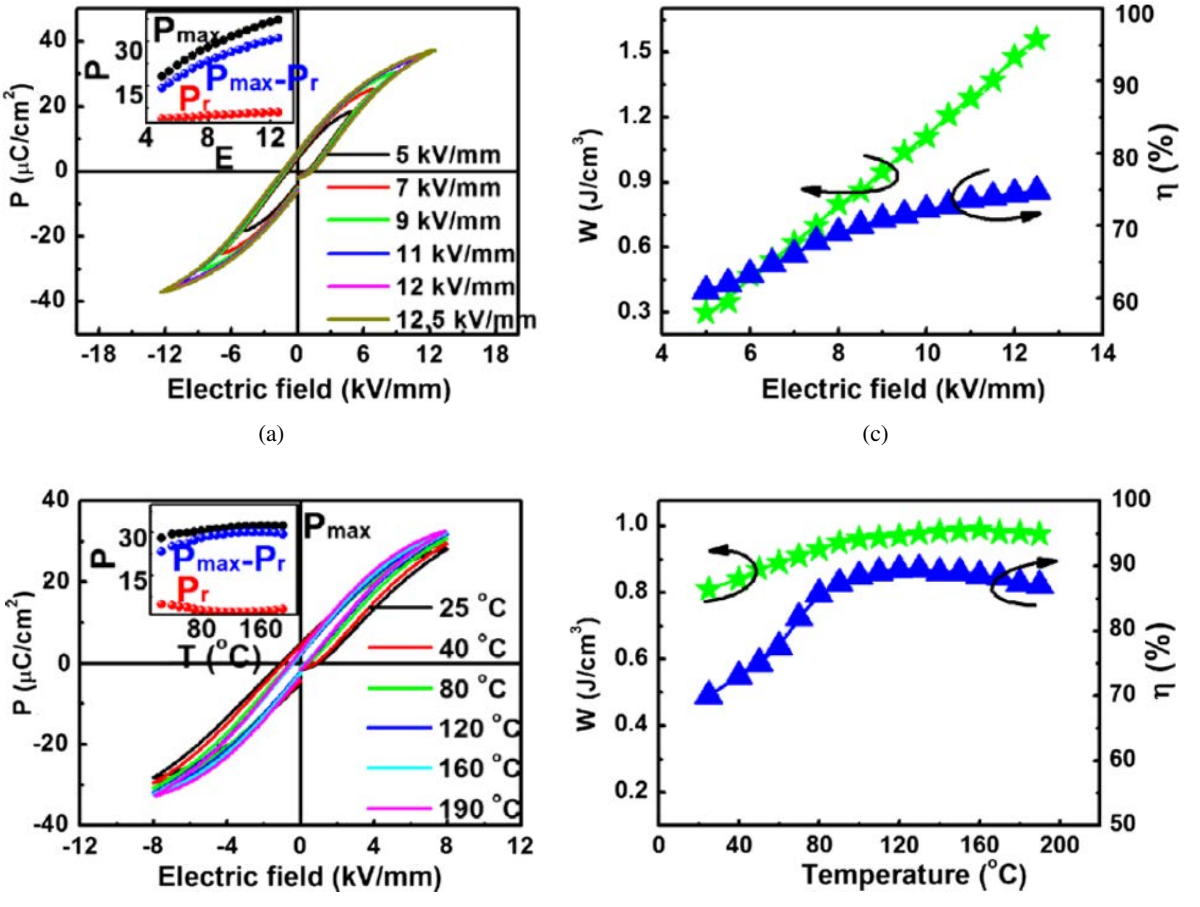

(a) (c)

(b) (d)

Fig. 38. *P-E* loops under different (a) electric fields and (b) temperature for 0.06Ba($Mg_{1/3}Nb_{2/3}$)O_3 (BMN) doped BF-BT (BF-BT-0.06BMN) ceramic, and both *W* and *η* values as a function of (c) electric field and (d) temperature.[144]

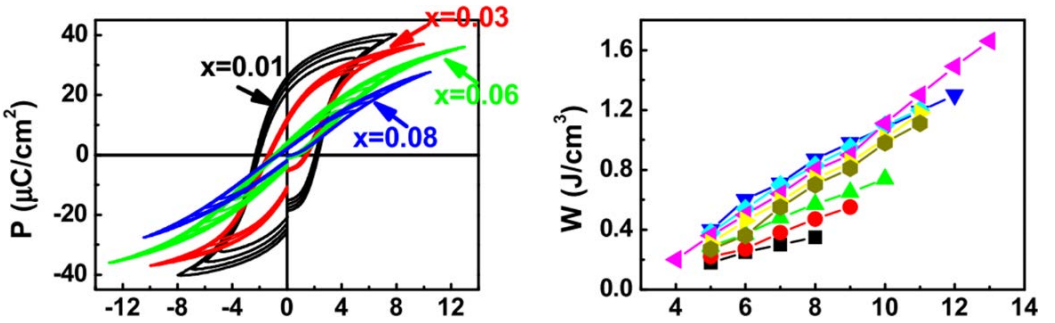

(a) (b)

Fig. 39. (a) *P-E* loops and (b) *W* for $La(Mg_{1/2}Ti_{1/2})O_3$ (LMT) doped BF-BT (BF-BT-*x*LMT) ceramics with different *x* concentration.[145]

P-E loops, $W_{rec} \sim 1.75\,J/cm^3$ and $\eta \sim 66\%$ at 15.5 kV/mm, as shown in Figs. 40(a) and 40(b),[146] with thermal stability from 30–120°C (Figs. 40(c) and 40(d)).

7.3. *Control of microstructure through doping*

The microstructural features in dielectric ceramics play an essential role on E_{BDS}, including porosity, grain boundary, inhomogeneity, second phase and grain size. The following relationship between E_{BDS} and average grain size (G) was proposed by Tunkasiri *et al.*,[147] confirming that smaller G leads to higher E_{BDS}.

$$E_{BDS} \propto \frac{1}{\sqrt{G}}. \tag{7}$$

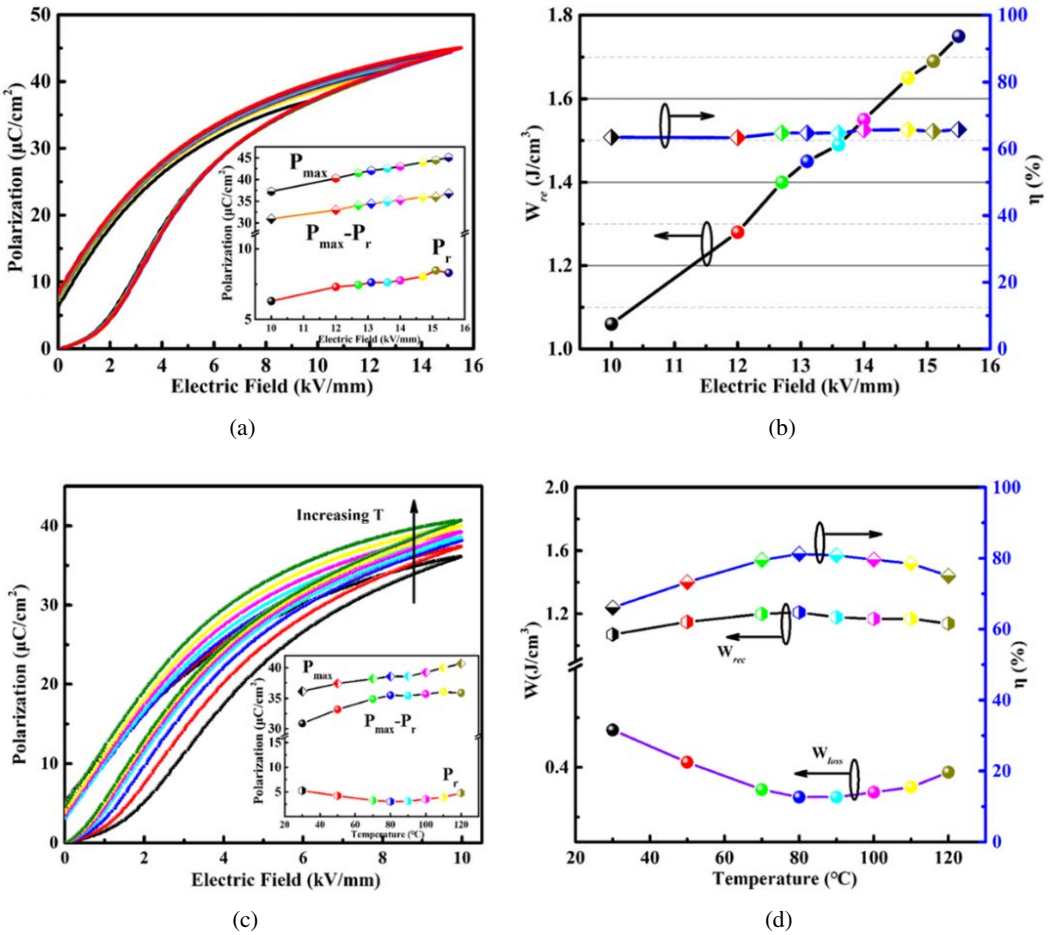

(a) (b)

(c) (d)

Fig. 40. Unipolar *P-E* loops under different (a) electric fields and (c) temperature for $0.06Sr(Al_{0.5}Nb_{0.5})O_3$ (SAN) doped BF-BT (0.6BF-0.34BT-0.06SAN) and W, W_{rec}, and η as a function (b) electric field and (d) temperature.[146]

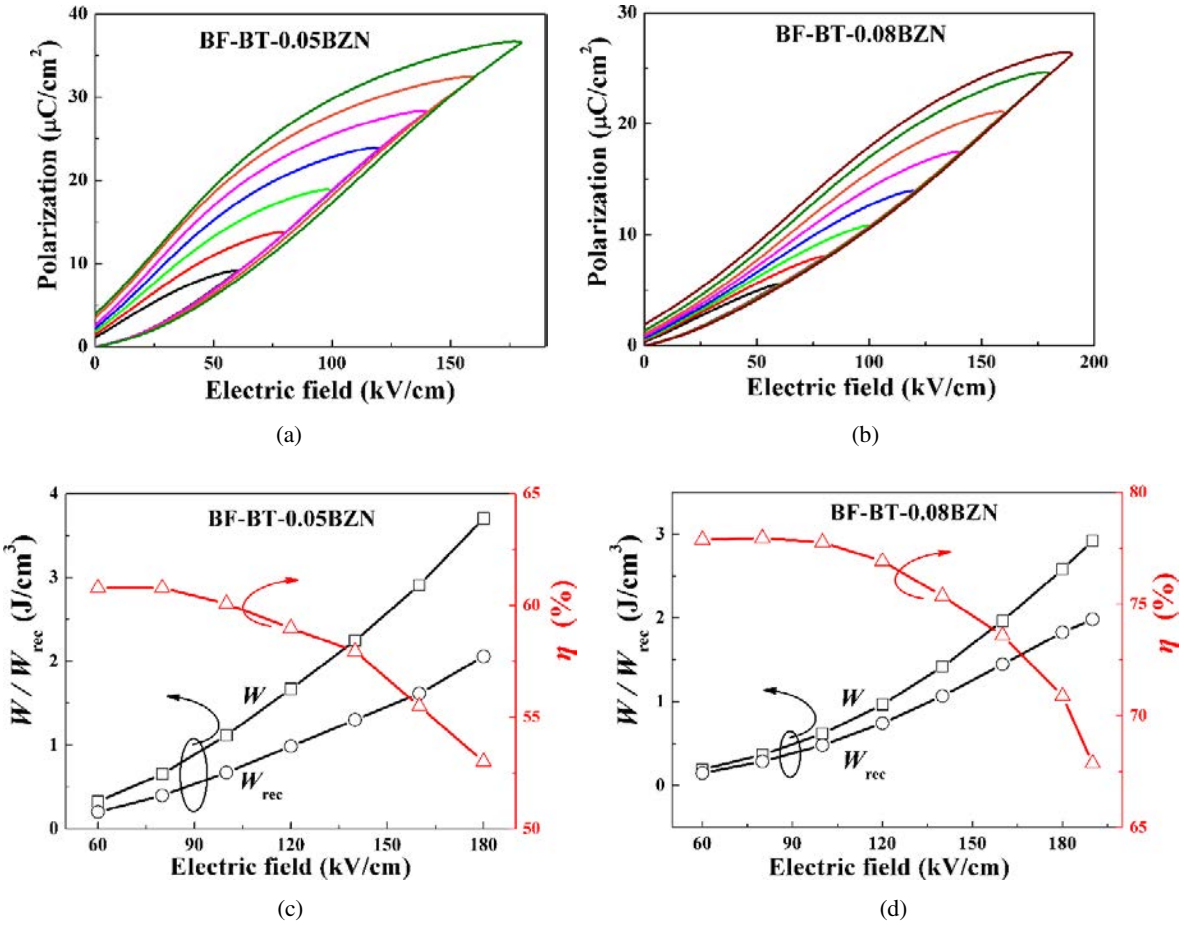

Fig. 41. Unipolar *P-E* loops under different electric fields for $Bi(Zn_{2/3}Nb_{1/3})O_3$ (BZN) doped BF-BT (BF-BT-*x*BZN) (a) BF-BT-0.05BZN and (b) BF-BT-0.08BZN. W, W_{rec}, and η as a function of electric field for (c) BF-BT-0.05BZN and (d) BF-BT-0.08BZN.[58]

In most of cases, G reduces with increasing dopant concentration with a commensurate improvement in E_{BDS}. E_{BDS} of dielectric ceramics is also greatly increased with a reduction in porosity and defects.[148,149] For example, a large G of $\sim 7\,\mu$m was observed in undoped 0.7BF-0.3BT ceramics (Fig. 35(b)) normally breaks down at 100 kV/cm.[58,61,83] With addition of dopants, such as Nd^{3+} reported by Wang *et al.*[61] a significant reduction of both G (1–2 μm) and porosity was

Table 4. Summary of the energy storage properties for reported BF-BT ceramics. (BMN = $Ba(Mg_{1/3}Nb_{2/3})O_3$, LMT = $La(Mg_{1/2}Ti_{1/2})O_3$, BZN = $Bi(Zn_{2/3}Nb_{1/3})O_3$, SAN = $Sr(Al_{0.5}Nb_{0.5})O_3$).

Compounds	E (kV/cm)	W (J/cm^3)	W_{rec} (J/cm^3)	η (%)	Ref.
0.97(0.65BF-0.35BT)-0.03Nb	90	/	0.71	/	143
0.75BF-0.25$B_{0.09}La_{0.01}$T	100	/	0.61	/	64
0.75$B_{0.85}Nd_{0.15}$F-0.25BT	170	4.1	1.82	41.3	61
0.75$B_{0.6}Nd_{0.4}$F-0.25BT	180	0.75	0.66	87.8	61
0.61BF-0.33BT-0.06BMN	125	2.08	1.56	75	144
0.61BF-0.33BT-0.06LMT	130	2.02	1.66	82	145
0.6BF-0.34BT-0.06SAN	155	2.69	1.75	65	146
0.65BF-0.3BT-0.05BZN	180	3.7	2.06	53	58
0.65BF-0.3BT-0.08BZN	190	2.9	1.98	68	58
BF-BT multilayers	540	8.75	6.74	77	61

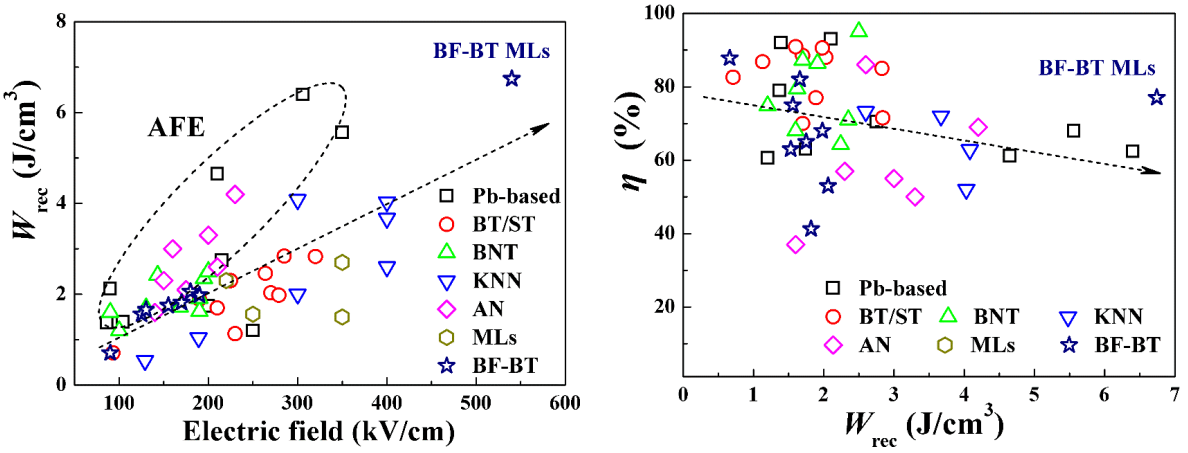

Fig. 42. Comparison of energy-storage properties among lead-based, lead-free and multilayer ceramics/capacitors (a) W_{rec} versus electric field and (b) η versus W_{rec}.[58,61,64,143–194]

achieved by Nd doping (Fig. 35(b)), increasing E_{BDS} (180–190 kV/cm), resulting in an improvement of $W \sim 4.1$ J/cm^3 and $W_{rec} \sim 1.82$ J/cm^3, as shown in Fig. 36.

Additionally, as discussed in Sec. 5.1, compositional inhomogeneity with core-shell microstructure is often observed in doped BF-BT ceramics. However, this is not considered detrimental to energy storage behavior. $W_{rec} \sim 2.1$ J/cm^3 and $\eta \sim 53\%$ under an electric field of ~ 180 kV/cm was reported in core-shell 0.65BF-0.3BT-0.05BZN compositions (Figs. 13, 14 and 41)[58] which they attributed to slim *P-E* loops.

The energy storage properties for reported BF-BT ceramics and MLs are summarized in Table 4 and the comparison of energy-storage properties among lead-based and lead-free ceramics/MLs are displayed in Fig. 42.[58,61,64,143–194] Among all reported BF-BT ceramics, 0.05BZN and 0.4Nd doped BF-BT exhibits the highest values of $W_{rec} \sim 2.1$ J/cm^3 and $\eta \sim 87.8\%$, respectively (Table 4). Compared with lead-based and other lead-free ceramics, as shown in Fig. 42, the values of W_{rec} for BF-BT ceramics are promising but antiferroelectrics (AFE, PLZT, $AgNbO_3$, some BNT-based ceramics) are higher. Authors however, do not often report the concomitant large strain associated with AFE/FE transitions which may prove detrimental to the longevity of a device in service due to mechanical fatigue during charge discharge.[194] Nd-doped BF-BT MLs exhibit the largest $W_{rec} \sim 6.74$ J cm^{-3} with high $\eta \sim 77\%$ in BF-BT based systems but we note that recent unpublished data by the present authors have now surpassed these values with $W_{rec} > 10$ J/cm^3. This latter value exceeds that reported by Li *et al.*[194] for (Bi,Sr)TiO_3 doped NBT MLs (> 9 J/cm^3).

In summary, the methodologies for developing high energy density materials are now known and BF-BT compositions can be readily adapted to have high E_{BDS} and large ΔP. The role of dopants/third end member in the solid solution is many fold. The dopants decrease P_r, increase E_{BDS} through improved density, decreased grain size and possibly inducing a core-shell microstructure. Multilayering compositions further increases E_{BDS} and improves the η with respect to bulk performance. We encourage researchers to explore the compositional design space that this methodology permits to improve the performance of BF-BT systems with $W_{rec} \sim 15$ J/cm^3 a realistic target. The low strains associated with RFE, BF-BT based MLs offer significant advantages over their AFE counterparts, and work is now required to explore cheaper internal electrode options (current prototypes are fabricated from Pt internal electrodes) to reduce manufacturing costs.

8. BF-BT films

BF-BT films have attracted recent attention for potential applications in ferroelectric random access memory (FeRAM) and microelectromechanical systems (MEMS).[195–215] Compared with PZT or other lead-free materials, only few studies have focused on BF-BT films. Ueda *et al.*[216] prepared BF-0.3BT films by the pulsed-laser deposition technique in 1999, which found coexistence of weak ferroelectricity and ferromagnetism ($P_r \sim 2.5$ μC/cm^2, Fig. 43). Ito *et al.*[217] prepared BF-0.3BT films by chemical solution deposition and Mn doping reduced the leakage current, leading to improvement in ferroelectric properties to $P_S \sim 60$ μC/cm^2 and $P_r \sim 27$ μC/cm^2 at a field of 800 kV/cm. Liu *et al.*[218] grew BF-*x*BT films by chemical solution deposition and achieved high values of $P_r \sim 19.7$–76.6 μC/cm^2 at 940 kV/cm. Although there are only a few papers on BF-BT film, Lee *et al.*[219] (2016) recently reported that 300 nm thick BF-0.33BT achieved local piezoelectric constant ($d_{33,PFM}$) of 92.5 pm/V with high T_C of 405°C (Fig. 44). In addition, Lee *et al.*[219] further compared the temperature dependence of ε_r between film and bulk of the same composition observing

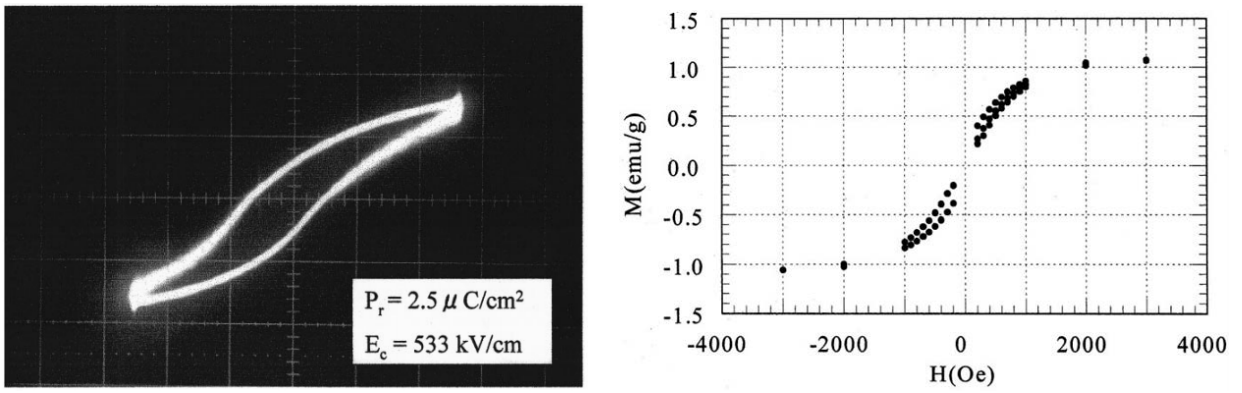

(a) (b)

Fig. 43. (a) Electric and (b) magnetic hysteresis curves of 0.7BF-0.3BT film (~ 3000 Å) at RT. $P_r = 2.5\,\mu$C/cm^2, $E_C = 533$ kV/cm, $M_r = 0.2$ emu/g, $H_C = 200$ Oe.[216]

that the dielectric anomaly of the film was broader than that of the bulk (Figs. 44(b) and 44(c)), due to stress effects relating to the presence of a high volume fraction of grain boundary compared with bulk and differences in thermal expansion between film and substrate. To our knowledge however, there are still no reports on BF-BT films for energy storage. A Mn-doped $0.4BiFeO_3$-$0.6SrTiO_3$ (BF-ST) thin film capacitor was reported by Pan *et al.*[220] which achieved

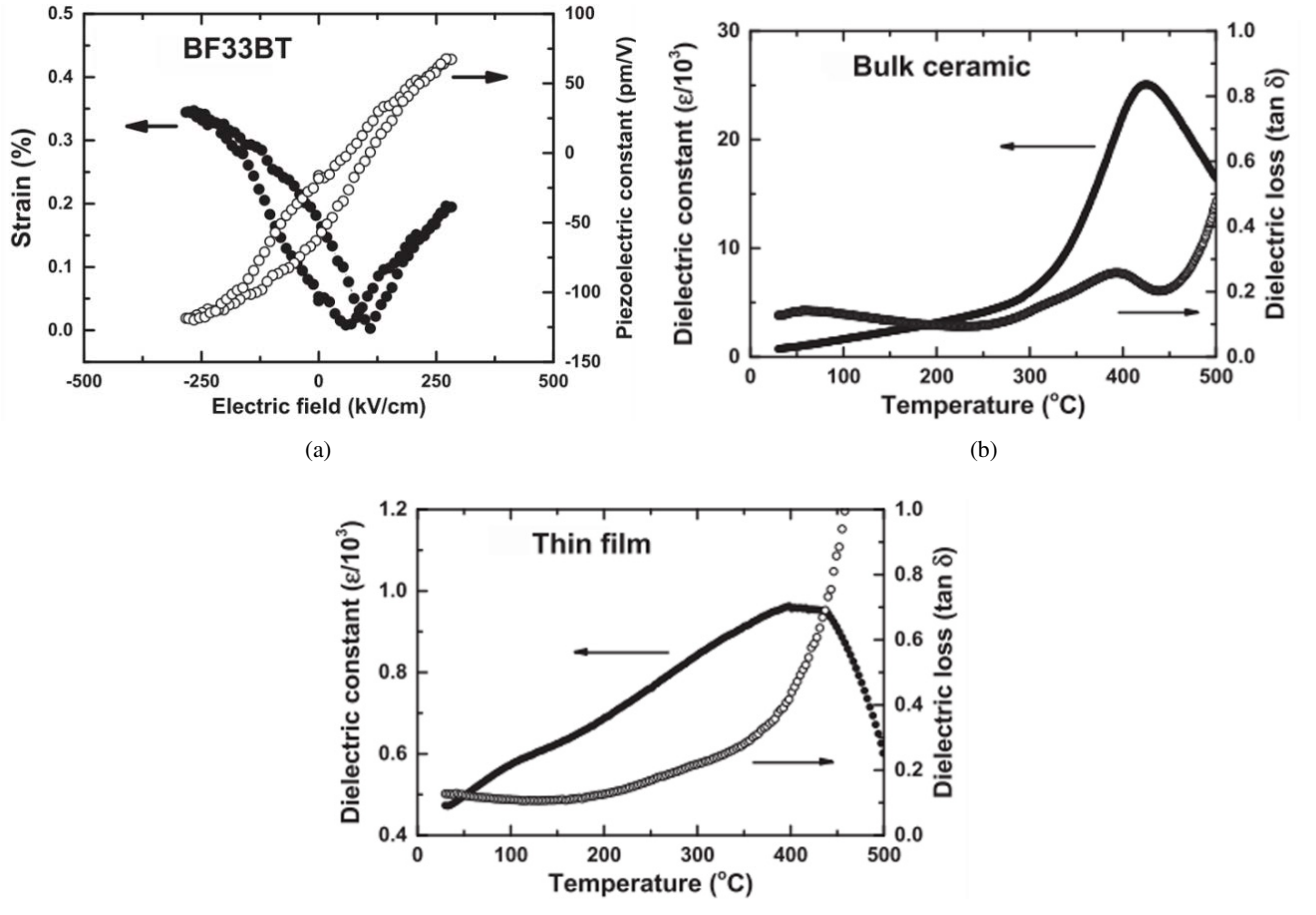

(a) (b)

(c)

Fig. 44. (a) The local piezoelectric hysteresis loops of electric field dependent strain and $d_{33,\mathrm{PFM}}$ of 0.67BF-0.33BT (BF-33BT) thin film; Temperature dependence of ε_r and dielectric loss ($\tan\delta$) of BF-33BT (b) bulk ceramic and (c) thin film.[219]

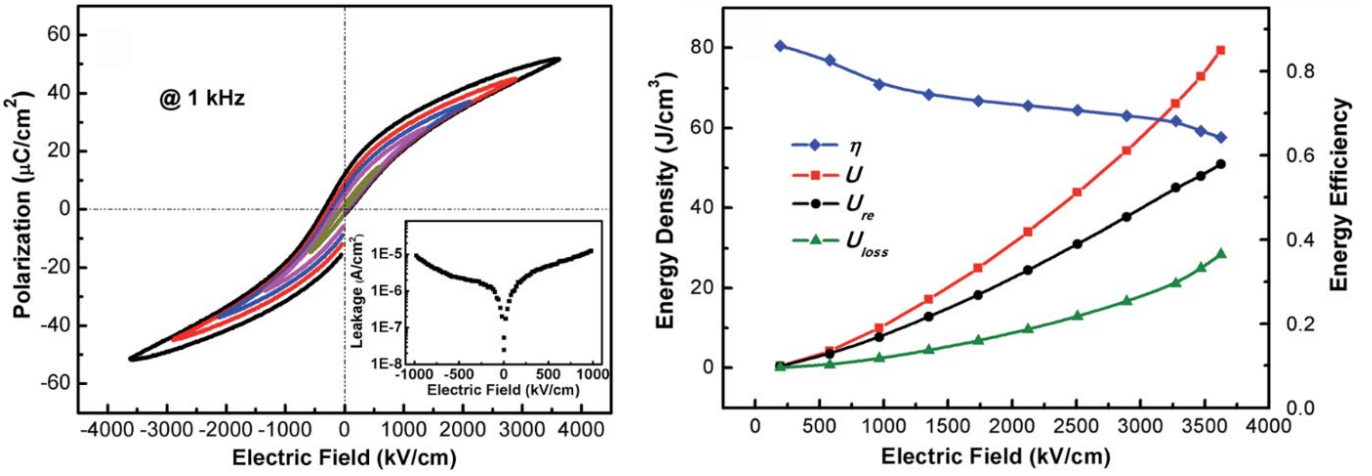

(a) (b)

Fig. 45. (a) *P-E* loops of $0.4BiFeO_3$-$0.6SrTiO_3$ (BF-ST) film with various applied electric fields at 1 kHz. The inset is the *J* of BF-ST film at various DC biased electric fields. (b) Stored energy density *U*, recoverable energy density U_{re}, hysteresis loss U_{loss}, and η as a function of the applied electric field.[220]

an ultrahigh $W_{rec} \sim 51\,J/cm^3$ (Fig. 45), superior to other lead-free systems and comparable with the best lead-based films. Similar high energy storage performance in BF-BT films are realistic based on the excellent properties of ceramics and MLs.

9. Further Potential Applications of BF-BT

In comparison to PZT, BF-BT ceramics are in their infancy with significant scientific interest only emerging after the work of Leontsiev *et al.*[53] Since this publication, BF-BT systems have been shown to be suitable for sensor, actuator and energy storage applications. However, there are a number of further attractive features/properties that show promise for other applications. Electrocalorics are required to progress through the Carnot cycle (Fig. 46).[221–228] The design metrics are low strain to prevent mechanical fatigue, high E_{BDS} and the ability to induce a large entropy change associated with the large polarization change though the application of cyclic field such as occurs in a field induced relaxor to ferroelectric transition. The ability to form robust multilayers is also an advantage for the fabrication of channelled device structures. It is evident that doped BF-BT compositions meet these criteria and thus should be considered as possible candidates for electrocaloric solid state cooling systems.

Pyroelectricity is the electrical response of an insulating dielectric to a change in temperature, which is found in polar materials with noncentrosymmetric structure.[227–230] Figures of merit (FOMs) are critical for pyroelectric materials and devices, which could be maximized by high pyroelectric coefficient (*p*, determined by P_S) as well as both low values of ε_r and $\tan\delta$.[227–230] To our knowledge, the pyroelectric properties of BF-BT systems remain unknown at this time but the ability to manipulate the system though an array of dopants that influence the phase assemblage and the relaxor to ferroelectric behavior suggest that research may yield interesting pyroelectric compositions.

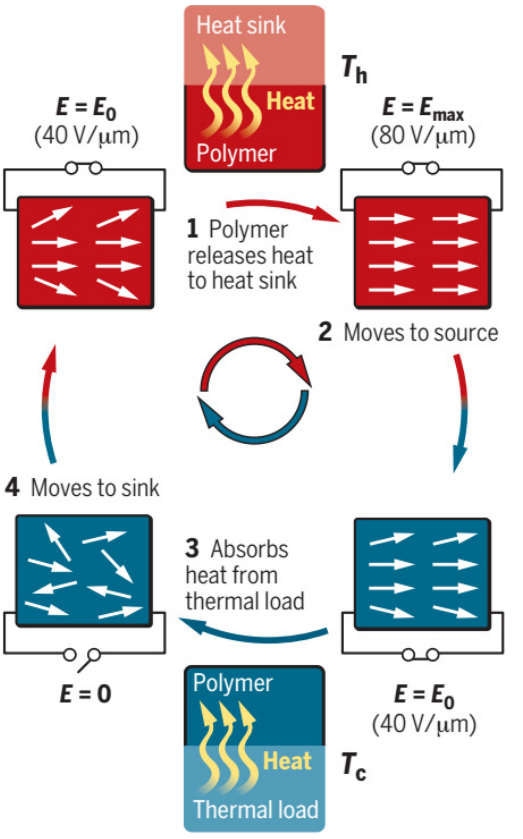

Fig. 46. Two half-cycles in Carnot cooler cycle.[221]

10. Summary and Future Work

(1) Crystal structure and microstructure is critical and can strongly affect the performance of BF-BT ceramics. The optimum piezoelectric properties ($d_{33} = 100 \sim 402$ pC/N, $d^*_{33} = 126 \sim 600$ pm/V) are commonly achieved at the *R-C* phase boundary. The crystal structure of compositions at this boundary is still ambiguous and further work is required to understand the average and local structure. Specifically, *in-situ* XRD and TEM is needed to determine the behavior as a function of applied field and temperature.

(2) Compositional inhomogeneity with core-shell microstructure (Ba/Ti-rich shell and Bi/Fe-rich core) have been investigated by BSE, EDS, TEM and impedance. Although compositional inhomogeneity is considered harmful to piezoelectric properties, enhanced energy storage property has been observed for core-shell BF-BT-*x*BZN. Further work is required to understand the role of chemical homogeneity on breakdown strength and polarisation.

(3) Thermal treatment (annealing and quenching) affect the crystal structure have been reported to eliminate compositional inhomogeneity and improve the ferroelectric/piezoelectric properties. Quenched Ga-doped BF-BT ceramics have been reported with mixed *R*3*c* and *P*4*mm* phases which possess $d_{33} \sim 402$ pC/N. Large strains are achieved in many compositions and d^*_{33} is routinely reported to exceed 400 pm/V but to date large conventional d_{33} values have not been reproduced on either furnace cooled or quenched samples. Further studies are required to reproduce this data and assess whether processing methodologies are suitable for scale-up.

(4) A/B site doping and extension of the solid solution with a third end member have proved to be effective in achieving slim *P-E* loops and enhancing E_{BDS} in the BF-BT system. Multilayering further increases E_{BDS} and improves η. We recommend that the outlined methodologies are utilized by researchers to improve iteratively the energy storage properties in the BF-BT system with $W_{rec} \sim 15$ J/cm^3 a realistic target.

(5) BF-BT films have been successfully prepared by different methods, including pulsed-laser and chemical solution deposition. The energy storage properties have not been reported in BF-BT films so far but given the high E_{BDS} of MLs and ceramics and the high W_{rec} (~ 51 J/cm^3) reported for BF-ST thin films, we strongly recommend that further studies are carried out.

(6) We note that long term reliability of BF-BT based systems has not been investigated and it is critical that such work is undertaken in the near future if the potential of this novel system is to be achieved.

(7) Although there is clear evidence that the electrostrictive, piezoelectric and energy storage properties of BF-BF are promising for real world applications, there are no studies on pyroelectric and electrocaloric behavior. This oversight in the literature needs redressing.

Acknowledgments

This work was supported by the Engineering and Physical Sciences Research Council (EP/L017563/1 and EP/N010493/1) and National Natural Science Foundation of China (51602060 and 51402005). D. Wang, G. Wang and S. Murakami contributed equally to this work and should be considered as co-first authors.

References

[1]N. Setter and R. Waser, Electroceramic materials, *Acta Mater.* **48**, 151 (2000).
[2]J. Curie and P. Curie, Development, via compression, of electric polarization in hemihedral crystals with inclined faces, *Bulletin de la Societe de Minerologique de France*, **3**, 90 (1880).
[3]G. Lippmann, Principe de la conservation de l'électricité, ou second principe de la théorie des phénomènes électriques, *Ann. Chimie Phys.* **24**, 145 (1881).
[4]G. Shirane, K. Suzuki and A. Takeda, Phase transitions in solid solutions of $PbZrO_3$ and $PbTiO_3$ (II) X-ray study, *J. Phys. Soc. Jpn.* **7**, 12 (1952).
[5]E. Sawaguchi, Ferroelectricity versus antiferroelectricity in the solid solutions of $PbZrO_3$ and $PbTiO_3$, *J. Phys. Soc. Jpn.* **8**, 615 (1953).
[6]T. R. Shrout and S. Zhang, Lead-free piezoelectric ceramics: Alternatives for PZT?, *J. Electroceram.* **19**, 185 (2007).
[7]B. Jaffe, R. S. Roth and S. Marzullo, Piezoelectric properties of lead zirconate-lead titanate solid-solution ceramics, *J. Appl. Phys.* **25**, 809 (1954).
[8]B. Noheda, D. E. Cox, G. Shirane, J. A. Gonzalo, L. E. Cross, and S. E. Park, A monoclinic ferroelectric phase in the $PbZr1_{-x}TixO_3$ solid solution, *Appl. Phys. Lett.* **74**, 2059 (1999).
[9]B. Noheda, J. A. Gonzalo, L. E. Cross, R. Guo, S. E. Park, D. E. Cox and G. Shirane, Tetragonal-to-monoclinic phase transition in a ferroelectric perovskite: The structure of $PbZr_{0.52}Ti_{0.48}O_3$, *Phys. Rev. B* **61**, 8687 (2000).
[10]D. Wang, Y. Fotinich and G. P. Carman, Influence of temperature on the electromechanical and fatigue behavior of piezoelectric ceramics, *J. Appl. Phys.* **83**, 5342 (1998).
[11]A. B. Schäufele and K. Heinz Härdtl, Ferroelastic properties of lead zirconate titanate ceramics, *J. Am. Ceram. Soc.* **79**, 2637 (1996).
[12]G. H. Haertling, Ferroelectric ceramics: History and technology, *J. Am. Ceram. Soc.* **82**, 797 (2004).
[13]D. W. Wang, M. S. Cao, J. Yuan, Q. L. Zhao, H. B. Li, D. Q. Zhang and S. Agathopoulos, Enhanced piezoelectric and ferroelectric properties of Nb_2O_5 modified lead zirconate titanate-based composites, *J. Am. Ceram. Soc.* **94**, 647 (2011).
[14]M. S. Cao, D. W. Wang, J. Yuan, H. B. Lin, Q. L. Zhao, W. L. Song and D. Q. Zhang, Enhanced piezoelectric and mechanical properties of ZnO whiskers and Sb_2O_3 co-modified lead zirconate titanate composites, *Mater. Lett.* **64**, 1798 (2010).
[15]Directive 2002/95/EC of the European Parliament and of the Council of 27 January 2003 on the restriction of the use of certain

hazardous substances in electrical and electronic equipment, *Off. J. Eur. Union* **13**, 2 (2003)

[16]Y. Saito, H. Takao, T. Tani, T. Nonoyama, K. Takatori, T. Homma, T. Nagaya and M. Nakamura, Lead-free piezoceramics, *Nature* **432**, 84 (2004).

[17]E. K. Akdoğan, K. Kerman, M. Abazari and A. Safari, Origin of high piezoelectric activity in ferroelectric $(K_{0.44}Na_{0.52}Li_{0.04})$-$(Nb_{0.84}Ta_{0.1}Sb_{0.06})O_3$ ceramics, *Appl. Phys. Lett.* **92**, 112908 (2008).

[18]E. Hollenstein, D. Damjanovic and N. Setter, Temperature stability of the piezoelectric properties of Li-modified KNN ceramics, *J. Eur. Ceram. Soc.* **27**, 4093 (2007).

[19]H. Shi, J. Chen, R. Wang and S. Dong, Full set of material constants of $(Na_{0.5}K_{0.5})NbO_3$–$BaZrO_3$–$(Bi_{0.5}Li_{0.5})TiO_3$ lead-free piezoelectric ceramics at the morphotropic phase boundary, *J. Alloys Compd.* **655**, 290 (2016).

[20]K. Xu, J. Li, X. Lv, J. Wu, X. Zhang, D. Xiao and J. Zhu, Superior piezoelectric properties in potassium–sodium niobate lead-free ceramics, *Adv. Mater.* **28**, 8519 (2016).

[21]R. Zuo and J. Fu, Rhombohedral–Tetragonal phase coexistence and piezoelectric properties of $(NaK)(NbSb)O_3$–$LiTaO_3$–$BaZrO_3$ lead-free ceramics, *J. Am. Ceram. Soc.* **94**, 1467 (2011).

[22]R. Zuo, J. Fu, S. Lu and Z. Xu, Normal to relaxor ferroelectric transition and Domain morphology evolution in (K,Na)(Nb,Sb)O_3–$LiTaO_3$–$BaZrO_3$ lead-free ceramics, *J. Am. Ceram. Soc.* **94**, 4352 (2011).

[23]J. Fu, R. Zuo, S. C. Wu, J. Z. Jiang, L. Li, T. Y. Yang, X. Wang and L. Li, Electric field induced intermediate phase and polarization rotation path in alkaline niobate based piezoceramics close to the rhombohedral and tetragonal phase boundary, *Appl. Phys. Lett.* **100**, 122902 (2012).

[24]B. Zhang, J. Wu, X. Cheng, X. Wang, D. Xiao, J. Zhu, X. Wang and X. Lou, Lead-free piezoelectrics based on potassium–sodium niobate with giant d33, *ACS Appl. Mater. Interfaces* **5**, 7718 (2013).

[25]C. Liu, D. Xiao, T. Huang, J. Wu, F. Li, B. Wu and J. Zhu, Composition induced rhombohedral–tetragonal phase boundary in $BaZrO_3$ modified $(K_{0.445}Na_{0.5}0Li_{0.055})NbO_3$ lead-free ceramics, *Mater. Lett.* **120**, 275 (2014).

[26]X. Wang, J. Wu, D. Xiao, J. Zhu, X. Cheng, T. Zheng, B. Zhang, X. Lou and X. Wang, Giant piezoelectricity in potassium–sodium niobate lead-free ceramics, *J. Am. Chem. Soc.* **136**, 2905 (2014).

[27]T. Zheng, J. Wu, D. Xiao, J. Zhu, X. Wang, L. Xin and X. Lou, Strong piezoelectricity in $(1–x)(K_{0.4}Na_{0.6})(Nb_{0.96}Sb_{0.04})O_3$-$xBi_{0.5}K_{0.5}Zr_{1-y}SnyO_3$ lead-free binary system: Identification and rrole of multiphase coexistence, *ACS Appl. Mater. Interfaces* **7**, 5927 (2015).

[28]T. Zheng, J. Wu, D. Xiao, J. Zhu, X. Wang and X. Lou, Potassium–sodium niobate lead-free ceramics: Modified strain as well as piezoelectricity, *J. Mater. Chem. A* **3**, 1868 (2015).

[29]J. S. Zhou, K. Wang, F. Z. Yao, T. Zheng, J. Wu, D. Xiao, J. Zhu and J. F. Li, Multi-scale thermal stability of niobate-based lead-free piezoceramics with large piezoelectricity, *J. Mater. Chem. C* **3**, 8780 (2015).

[30]Y. Wang, L. Hu, Q. Zhang and H. Yang, Phase transition characteristics and associated piezoelectricity of potassium-sodium niobate lead-free ceramics, *Dalton Trans.* **44**, 13688 (2015).

[31]Z. Wang, D. Xiao, J. Wu, M. Xiao, F. Li and J. Zhu, New lead-free $(1 - x)(K_{0.5}Na_{0.5})NbO_3$–$x(Bi_{0.5}Na_{0.5})ZrO_3$ ceramics with high piezoelectricity, *J. Am. Ceram. Soc.* **97**, 688 (2014).

[32]S. T. Zhang, A. B. Kounga, E. Aulbach, H. Ehrenberg and J. Rödel, Giant strain in lead-free piezoceramics $Bi_{0.5}Na_{0.5}TiO_3$–$BaTiO_3$–$K_{0.5}Na_{0.5}NbO_3$ system, *Appl. Phys. Lett.* **91**, 112906 (2007).

[33]S. T. Zhang, A. B. Kounga, E. Aulbach, T. Granzow, W. Jo, H. J. Kleebe and J. Rödel, Lead-free piezoceramics with giant strain in the system $Bi_{0.5}Na_{0.5}TiO_3$–$BaTiO_3$–$K_{0.5}Na_{0.5}NbO_3$. I. Structure and room temperature properties, *J. Appl. Phys.* **103**, 034107 (2008).

[34]Y. Wang, N. Kounga A. Brice and C. Hoffmann, Piezo-electric ceramic composition, method for producing the composition, and electric component comprising the composition, Patent, WO/2011/012682, 2011.

[35]W. Bai, P. Li, L. Li, J. Zhang, B. Shen and J. Zhai, Structure evolution and large strain response in BNT–BT lead-free piezoceramics modified with $Bi(Ni_{0.5}Ti_{0.5})O_3$, *J. Alloys Compd.* **649**, 772 (2015).

[36]A. Maqbool, A. Hussain, J. Ur Rahman, T. Kwon Song, W.-J. Kim, J. Lee and M.-H. Kim, Enhanced electric field-induced strain and ferroelectric behavior of $(Bi_{0.5}Na_{0.5})TiO_3$–$BaTiO_3$–$SrZrO_3$ lead-free ceramics, *Ceram. Int.* **40**, 11905 (2014).

[37]Y. Kazushige, H. Yuji, N. Hajime and T. Tadashi, Electrical properties and depolarization temperature of $(Bi_{1/2}Na_{1/2})TiO_3$–$(Bi_{1/2}K_{1/2})TiO_3$ lead-free piezoelectric ceramics, *Jpn. J. Appl. Phys.* **45**, 4493 (2006).

[38]K. N. Pham, A. Hussain, C. W. Ahn, W. Kim, S. J. Jeong and J. S. Lee, Giant strain in Nb-doped $Bi_{0.5}(Na_{0.8}2K_{0.1}8)_{0.5}TiO_3$ lead-free electromechanical ceramics, *Mater. Lett.* **64**, 2219 (2010).

[39]V. Q. Nguyen, H. S. Han, K. J. Kim, D. D. Dang, K. K. Ahn and J. S. Lee, Strain enhancement in $Bi_{1/2}(Na_{0.82}K_{0.18})_{1/2}TiO_3$ lead-free electromechanical ceramics by co-doping with Li and Ta, *J. Alloys Compd.* **511**, 237 (2012).

[40]H. Yuji, N. Hajime and T. Tadashi, Formation of morphotropic Phase boundary and electrical properties of $(Bi_{1/2}Na_{1/2})TiO_3$–$Ba(Al_{1/2}Nb_{1/2})O_3$ solid solution ceramics, *Jpn. J. Appl. Phys.* **48**, 09KC08 (2009).

[41]X. Liu and X. Tan, Giant strain with low cycling degradation in Ta-doped $[Bi_{1/2}(Na_{0.8}K_{0.2})_{1/2}]TiO_3$ lead-free ceramics, *J. Appl. Phys.* **120**, 034102 (2016).

[42]W. Liu and X. Ren, Large piezoelectric effect in Pb-Free ceramics, *Phys. Rev. Lett.* **103**, 257602 (2009).

[43]M. Acosta, N. Novak, V. Rojas, S. Patel, R. Vaish, J. Koruza, G. A. Rossetti, and J. Rödel, $BaTiO_3$-based piezoelectrics: Fundamentals, current status, and perspectives, *Appl. Phys. Rev.* **4**, 041305 (2017).

[44]R. Yuan, Z. Liu, P. V. Balachandran, D. Xue, Y. Zhou, X. Ding, J. Sun, D. Xue and T. Lookman, Accelerated discovery of large electrostrains in $BaTiO_3$-based piezoelectrics using active learning, *Adv. Mater.* **30**, 1702884 (2018).

[45]Y. Liu, Y. Chang, F. Li, B. Yang, Y. Sun, J. Wu, S. Zhang, R. Wang and W. Cao, Exceptionally high piezoelectric coefficient and low strain hysteresis in grain-oriented (Ba, Ca)(Ti, Zr)O_3 through integrating crystallographic texture and domain engineering, *ACS Appl. Mater. Interfaces* **9**, 29863 (2017).

[46]H. Sun, S. Duan, X. Liu, D. Wang and H. Sui, Lead-free $Ba_{0.98}Ca_{0.02}Zr_{0.02}Ti_{0.98}O_3$ ceramics with enhanced electrical performance by modifying MnO_2 doping content and sintering temperature, *J. Alloys Compd.* **670**, 262 (2016).

[47]Z. Wang, J. Wang, X. Chao, L. Wei, B. Yang, D. Wang and Z. Yang, Synthesis, structure, dielectric, piezoelectric, and energy storage performance of $(Ba_{0.85}Ca_{0.15})(Ti_{0.9}Zr_{0.1})O_3$ ceramics

prepared by different methods, *J. Mater. Sci. Mater. Electron.* **27**, 5047 (2016).
[48]G. Catalan and J. F. Scott, Physics and applications of bismuth ferrite, *Adv. Mater.* **21**, 2463 (2009).
[49]T. Rojac, A. Bencan, B. Malic, G. Tutuncu, J. L. Jones, J. E. Daniels and D. Damjanovic, $BiFeO_3$ Ceramics: Processing, electrical, and electromechanical properties, *J. Am. Ceram. Soc.* **97**, 1993 (2014).
[50]D. Wang, M. Wang, F. Liu, Y. Cui, Q. Zhao, H. Sun, H. Jin and M. Cao, Sol–gel synthesis of Nd-doped $BiFeO_3$ multiferroic and its characterization, *Ceram. Int.* **41**, 8768 (2015).
[51]I. H. Ismailzade, R. M. Ismailov, A. I. Alekberov and F. M. Salaev, Investigation of the magnetoelectric (ME)H effect in solid solutions of the systems $BiFeO_3$-$BaTiO_3$ and $BiFeO_3$-$PbTiO_3$, *Phys. Status Solidi A* **68**, K81 (1981).
[52]M. M. Kumar, A. Srinivas and S. V. Suryanarayana, Structure property relations in $BiFeO_3$/$BaTiO_3$ solid solutions, *J. Appl. Phys.* **87**, 855 (1999).
[53]S. O. Leontsev and R. E. Eitel, Dielectric and piezoelectric properties in Mn-modified $(1-x)BiFeO_{3-x}BaTiO_3$ ceramics, *J. Am. Ceram. Soc.* **92**, 2957 (2009).
[54]M. H. Lee, D. J. Kim, J. S. Park, S. W. Kim, T. K. Song, M. H. Kim, W. J. Kim, D. Do and I. K. Jeong, High-performance lead-free piezoceramics with high Curie temperatures, *Adv. Mater.* **27**, 6976 (2015).
[55]R. A. M. Gotardo, D. S. F. Viana, M. Olzon-Dionysio, S. D. Souza, D. Garcia, J. A. Eiras, M. F. S. Alves, L. F. Cótica, I. A. Santos and A. A. Coelho, Ferroic states and phase coexistence in $BiFeO_3$-$BaTiO_3$ solid solutions, *J. Appl. Phys.* **112**, 104112 (2012).
[56]S. Murakami, D. Wang, A. Mostaed, A. Khesro, A. Feteira, D. C. Sinclair, Z. Fan, X. Tan and I. M. Reaney, High strain (0.4%) Bi$(Mg_{2/3}Nb_{1/3})O_3$-$BaTiO_3$-$BiFeO_3$ lead-free piezoelectric ceramics and multilayers, *J. Am. Ceram. Soc.* doi.org/10.1111/jace.15749 (2018).
[57]S. Murakami, N. T. A. F. Ahmed, D. Wang, A. Feteira, D. C. Sinclair and I. M. Reaney, Optimising dopants and properties in $BiMeO_3$ (Me = Al, Ga, Sc, Y, $Mg_{2/3}Nb_{1/3}$, $Zn_{2/3}Nb_{1/3}$, $Zn_{1/2}Ti_{1/2}$) lead-free $BaTiO_3$-$BiFeO_3$ based ceramics for actuator applications, *J. Eur. Ceram. Soc.* **38**, 4220 (2018).
[58]D. Wang, Z. Fan, W. Li, D. Zhou, A. Feteira, G. Wang, S. Murakami, S. Sun, Q. Zhao, X. Tan and I. M. Reaney, High energy storage density and large strain in $Bi(Zn_{2/3}Nb_{1/3})O_3$-doped $BiFeO_3$–$BaTiO_3$ ceramics, *ACS Appl. Energy Mater.* **1**, 4403 (2018).
[59]S. Kitagawa, T. Ozaki, Y. Horibe, K. Yoshii and S. Mori, Ferroelectric domain structures in $BiFeO_3$-$BaTiO_3$, *Ferroelectrics* **376**, 122 (2008).
[60]T. Ozaki, S. Kitagawa, S. Nishihara, Y. Hosokoshi, M. Suzuki, Y. Noguchi, M. Miyayama and S. Mori, Ferroelectric properties and nano-scaled domain structures in (1-x)$BiFeO_{3-x}BaTiO_3$ ($0.33 < x < 0.50$), *Ferroelectr.* **385**, 6155 (2009).
[61]D. Wang, Z. Fan, D. Zhou, A. Khesro, S. Murakami, A. Feteira, Q. Zhao, X. Tan and I. M. Reaney, Bismuth ferrite-based lead-free ceramics and multilayers with high recoverable energy density, *J. Mater. Chem. A* **6**, 4133 (2018).
[62]D. S. Kim, C. I. Cheon, S. S. Lee and J. S. Kim, Effect of cooling rate on phase transitions and ferroelectric properties in 0.75$BiFeO_3$-0.25$BaTiO_3$ ceramics, *Appl. Phys. Lett.* **109**, 202902 (2016).
[63]I. Calisir and D. A. Hall, Chemical heterogeneity and approaches to its control in $BiFeO_3$–$BaTiO_3$ lead-free ferroelectrics, *J. Mater. Chem. C* **6**, 134 (2018).
[64]I. Calisir, A. A. Amirov, A. K. Kleppe and D. A. Hall, Optimisation of functional properties in lead-free $BiFeO_3$–$BaTiO_3$ ceramics through La^{3+} substitution strategy, *J. Mater. Chem. A* **6**, 5378 (2018).
[65]D. Lin, Q. Zheng, Y. Li, Y. Wan, Q. Li and W. Zhou, Microstructure, ferroelectric and piezoelectric properties of $Bi_{0.5}K_{0.5}TiO_3$-modified $BiFeO_3$–$BaTiO_3$ lead-free ceramics with high Curie temperature, *J. Eur. Ceram. Soc.* **33**, 3023 (2013).
[66]Y. Guo, T. Wang, D. Shi, P. Xiao, Q. Zheng, C. Xu, K. H. Lam and D. Lin, Strong piezoelectricity and multiferroicity in $BiFeO_3$–$BaTiO_3$–$NdCoO_3$ lead-free piezoelectric ceramics with high Curie temperature for current sensing application, *J. Mater. Sci. Mater. Electron.* **28**, 5531 (2017).
[67]Y. Hisato, S. Mikio, W. Takayuki, H. Jumpei, K. Makoto, M. Kaoru, F. Tetsuro, F. Ichiro and W. Satoshi, Microstructure of $BaTiO_3$–$Bi(Mg_{1/2}Ti_{1/2})O_3$–$BiFeO_3$ piezoelectric ceramics, *Jpn. J. Appl. Phys.* **51**, 09LD04 (2012).
[68]Z. J. Li, Z. L. Hou, W. L. Song, X. D. Liu, D. W. Wang, J. Tang and X. H. Shao, Mg-substitution for promoting magnetic and ferroelectric properties of $BiFeO_3$ multiferroic nanoparticles, *Mater. Lett.* **175**, 207 (2016).
[69]Y. Li, W. Q. Cao, J. Yuan, D. W. Wang and M. S. Cao, Nd doping of bismuth ferrite to tune electromagnetic properties and increase microwave absorption by magnetic–dielectric synergy, *J. Mater. Chem. C* **3**, 9276 (2015).
[70]Y. Li, M. S. Cao, D. W. Wang and J. Yuan, High-efficiency and dynamic stable electromagnetic wave attenuation for La doped bismuth ferrite at elevated temperature and gigahertz frequency, *RSC Adv.* **5**, 77184 (2015).
[71]J. Chen and J. Cheng, Enhanced thermal stability of lead-free high temperature 0.75$BiFeO_3$–0.25$BaTiO_3$ ceramics with excess Bi content, *J. Alloys Compd.* **589**, 115 (2014).
[72]T. Zheng, Y. Ding and J. Wu, Bi nonstoichiometry and composition engineering in $(1-x)Bi_{1+y}FeO_{3+3y/2}-xBaTiO_3$ ceramics, *RSC Adv.* **6**, 90831 (2016).
[73]L. F. Zhu, B. P. Zhang, S. Li and G. L. Zhao, Large piezoelectric responses of Bi(Fe,Mg,Ti)O_3-$BaTiO_3$ lead-free piezoceramics near the morphotropic phase boundary, *J. Alloys Compd.* **727**, 382 (2017).
[74]Y. Guo, P. Xiao, R. Wen, Y. Wan, Q. Zheng, D. Shi, K. H. Lam, M. Liu and D. Lin, Critical roles of Mn-ions in enhancing the insulation, piezoelectricity and multiferroicity of $BiFeO_3$-based lead-free high temperature ceramics, *J. Mater. Chem. C* **3**, 5811 (2015).
[75]Y. Lin, L. Zhang and J. Yu, Stable piezoelectric property of modified $BiFeO_3$–$BaTiO_3$ lead-free piezoceramics, *J. Mater. Sci. Mater. Electron.* **26**, 8432 (2015).
[76]S. Hao, J. Yi, X. Chao, L. Wei and Z. Yang, Multiferroic properties in Mn-modified 0.7$BiFeO_3$-0.3$(Ba_{0.85}Ca_{0.15})(Zr_{0.1}Ti_{0.9})O_3$ ceramics, *Mater. Res. Bull.* **84**, 25 (2016).
[77]Q. Li, J. Wei, J. Cheng and J. Chen, High temperature dielectric, ferroelectric and piezoelectric properties of Mn-modified $BiFeO_3$-$BaTiO_3$ lead-free ceramics, *J. Mater. Sci.* **52**, 229 (2017).
[78]Q. Fan, C. Zhou, W. Zeng, L. Cao, C. Yuan, G. Rao and X. Li, Normal-to-relaxor ferroelectric phase transition and electrical properties in Nb-modified 0.72$BiFeO_3$-0.28$BaTiO_3$ ceramics, *J. Electroceram.* **36**, 1 (2016).

[79]X. Wu, L. Luo, N. A. Jiang, X. Wu and Q. Zheng, Effects of Nb doping on the microstructure, ferroelectric and piezoelectric properties of $0.7BiFeO_3$–$0.3BaTiO_3$ lead-free ceramics, *Bull. Mater. Sci.* **39**, 737 (2016).

[80]C. Zhou, H. Yang, Q. Zhou, Z. Cen, W. Li, C. Yuan and H. Wang, Dielectric, ferroelectric and piezoelectric properties of La-substituted $BiFeO_3$–$BaTiO_3$ ceramics, *Ceram. Int.* **39**, 4307 (2013).

[81]X. Wu, M. Tian, Y. Guo, Q. Zheng, L. Luo and D. Lin, Phase transition, dielectric, ferroelectric and ferromagnetic properties of La-doped $BiFeO_3$–$BaTiO_3$ multiferroic ceramics, *J. Mater. Sci. Mater. Electron.* **26**, 978 (2015).

[82]Q. Zheng, L. Luo, K. H. Lam, N. Jiang, Y. Guo and D. Lin, Enhanced ferroelectricity, piezoelectricity, and ferromagnetism in Nd-modified $BiFeO_3$-$BaTiO_3$ lead-free ceramics, *J. Appl. Phys.* **116**, 184101 (2014).

[83]D. Wang, A. Khesro, S. Murakami, A. Feteira, Q. Zhao and I. M. Reaney, Temperature dependent, large electromechanical strain in Nd-doped $BiFeO_3$-$BaTiO_3$ lead-free ceramics, *J. Eur. Ceram. Soc.* **37**, 1857 (2017).

[84]W. Zhou, Q. Zheng, Y. Li, Q. Li, Y. Wan, M. Wu and D. Lin, Structure, ferroelectric, ferromagnetic, and piezoelectric properties of Al-modified $BiFeO_3$–$BaTiO_3$ multiferroic ceramics, *Phys. Status Solidi A* **212**, 632 (2014).

[85]Z. Cen, C. Zhou, H. Yang, Q. Zhou, W. Li, C. Yan, L. Cao, J. Song and L. Peng, Remarkably high-temperature stability of $Bi(Fe_{1-x}Al_x)O_3$–$BaTiO_3$ solid solution with near-zero temperature coefficient of piezoelectric properties, *J. Am. Ceram. Soc.* **96**, 2252 (2013).

[86]Q. Zhou, C. Zhou, H. Yang, G. Chen, W. Li and H. Wang, Dielectric, ferroelectric, and piezoelectric properties of Bi $(Ni_{1/2}Ti_{1/2})O_3$-modified $BiFeO_3$–$BaTiO_3$ ceramics with high Curie temperature, *J. Am. Ceram. Soc.* **95**, 3889 (2012).

[87]C. Zhou, Z. Cen, H. Yang, Q. Zhou, W. Li, C. Yuan and H. Wang, Structure, electrical properties of Bi(Fe, Co)O_3–$BaTiO_3$ piezoelectric ceramics with improved Curie temperature, *Phys. B: Condens. Matter* **410**, 13 (2013).

[88]L. Luo, N. Jiang, X. Zou, D. Shi, T. Sun, Q. Zheng, C. Xu, K. H. Lam and D. Lin, Phase transition, piezoelectric, and multiferroic properties of $La(Co_{0.5}Mn_{0.5})O_3$-modified $BiFeO_3$–$BaTiO_3$ lead-free ceramics, *Phys. Status Solidi A* **212**, 2012 (2015).

[89]Q. Zheng, Y. Guo, F. Lei, X. Wu and D. Lin, Microstructure, ferroelectric, piezoelectric and ferromagnetic properties of $BiFeO_3$–$BaTiO_3$–$Bi(Zn_{0.5}Ti_{0.5})O_3$ lead-free multiferroic ceramics, *J. Mater. Sci. Mater. Electron.* **25**, 2638 (2014).

[90]Y. Li, N. Jiang, K. H. Lam, Y. Guo, Q. Zheng, Q. Li, W. Zhou, Y. Wan and D. Lin, Structure, ferroelectric, piezoelectric, and ferromagnetic properties of $BiFeO_3$-$BaTiO_3$-$Bi_{0.5}Na_{0.5}TiO_3$ lead-free multiferroic ceramics, *J. Am. Ceram. Soc.* **97**, 3602 (2014).

[91]T. Zheng, Z. Jiang and J. Wu, Enhanced piezoelectricity in $(1-x)$ $Bi_{1.05}Fe_{1-y}A_yO_3$–$xBaTiO_3$ lead-free ceramics: Site engineering and wide phase boundary region, *Dalton Trans.* **45**, 11277 (2016).

[92]T. Zheng, Y. Ding and J. Wu, Effects of oxide additives on structure and properties of bismuth ferrite-based ceramics, *J. Mater. Sci. Mater. Electron.* **28**, 11534 (2017).

[93]Z. Liu, T. Zheng, C. Zhao and J. Wu, Composition design and electrical properties in $BiFeO_3$–$BaTiO_3$–$Bi(Zn_{0.5}Ti_{0.5})O_3$ lead-free ceramics, *J. Mater. Sci. Mater. Electron.* **28**, 13076 (2017).

[94]W. Gao, J. Lv and X. Lou, Large electric-field-induced strain and enhanced piezoelectric constant in CuO-modified $BiFeO_3$-$BaTiO_3$ ceramics, *J. Am. Ceram. Soc.* **101**, 3383 (2018).

[95]Q. Li, J. Wei, T. Tu, J. Cheng and J. Chen, Remarkable piezoelectricity and stable high-temperature dielectric properties of quenched $BiFeO_3$–$BaTiO_3$ ceramics, *J. Am. Ceram. Soc.* **100**, 5573 (2017).

[96]G. H. Ryu, A. Hussain, M. H. Lee, R. A. Malik, T. K. Song, W. J. Kim and M. H. Kim, Lead-free high performance $Bi(Zn_{0.5}Ti_{0.5})$ O_3-modified $BiFeO_3$-$BaTiO_3$ piezoceramics, *J. Eur. Ceram. Soc.* **38**, 4414 (2018).

[97]R. Ahmed Malik, A. Hussain, T. Kwon Song, W. J. Kim, R. Ahmed, Y. Soo Sung and M. H. Kim, Enhanced electromechanical properties of (1-x)$BiFeO_3$–$BaTiO_3$–$xLiNbO_3$ ceramics by quenching process, *Ceram. Int.* **43**, S198 (2017).

[98]F. Ichiro, M. Ryuta, N. Kouichi, K. Nobuhiro, S. Mikio, W. Takayuki, H. Jumpei, Y. Hisato, K. Makoto, F. Tetsuro and W. Satoshi, Structural, dielectric, and Piezoelectric properties of Mn-Doped $BaTiO_3$–$Bi(Mg_{1/2}Ti_{1/2})O_3$–$BiFeO_3$ ceramics, *Jpn. J. Appl. Phys.* **50**, 09ND07 (2011).

[99]S. Kim, G. P. Khanal, S. Ueno, C. Moriyoshi, Y. Kuroiwa and S. Wada, Revealing the role of heat treatment in enhancement of electrical properties of lead-free piezoelectric ceramics, *J. Appl. Phys.* **122**, 014103 (2017).

[100]I. Fujii, R. Iizuka, Y. Nakahira, Y. Sunada, S. Ueno, K. Nakashima, E. Magome, C. Moriyoshi, Y. Kuroiwa and S. Wada, Electric field induced lattice strain in pseudocubic Bi $(Mg_{1/2}Ti_{1/2})O_3$-modified $BaTiO_3$-$BiFeO_3$ piezoelectric ceramics, *Appl. Phys. Lett.* **108**, 172903 (2016).

[101]S. Kim, G. P. Khanal, H. W. Nam, M. Kim, I. Fujii, S. Ueno, C. Moriyoshi, Y. Kuroiwa and S. Wada, In-situ electric field induced lattice strain response observation in $BiFeO_3$–$BaTiO_3$ lead-free piezoelectric ceramics, *J. Ceram. Soc. Jpn.* **126**, 316 (2018).

[102]D. W. Wang, D. Q. Zhang, J. Yuan, Q. L. Zhao, H. M. Liu, Z. Y. Wang and M. S. Cao, Structural and electrical properties of Nd ion modified lead zirconate titanate nanopowders and ceramics, *Chin. Phys. B* **18**, 2596 (2009).

[103]D. W. Wang, H. B. Jin, J. Yuan, B. L. Wen, Q. L. Zhao, D. Q. Zhang and M. S. Cao, Mechanical reinforcement and piezoelectric properties of PZT ceramics embedded with nano-crystalline, *Chin. Phys. Lett.* **27**, 047701 (2010).

[104]D. W. Wang, J. Yuan, H. B. Li, R. Lu, Q. L. Zhao, D. Q. Zhang and M. S. Cao, Effects of Nb_2O_5 addition on the microstructure, electrical, and mechanical properties of PZT/ZnO nanowhisker piezoelectric composites, *J. Mater. Sci.* **47**, 2687 (2012).

[105]D. W. Wang, M. S. Cao, J. Yuan, Q. L. Zhao, H. B. Li, H. B. Lin and D. Q. Zhang, Piezoelectric, ferroelectric and mechanical properties of lead zirconate titanate/zinc oxide nanowhisker ceramics, *J. Mater. Sci. Mater. Electron.* **22**, 1393 (2011).

[106]D. Wang, M. Cao and S. Zhang, Investigation of ternary system $Pb(Sn,Ti)O_3$–$Pb(Mg_{1/3}Nb_{2/3})O_3$ with morphotropic phase boundary compositions, *J. Eur. Ceram. Soc.* **32**, 441 (2012).

[107]Y. Li, D. Wang, W. Cao, B. Li, J. Yuan, D. Zhang, S. Zhang and M. Cao, Effect of MnO_2 addition on relaxor behavior and electrical properties of PMNST ferroelectric ceramics, *Ceram. Int.* **41**, 9647 (2015).

[108]Y. Li, J. Yuan, D. Wang, D. Zhang, H. Jin and M. Cao, Effects of Nb, Mn doping on the structure, piezoelectric, and dielectric properties of $0.8Pb(Sn_{0.4}6Ti_{0.5}4)O_3$–$0.2Pb(Mg_{1/3}Nb_{2/3})O_3$ piezoelectric ceramics, *J. Am. Ceram. Soc.* **96**, 3440 (2013).

[109]D. Wang, Q. Zhao, M. Cao, Y. Cui and S. Zhang, Dielectric, piezoelectric, and ferroelectric properties of Al_2O_3 and MnO_2 modified $PbSnO_3$–$PbTiO_3$–$Pb(Mg_{1/3}Nb_{2/3})O_3$ ternary ceramics, *Phys. Status Solidi A* **210**, 1363 (2013).

[110]D. Wang, M. Cao and S. Zhang, Piezoelectric properties of $PbHfO_3$–$PbTiO_3$–$Pb(Mg_{1/3}Nb_{2/3})O_3$ ternary ceramics, *Phys. Status Solidi Rapid Res. Lett.* **6**, 135 (2012).

[111]D. Wang, M. Cao and S. Zhang, Investigation of ternary system $PbHfO_3$–$PbTiO_3$–$Pb(Mg_{1/3}Nb_{2/3})O_3$ with morphotropic phase boundary compositions, *J. Am. Ceram. Soc.* **95**, 3220 (2012).

[112]D. Wang, J. Li, M. Cao and S. Zhang, Effects of Nb_2O_5 additive on the piezoelectric and dielectric properties of PHT-PMN ternary ceramics near the morphotropic phase boundary, *Phys. Status Solidi A* **211**, 226 (2013).

[113]D. Wang, M. Cao and S. Zhang, Phase diagram and properties of $Pb(In_{1/2}Nb_{1/2})O_3$–$Pb(Mg_{1/3}Nb_{2/3})O_3$–$PbTiO_3$ polycrystalline ceramics, *J. Eur. Ceram. Soc.* **32**, 433 (2012).

[114]K. Wang, J. F. Li and J. J. Zhou, High normalized strain obtained in Li-modified (K,Na)NbO_3 lead-free piezoceramics, *Appl. Phys. Express* **4**, 061501 (2011).

[115]F. Li, D. Lin, Z. Chen, Z. Cheng, J. Wang, C. Li, Z. Xu, Q. Huang, X. Liao, L. Q. Chen, T. R. Shrout and S. Zhang, Ultrahigh piezoelectricity in ferroelectric ceramics by design, *Nat. Mater.* **17**, 349 (2018).

[116]H. Qi, R. Zuo, D. Zheng and A. Xie, Evolution of relaxor behavior and high-field strain responses in $Bi(Mg_{1/2}Ti_{1/2})O_3$-$PbTiO_3$-$Pb(Ni_{1/3}Nb_{2/3})O_3$ ferroelectric ceramics, *J. Alloys Compd.* **724**, 774 (2017).

[117]N. J. Donnelly, T. R. Shrout and C. A. Randall, Addition of a Sr, K, Nb (SKN) combination to PZT(53/47) for high strain applications, *J. Am. Ceram. Soc.* **90**, 490 (2007).

[118]Q. Zhang, J. Chen, Y. Lu, T. Yang, X. Yao and Y. He, (Pb,Sm)(Zr,Sn,Ti)O_3 Multifunctional ceramics with large electric-field-induced strain and high-energy storage density, *J. Am. Ceram. Soc.* **99**, 3853 (2016).

[119]Z. Liu, C. Zhao, J. F. Li, K. Wang and J. Wu, Large strain and temperature-insensitive piezoelectric effect in high-temperature piezoelectric ceramics, *J. Mater. Chem. C* **6**, 456 (2018).

[120]B. Narayan, J. S. Malhotra, R. Pandey, K. Yaddanapudi, P. Nukala, B. Dkhil, A. Senyshyn and R. Ranjan, Electrostrain in excess of 1% in polycrystalline piezoelectrics, *Nat. Mater.* **17**, 427 (2018).

[121]X. Gao, J. Wu, Y. Yu, Z. Chu, H. Shi and S. Dong, Giant piezoelectric coefficients in relaxor piezoelectric ceramic PNN-PZT for vibration energy harvesting, *Adv. Funct. Mater.* **28**, 1706895 (2018).

[122]H. Tang, M. F. Zhang, S. J. Zhang, Y. J. Feng, F. Li and T. R. Shrout, Investigation of dielectric and piezoelectric properties in $Pb(Ni_{1/3}Nb_{2/3})O_3$–$PbHfO_3$–$PbTiO_3$ ternary system, *J. Eur. Ceram. Soc.* **33**, 2491 (2013).

[123]R. E. Eitel, S. J. Zhang, T. R. Shrout, C. A. Randall and I. Levin, Phase diagram of the perovskite system $(1-x)BiScO_3$-$xPbTiO_3$, *J. Appl. Phys.* **96**, 2828 (2004).

[124]J. Cheng, Z. Meng and L. E. Cross, High-field and high-Tc piezoelectric ceramics based on $Bi(Ga,Fe)O_3$-$PbTiO_3$ crystalline solutions, *J. Appl. Phys.* **98**, 084102 (2005).

[125]H. Tao, J. Wu, D. Xiao, J. Zhu, X. Wang and X. Lou, High strain in (K,Na)NbO_3-based lead-free piezoceramics, *ACS Appl. Mater. Interfaces.* **6**, 20358 (2014).

[126]T. Zheng, J. Wu, D. Xiao, J. Zhu, X. Wang and X. Lou, Composition-driven phase boundary and piezoelectricity in potassium–sodium niobate-based ceramics, *ACS Appl. Mater. Interfaces* **7**, 20332 (2015).

[127]Y. Qin, J. Zhang, W. Yao, C. Lu and S. Zhang, Domain configuration and thermal stability of $(K_{0.48}Na_{0.52})(Nb_{0.96}Sb_{0.04})O_3$–$Bi_{0.50}(Na_{0.8}2K_{0.18})_{0.50}ZrO_3$ piezoceramics with high d33 coefficient, *ACS Appl. Mater. Interfaces* **8**, 7257 (2016).

[128]J. Fu, R. Zuo, H. Qi, C. Zhang, J. Li and L. Li, Low electric-field driven ultrahigh electrostrains in Sb-substituted (Na,K)NbO_3 lead-free ferroelectric ceramics, *Appl. Phys. Lett.* **105**, 242903 (2014).

[129]K. Wang, F. Z. Yao, W. Jo, D. Gobeljic, V. V. Shvartsman, D. C. Lupascu, J. F. Li and J. Rödel, Temperature-insensitive (K,Na)NbO_3-based lead-free piezoactuator ceramics, *Adv. Funct. Mater.* **23**, 4079 (2013).

[130]J. H. Lee, D. H. Kim, I. T. Seo, J. H. Kim, J. S. Park, J. Ryu, S. H. Han, B. Y. Jang and S. Nahm, Large strain in CuO-added $(Na_{0.2}K_{0.8})NbO_3$ ceramic for use in piezoelectric multilayer actuators, *J. Am. Ceram. Soc.* **99**, 938 (2015).

[131]M. H. Zhang, K. Wang, Y.-J. Du, G. Dai, W. Sun, G. Li, D. Hu, H. C. Thong, C. Zhao, X. Q. Xi, Z. X. Yue and J. F. Li, High and temperature-insensitive piezoelectric strain in alkali niobate lead-free perovskite, *J. Am. Chem. Soc.* **139**, 3889 (2017).

[132]X. Wang, T. Zheng, J. Wu, D. Xiao, J. Zhu, H. Wang, X. Wang, X. Lou and Y. Gu, Characteristics of giant piezoelectricity around the rhombohedral-tetragonal phase boundary in (K,Na)NbO_3-based ceramics with different additives, *J. Mater. Chem. A* **3**, 15951 (2015).

[133]D. Wang, F. Hussain, A. Khesro, A. Feteira, Y. Tian, Q. Zhao and I. M. Reaney, Composition and temperature dependence of structure and piezoelectricity in $(1-x)(K_{1-y}Na_y)NbO_3$-x $(Bi_{1/2}Na_{1/2})ZrO_3$ lead-free ceramics, *J. Am. Ceram. Soc.* **100**, 627 (2016).

[134]J. Yin, C. Zhao, Y. Zhang and J. Wu, Ultrahigh strain in site engineering-independent $Bi_{0.5}Na_{0.5}TiO_3$-based relaxor-ferroelectrics, *Acta Mater.* **147**, 70 (2018).

[135]J. Yin, Y. Zhang, X. Lv and J. Wu, Ultrahigh energy-storage potential under low electric field in bismuth sodium titanate-based perovskite ferroelectrics, *J. Mater. Chem. A* **6**, 9823 (2018).

[136]P. Fan, Y. Zhang, Q. Zhang, B. Xie, Y. Zhu, M. A. Mawat, W. Ma, K. Liu, J. Xiao and H. Zhang, Large strain with low hysteresis in $Bi_4Ti_3O_{12}$ modified $Bi_{1/2}(Na_{0.82}K_{0.18})_{1/2}TiO_3$ lead-free piezoceramics, *J. Eur. Ceram. Soc.* **38**, 4404 (2018).

[137]B. Li, M. S. Cao, J. Liu and D. W. Wang, Domain structure and enhanced electrical properties in sodium bismuth titanate ceramics sintered from crystals with different morphologies, *J. Am. Ceram. Soc.* **99**, 2316 (2016).

[138]A. Khesro, D. Wang, F. Hussain, D. C. Sinclair, A. Feteira and I. M. Reaney, Temperature stable and fatigue resistant lead-free ceramics for actuators, *Appl. Phys. Lett.* **109**, 142907 (2016).

[139]I. Burn and D. M. Smyth, Energy storage in ceramic dielectrics, *J. Mater. Sci.* **7**, 339 (1972).

[140]G. R. Love, Energy storage in ceramic dielectrics, *J. Am. Ceram. Soc.* **73**, 323 (1990).

[141]B. Chu, X. Zhou, K. Ren, B. Neese, M. Lin, Q. Wang, F. Bauer and Q. M. Zhang, A dielectric polymer with high electric energy density and fast discharge speed, *Science* **313**, 334 (2006).

[142]H. Chen, T. N. Cong, W. Yang, C. Tan, Y. Li and Y. Ding, Progress in electrical energy storage system: A critical review, *Prog. Nat. Sci.* **19**, 291 (2009).

[143]T. Wang, L. Jin, Y. Tian, L. Shu, Q. Hu and X. Wei, Microstructure and ferroelectric properties of Nb_2O_5-modified $BiFeO_3$-$BaTiO_3$ lead-free ceramics for energy storage, *Mater. Lett.* **137**, 79 (2014).

[144]D. Zheng, R. Zuo, D. Zhang and Y. Li, Novel $BiFeO_3$–$BaTiO_3$–$Ba(Mg_{1/3}Nb_{2/3})O_3$ lead-free relaxor ferroelectric ceramics for energy-storage capacitors, *J. Am. Ceram. Soc.* **98**, 2692 (2015).

[145]D. Zheng and R. Zuo, Enhanced energy storage properties in La $(Mg_{1/2}Ti_{1/2})O_3$-modified $BiFeO_3$-$BaTiO_3$ lead-free relaxor ferroelectric ceramics within a wide temperature range, *J. Eur. Ceram. Soc.* **37**, 413 (2017).

[146]N. Liu, R. Liang, X. Zhao, C. Xu, Z. Zhou and X. Dong, Novel bismuth ferrite-based lead-free ceramics with high energy and power density, *J. Am. Ceram. Soc.* **101**, 3259 (2018).

[147]T. Tunkasiri and G. Rujijanagul, Dielectric strength of fine grained barium titanate ceramics, *J. Mater. Sci. Lett.* **15**, 1767 (1996).

[148]R. Gerson and T. C. Marshall, Dielectric breakdown of porous ceramics, *J. Appl. Phys.* **30**, 1650 (1959).

[149]Y. J. Wu, Y. H. Huang, N. Wang, J. Li, M. S. Fu and X. M. Chen, Effects of phase constitution and microstructure on energy storage properties of barium strontium titanate ceramics, *J. Eur. Ceram. Soc.* **37**, 2099 (2017).

[150]L. Zhang, S. Jiang, B. Fan and G. Zhang, Enhanced energy storage performance in $(Pb_{0.85}8Ba_{0.1}La_{0.02}Y_{0.008})(Zr_{0.65}Sn_{0.3}Ti_{0.05})O_3$–$(Pb_{0.9}7La_{0.02})(Zr_{0.9}Sn_{0.05}Ti_{0.05})O_3$ anti-ferroelectric composite ceramics by spark plasma sintering, *J. Alloys Compd.* **622**, 162 (2015).

[151]Z. Liu, X. Chen, W. Peng, C. Xu, X. Dong, F. Cao and G. Wang, Temperature-dependent stability of energy storage properties of $Pb_{0.97}La_{0.02}(Zr_{0.58}Sn_{0.335}Ti_{0.085})O_3$ antiferroelectric ceramics for pulse power capacitors, *Appl. Phys. Lett.* **106**, 262901 (2015).

[152]Q. Zhang, H. Tong, J. Chen, Y. Lu, T. Yang, X. Yao and Y. He, High recoverable energy density over a wide temperature range in Sr modified (Pb,La)(Zr,Sn,Ti)O_3 antiferroelectric ceramics with an orthorhombic phase, *Appl. Phys. Lett.* **109**, 262901 (2016).

[153]R. Xu, B. Li, J. Tian, Z. Xu, Y. Feng, X. Wei, D. Huang and L. Yang, $Pb_{0.94}La_{0.04}[(Zr_{0.70}Sn_{0.30})_{0.9}0Ti_{0.10}]O_3$ antiferroelectric bulk ceramics for pulsed capacitors with high energy and power density, *Appl. Phys. Lett.* **110**, 142904 (2017).

[154]Q. Zhao, H. Lei, G. He, J. Di, D. Wang, P. Tan, H. Jin and M. Cao, Effects of thickness on energy storage of (Pb, La)(Zr, Sn, Ti)O_3 antiferroelectric films deposited on $LaNiO_3$ electrodes, *Ceram. Int.* **42**, 1314 (2016).

[155]Y. Wang, X. Chen, H. Zhou, L. Fang, L. Liu and H. Zhang, Evolution of phase transformation behavior and dielectric temperature stability of $BaTiO_3$–$Bi(Zn_{0.5}Zr_{0.5})O_3$ ceramics system, *J. Alloys Compd.* **551**, 365 (2013).

[156]B. Liu, X. Wang, Q. Zhao and L. Li, Improved energy storage properties of fine-crystalline $BaTiO_3$ ceramics by coating powders with Al_2O_3 and SiO_2, *J. Am. Ceram. Soc.* **98**, 2641 (2015).

[157]Q. Zhang, L. Wang, J. Luo, Q. Tang and J. Du, $Ba_{0.4}Sr_{0.6}TiO_3$/MgO Composites with enhanced energy storage density and low dielectric loss for solid-state pulse-forming line, *Inter. J. Appl. ceram. Technol.* **7**, E124 (2009).

[158]Y. H. Huang, Y. J. Wu, W. J. Qiu, J. Li and X. M. Chen, Enhanced energy storage density of $Ba_{0.4}Sr_{0.6}TiO_3$–MgO composite prepared by spark plasma sintering, *J. Eur. Ceram. Soc.* **35**, 1469 (2015).

[159]W. B. Li, D. Zhou and L. X. Pang, Enhanced energy storage density by inducing defect dipoles in lead free relaxor ferroelectric $BaTiO_3$-based ceramics, *Appl. Phys. Lett.* **110**, 132902 (2017).

[160]W. B. Li, D. Zhou, L. X. Pang, R. Xu and H. H. Guo, Novel barium titanate based capacitors with high energy density and fast discharge performance, *J. Mater. Chem. A* **5**, 19607 (2017).

[161]Q. Yuan, F. Yao, Y. Wang, R. Ma and H. Wang, Relaxor ferroelectric $0.9BaTiO_3$–$0.1Bi(Zn_{0.5}Zr_{0.5})O_3$ ceramic capacitors with high energy density and temperature stable energy storage properties, *J. Mater. Chem. C* **5**, 9552 (2017).

[162]T. Wang, L. Jin, C. Li, Q. Hu and X. Wei, Relaxor ferroelectric $BaTiO_3$–$Bi(Mg_{2/3}Nb_{1/3})O_3$ ceramics for energy storage application, *J. Am. Ceram. Soc.* **98**, 559 (2014).

[163]Q. Hu, L. Jin, T. Wang, C. Li, Z. Xing and X. Wei, Dielectric and temperature stable energy storage properties of $0.88BaTiO_3$–$0.12Bi(Mg_{1/2}Ti_{1/2})O_3$ bulk ceramics, *J. Alloys Compd.* **640**, 416 (2015).

[164]Z. Shen, X. Wang, B. Luo and L. Li, $BaTiO_3$–$BiYbO_3$ perovskite materials for energy storage applications, *J. Mater. Chem. A* **3**, 18146 (2015).

[165]L. Wu, X. Wang and L. Li, Lead-free $BaTiO_3$–$Bi(Zn_{2/3}Nb_{1/3})O_3$ weakly coupled relaxor ferroelectric materials for energy storage, *RSC Adv.* **6**, 14273 (2016).

[166]H. Yang, F. Yan, Y. Lin and T. Wang, Novel strontium titanate-based lead-free ceramics for high-Energy storage applications, *ACS Sustain. Chem. Eng.* **5**, 10215 (2017).

[167]F. Yan, H. Yang, Y. Lin and T. Wang, Dielectric and ferroelectric properties of $SrTiO_3$–$Bi_{0.5}Na_{0.5}TiO_3$–$BaAl_{0.5}Nb_{0.5}O_3$ lead-free ceramics for high-energy-storage applications, *Inorg. Chem.* **56**, 13510 (2017).

[168]H. Yang, F. Yan, Y. Lin and T. Wang, Enhanced recoverable energy storage density and high efficiency of $SrTiO_3$-based lead-free ceramics, *Appl. Phys. Lett.* **111**, 253903 (2017).

[169]H. Yang, F. Yan, Y. Lin, T. Wang, L. He and F. Wang, A lead free relaxation and high energy storage efficiency ceramics for energy storage applications, *J. Alloys Compd.* **710**, 436 (2017).

[170]H. Yang, F. Yan, Y. Lin, T. Wang, F. Wang, Y. Wang, L. Guo, W. Tai and H. Wei, Lead-free $BaTiO_3$-$Bi_{0.5}Na_{0.5}TiO_3$-$Na_{0.73}Bi_{0.09}NbO_3$ relaxor ferroelectric ceramics for high energy storage, *J. Eur. Ceram. Soc.* **37**, 3303 (2017).

[171]Y. H. Huang, Y. J. Wu, B. Liu, T. N. Yang, J. J. Wang, J. Li, L. Q. Chen and X. M. Chen, From core–shell $Ba_{0.4}Sr_{0.6}TiO_3@SiO_2$ particles to dense ceramics with high energy storage performance by spark plasma sintering, *J. Mater. Chem. A* **6**, 4477 (2018).

[172]Q. Xu, J. Xie, Z. He, L. Zhang, M. Cao, X. Huang, M. T. Lanagan, H. Hao, Z. Yao and H. Liu, Energy-storage properties of $Bi_{0.5}Na_{0.5}TiO_3$-$BaTiO_3$-$KNbO_3$ ceramics fabricated by wet-chemical method, *J. Eur. Ceram. Soc.* **37**, 99 (2017).

[173]Q. Xu, H. Liu, L. Zhang, J. Xie, H. Hao, M. Cao, Z. Yao and M. T. Lanagan, Structure and electrical properties of lead-free $Bi_{0.5}Na_{0.5}TiO_3$-based ceramics for energy-storage applications, *RSC Adv.* **6**, 59280 (2016).

[174]J. Yin, X. Lv and J. Wu, Enhanced energy storage properties of $\{Bi_{0.5}[(Na_{0.8}K_{0.2)1-z}Li_z]_{0.5}\}_{0.96}Sr_{0.04}(Ti_{1-x-y}Ta_xNb_y)O_3$ lead-free ceramics, *Ceram. Int.* **43**, 13541 (2017).

[175]Y. Pu, M. Yao, L. Zhang and M. Chen, Enhanced energy storage density of $0.55Bi_{0.5}Na_{0.5}TiO_3$-$0.45Ba_{0.85}Ca_{0.15}Ti_{0.85}Zr_{0.1}Sn_{0.05}O_3$ with MgO addition, *J. Alloys Compd.* **702**, 171 (2017).

[176]L. Zhang, X. Pu, M. Chen, S. Bai and Y. Pu, Influence of $BaSnO_3$ additive on the energy storage properties of $Na_{0.5}Bi_{0.5}TiO_3$-based relaxor ferroelectrics, *J. Eur. Ceram. Soc.* **38**, 2304 (2018).

[177]Y. Pu, L. Zhang, Y. Cui and M. Chen, High energy storage density and optical transparency of microwave sintered homogeneous $(Na_{0.5}Bi_{0.5})_{(1-x)}BaxTi_{(1-y)}Sn_yO_3$ ceramics, *ACS Sustain. Chem. Eng.* **6**, 6102 (2018).

[178]J. Wu, A. Mahajan, L. Riekehr, H. Zhang, B. Yang, N. Meng, Z. Zhang and H. Yan, Perovskite $Sr_x(Bi_{1-x}Na_{0.97-x}Li_{0.03})_{0.5}TiO_3$ ceramics with polar nano regions for high power energy storage, *Nano Energy* **50**, 723 (2018).

[179]J. Li, F. Li, Z. Xu and S. Zhang, Multilayer lead-free ceramic capacitors with ultrahigh energy density and efficiency, *Adv. Mater.* **30**, 1802155 (2018).

[180]Z. Yang, H. Du, S. Qu, Y. Hou, H. Ma, J. Wang, J. Wang, X. Wei and Z. Xu, Significantly enhanced recoverable energy storage density in potassium–sodium niobate-based lead free ceramics, *J. Mater. Chem. A* **4**, 13778 (2016).

[181]T. Shao, H. Du, H. Ma, S. Qu, J. Wang, J. Wang, X. Wei and Z. Xu, Potassium–sodium niobate based lead-free ceramics: Novel electrical energy storage materials, *J. Mater. Chem. A* **5**, 554 (2017).

[182]H. Tao, W. Wu and J. Wu, Electrical properties of holmium doped (K,Na)(Nb,Sb)O_3-(Bi,Na)HfO_3 ceramics with wide sintering and poling temperature range, *J. Alloys Compd.* **689**, 759 (2016).

[183]B. Qu, H. Du, Z. Yang, Q. Liu and T. Liu, Enhanced dielectric breakdown strength and energy storage density in lead-free relaxor ferroelectric ceramics prepared using transition liquid phase sintering, *RSC Adv.* **6**, 34381 (2016).

[184]H. Tao and J. Wu, Optimization of energy storage density in relaxor (K, Na, Bi)NbO_3 ceramics, *J. Mater. Sci. Mater. Electron.* **28**, 16199 (2017).

[185]Y. Tian, L. Jin, H. Zhang, Z. Xu, X. Wei, E. D. Politova, S. Y. Stefanovich, N. V. Tarakina, I. Abrahams and H. Yan, High energy density in silver niobate ceramics, *J. Mater. Chem. A* **4**, 17279 (2016).

[186]L. Zhao, Q. Liu, S. Zhang and J. F. Li, Lead-free $AgNbO_3$ antiferroelectric ceramics with an enhanced energy storage performance using MnO_2 modification, *J. Mater. Chem. C* **4**, 8380 (2016).

[187]L. Zhao, Q. Liu, J. Gao, S. Zhang and J. F. Li, Lead-free antiferroelectric silver niobate tantalate with high energy storage performance, *Adv. Mater.* **29**, 1701824 (2017).

[188]Y. Tian, L. Jin, H. Zhang, Z. Xu, X. Wei, G. Viola, I. Abrahams and H. Yan, Phase transitions in bismuth-modified silver niobate ceramics for high power energy storage, *J. Mater. Chem. A* **5**, 17525 (2017).

[189]L. Zhao, J. Gao, Q. Liu, S. Zhang and J. F. Li, Silver niobate lead-free antiferroelectric ceramics: Enhancing energy storage density by B-site doping, *ACS Appl. Mater. Interfaces* **10**, 819 (2018).

[190]H. Ogihara, C. A. Randall and S. Trolier-Mckinstry, High-energy density capacitors utilizing 0.7 $BaTiO_3$–0.3 $BiScO_3$ ceramics, *J. Am. Ceram. Soc.* **92**, 1719 (2009).

[191]Y. Gao, H. Liu, Z. Yao, H. Hao, Z. Yu and M. Cao, Effect of layered structure on dielectric properties and energy storage density in $xBa_{0.7}Sr_{0.3}TiO_3$-$SrTiO_3$ multilayer ceramics, *Ceram. Int.* **43**, 8418 (2017).

[192]D. P. Shay, N. J. Podraza, N. J. Donnelly and C. A. Randall, High energy density, high temperature capacitors utilizing Mn-Doped $0.8CaTiO_3$–$0.2CaHfO_3$ ceramics, *J. Am. Ceram. Soc.* **95**, 1348 (2011).

[193]H. Lee, J. R. Kim, M. J. Lanagan, S. Trolier-Mckinstry and C. A. Randall, High-energy density dielectrics and capacitors for elevated temperatures: Ca(Zr,Ti)O_3, *J. Am. Ceram. Soc.* **96**, 1209 (2013).

[194]L. Chen, N. Sun, Y. Li, Q. Zhang, L. Zhang and X. Hao, Multifunctional antiferroelectric MLCC with high-energy-storage properties and large field-induced strain, *J. Am. Ceram. Soc.* **101**, 2313 (2017).

[195]S. Trolier-Mckinstry and P. Muralt, Thin film piezoelectrics for MEMS, *J. Electroceram.* **12**, 7 (2004).

[196]G. L. Smith, J. S. Pulskamp, L. M. Sanchez, D. M. Potrepka, R. M. Proie, T. G. Ivanov, R. Q. Rudy, W. D. Nothwang, S. S. Bedair, C. D. Meyer and R. G. Polcawich, PZT-Based Piezoelectric MEMS Technology, *J. Am. Ceram. Soc.* **95**, 1777 (2012).

[197]H. Funakubo, M. Dekkers, A. Sambri, S. Gariglio, I. Shklyarevskiy and G. Rijnders, Epitaxial PZT films for MEMS printing applications, *MRS Bull.* **37**, 1030 (2012).

[198]J. S. Pulskamp, R. G. Polcawich, R. Q. Rudy, S. S. Bedair, R. M. Proie, T. Ivanov and G. L. Smith, Piezoelectric PZT MEMS technologies for small-scale robotics and RF applications, *MRS Bull.* **37**, 1062 (2012).

[199]C. G. Hindrichsen, R. Lou-Møller, K. Hansen and E. V. Thomsen, Advantages of PZT thick film for MEMS sensors, *Sens. Actuators A, Phys.* **163**, 9 (2010).

[200]Y. Wang, H. Zhao, L. Zhang, J. Chen and X. Xing, $PbTiO_3$-based perovskite ferroelectric and multiferroic thin films, *PCCP* **19**, 17493 (2017).

[201]H. Ishiwara, Impurity substitution effects in $BiFeO_3$ thin films — From a viewpoint of FeRAM applications, *Curr. Appl. Phys.* **12**, 603 (2012).

[202]A. Safari and M. Abazari, Lead-free piezoelectric ceramics and thin films, *IEEE Trans. Ultrason. Ferroelectr. Freq. Control* **57**, 2165 (2010).

[203]A. Rajashekhar, H.-R. Zhang, B. Srowthi, I. M. Reaney and S. Trolier-Mckinstry, Microstructure evolution of in situ pulsed-laser crystallized $Pb(Zr_{0.52}Ti_{0.48})O_3$ thin films, *J. Am. Ceram. Soc.* **99**, 43 (2015).

[204]H. Zhang, I. M. Reaney, D. M. Marincel, S. Trolier-Mckinstry, Q. M. Ramasse, I. Maclaren, S. D. Findlay, R. D. Fraleigh, I. M. Ross, S. Hu, W. Ren and W. Mark Rainforth, Stabilisation of Fe_2O_3-rich perovskite nanophase in epitaxial rare-earth doped $BiFeO_3$ films, *Sci Rep.* **5**, 13066 (2015).

[205]Q. Zhao, P. Tan, G. He, J. Di, D. Wang, L. Qi, H. Jin and M. Cao, Effects of electrodes on ferroelectric properties of PNZT films prepared by sol–gel method, *J. Sol-Gel Sci. Technol.* **78**, 258 (2016).

[206]Q. Zhao, M. Cao, J. Yuan, R. Lu, G. He and D. Wang, Fabrication and characterization of a piezoelectric micromirror using for optical data tracking of high-density storage, *Microsystem Technologies* **20**, 1317 (2014).

[207]Q. Zhao, D. Su, M. Cao, G. He, J. Di, J. Yuan and D. Wang, Thickness-dependent electrical properties of sol–gel derived Pb$(Zr_{0.52}Ti_{0.48})O_3$ thick films using $PbTiO_3$ buffer layers, *J. Mater. Sci. Mater. Electron.* **24**, 3521 (2013).

[208]Q. L. Zhao, M. S. Cao, J. Yuan, R. Lu, D. W. Wang and D. Q. Zhang, Thickness effect on electrical properties of Pb $(Zr_{0.52}Ti_{0.48})O_3$ thick films embedded with ZnO nanowhiskers prepared by a hybrid sol–gel route, *Mater. Lett.* **64**, 632 (2010).
[209]Q. L. Zhao, M. S. Cao, J. Yuan, W. L. Song, R. Lu, D. W. Wang and D. Q. Zhang, Preparation and electrical properties of Pb $(Zr_{0.52}Ti_{0.48})O_3$ thick films embedded with ZnO nanowhiskers by a hybrid sol–gel route, *J. Alloys Compd.* **492**, 264 (2010).
[210]H. Zhang, S. Jiang and K. Kajiyoshi, Nonlinear dielectric properties of $(Bi_{0.5}Na_{0.5})TiO_3$-based lead-free piezoelectric thick films, *Appl. Phys. Lett.* **98**, 072908 (2011).
[211]H. Zhang, S. Jiang, J. Xiao and K. Kajiyoshi, Low temperature preparation and electrical properties of sodium–potassium bismuth titanate lead-free piezoelectric thick films by screen printing, *J. Eur. Ceram. Soc.* **30**, 3157 (2010).
[212]H. Zhang, S. Jiang and K. Kajiyoshi, Pyroelectric and dielectric properties of Mn modified $0.82Bi_{0.5}Na_{0.5}TiO_3$–$0.18Bi_{0.5}K_{0.5}TiO_3$ lead-free thick films, *J. Am. Ceram. Soc.* **92**, 2147 (2009).
[213]H. Zhang, S. Jiang and Y. Zeng, Piezoelectric property in morphotropic phase boundary $Bi_{0.5}(Na_{0.82}K_{0.18})_{0.5}TiO_3$ lead free thick film deposited by screen printing, *Appl. Phys. Lett.* **92**, 152901 (2008).
[214]Y. Yao, Y. Li, N. Sun, J. Du, X. Li, L. Zhang, Q. Zhang and X. Hao, High energy-storage performance of BNT-BT-NN ferroelectric thin films prepared by RF magnetron sputtering, *J. Alloys Compd.* **750**, 228 (2018).
[215]J. Wang, N. Sun, Y. Li, Q. Zhang, X. Hao and X. Chou, Effects of Mn doping on dielectric properties and energy-storage performance of $Na_{0.5}Bi_{0.5}TiO_3$ thick films, *Ceram. Int.* **43**, 7804 (2017).
[216]K. Ueda, H. Tabata and T. Kawai, Coexistence of ferroelectricity and ferromagnetism in $BiFeO_3$–$BaTiO_3$ thin films at room temperature, *Appl. Phys. Lett.* **75**, 555 (1999).
[217]Y. Ito, W. Sakamoto, M. Moriya and T. Yogo, Synthesis and properties of multiferroic $0.7BiFeO_3-0.3BaTiO_3$ thin films by Mn doping, *Ceram. Int.* **39**, S451 (2013).
[218]H. Liu, R. Liu and T. Liu, Ferroelectricity of highly preferentially oriented $(BiFeO_3)_{1-x}$–$(BaTiO_3)_x$ solid solution film by sol–gel method, *J. Sol-Gel Sci. Technol.* **57**, 1 (2011).
[219]M. H. Lee, D. J. Kim, J. S. Park, M. H. Kim, T. K. Song, S. Kumar, W. J. Kim, D. Do, I. Hwang, B. H. Park and K. S. Choi, Lead-free piezoelectric $BiFeO_3$-$BaTiO_3$ thin film with high Curie temperature, *Curr. Appl. Phys.* **16**, 1449 (2016).
[220]H. Pan, Y. Zeng, Y. Shen, Y. H. Lin, J. Ma, L. Li and C. W. Nan, $BiFeO_3$–$SrTiO_3$ thin film as a new lead-free relaxor-ferroelectric capacitor with ultrahigh energy storage performance, *J. Mater. Chem. A* **5**, 5920 (2017).
[221]Q. M. Zhang and T. Zhang, The refrigerant is also the pump, *Science* **357**, 1094 (2017).
[222]R. Ma, Z. Zhang, K. Tong, D. Huber, R. Kornbluh, Y. S. Ju and Q. Pei, Highly efficient electrocaloric cooling with electrostatic actuation, *Science* **357**, 1130 (2017).
[223]S. G. Lu and Q. Zhang, Electrocaloric materials for solid-state refrigeration, *Adv. Mater.* **21**, 1983 (2009).
[224]B. Neese, B. Chu, S.-G. Lu, Y. Wang, E. Furman and Q. M. Zhang, Large electrocaloric effect in ferroelectric polymers near room temperature, *Science* **321**, 821 (2008).
[225]Y. Liu, J. F. Scott and B. Dkhil, Direct and indirect measurements on electrocaloric effect: Recent developments and perspectives, *Appl. Phys. Rev.* **3**, 031102 (2016).
[226]G. G. Guzmán-Verri and P. B. Littlewood, Why is the electrocaloric effect so small in ferroelectrics?, *APL Materials* **4**, 064106 (2016).
[227]X. Li, S. G. Lu, X. Z. Chen, H. Gu, X. S. Qian and Q. M. Zhang, Pyroelectric and electrocaloric materials, *J. Mater. Chem. C* **1**, 23 (2013).
[228]S. P. Alpay, J. Mantese, S. Trolier-Mckinstry, Q. Zhang and R. W. Whatmore, Next-generation electrocaloric and pyroelectric materials for solid-state electrothermal energy interconversion, *MRS Bull.* **39**, 1099 (2014).
[229]R. W. Whatmore, Pyroelectric devices and materials, *Rep. Prog. Phys.* **49**, 1335 (1986).
[230]Y. Tang, S. Zhang, Z. Shen, W. Jiang, J. Luo, R. Sahul and T. R. Shrout, Primary and secondary pyroelectric coefficients of rhombohedral and tetragonal single-domain relaxor-$PbTiO_3$ single crystals, *J. Appl. Phys.* **114**, 084105 (2013).